Hopf Bifurcations and Oscillatory Instabilities of Spike Solutions for the One-Dimensional Gierer-Meinhardt Model

Michael J. Ward,[*] Juncheng Wei[†]

Abstract

In the limit of small activator diffusivity ε, the stability of symmetric k-spike equilibrium solutions to the Gierer-Meinhardt reaction-diffusion system in a one-dimensional spatial domain is studied for various ranges of the reaction-time constant $\tau \geq 0$ and the diffusivity $D > 0$ of the inhibitor field dynamics. A nonlocal eigenvalue problem is derived that determines the stability on an $O(1)$ time-scale of these k-spike equilibrium patterns. The spectrum of this eigenvalue problem is studied in detail using a combination of rigorous, asymptotic, and numerical methods. For $k = 1$, and for various exponent sets of the nonlinear terms, we show that for each $D > 0$, a one-spike solution is stable only when $0 \leq \tau < \tau_0(D)$. As τ increases past $\tau_0(D)$, a pair of complex conjugate eigenvalues enters the unstable right half-plane, triggering an oscillatory instability in the amplitudes of the spikes. A large-scale oscillatory motion for the amplitudes of the spikes that occurs when τ is well beyond $\tau_0(D)$ is computed numerically and explained qualitatively. For $k \geq 2$, we show that a k-spike solution is unstable for any $\tau \geq 0$ when $D > D_k$, where $D_k > 0$ is the well known stability threshold of a multi-spike solution when $\tau = 0$. For $D > D_k$ and $\tau \geq 0$, there are eigenvalues of the linearization that lie on the (unstable) positive real axis of the complex eigenvalue plane. The resulting instability is of competition type whereby spikes are annihilated in finite time. For $0 < D < D_k$, we show that a k-spike solution is stable with respect to the $O(1)$ eigenvalues only when $0 \leq \tau < \tau_0(D; k)$. When τ increases past $\tau_0(D; k) > 0$, a synchronous oscillatory instability in the amplitudes of the spikes is initiated. For certain exponent sets and for $k \geq 2$, we show that $\tau_0(D; k)$ is a decreasing function of D with $\tau_0(D; k) \to \tau_{0k} > 0$ as $D \to D_k^-$.

1 Introduction

Since the pioneering work of Turing [29], there have been many studies determining the conditions for the onset of instabilities of spatially homogeneous patterns in reaction-diffusion systems in

[*]Department of Mathematics, University of British Columbia, Vancouver, Canada V6T 1Z2, (corresponding author)

[†]Department of Mathematics, Chinese University of Hong Kong, New Territories, Hong Kong

1

both bounded and unbounded spatial domains. Various types of weakly nonlinear theories, many of them associated with the complex Ginzburg-Landau equation, have been used to study the weakly nonlinear development of these Turing instabilities. There have been many results in this direction. A survey of pattern formation in many different physical settings is given in [2]. However, in the singularly perturbed limit, many reaction-diffusion systems can allow for the existence of equilibrium solutions that exhibit a high degree of spatial heterogeneity. A very common pattern of this type is a spike pattern, whereby one of the components of the system becomes spatially localized at certain points in the domain. In different contexts these localized patterns are referred to either as spots (cf. [18]) or pulses (cf. [4]). In contrast to the study of the stability of spatially homogeneous solutions, the instabilities and the dynamics of these spatially localized patterns are not nearly as well understood. In this paper, we determine the conditions for the onset of oscillatory instabilities for symmetric k-spike equilibrium solutions to the singularly perturbed Gierer-Meinhardt reaction-diffusion model in a bounded one-dimensional spatial domain. An equilibrium spike pattern is said to be symmetric when the spikes have a common amplitude. Asymmetric equilibrium spike patterns, where the spikes have different amplitudes, have been constructed asymptotically in [30].

The Gierer-Meinhardt (GM) model, introduced in [11], has been widely used to model localization processes in nature, such as cell differentiation and morphogenesis (cf. [12]), biological pattern formation (cf. [17]), and the formation of sea-shell patterns (cf. [18]). In Appendix A, we show that in the limit where the activator diffuses more slowly than the inhibitor, the GM system can be written in dimensionless form as

$$a_t = \varepsilon^2 a_{xx} - a + \frac{a^p}{h^q}, \qquad -1 < x < 1, \quad t > 0, \tag{1.1a}$$

$$\tau h_t = D h_{xx} - h + \varepsilon^{-1} \frac{a^m}{h^s}, \qquad -1 < x < 1, \quad t > 0, \tag{1.1b}$$

$$a_x(\pm 1, t) = h_x(\pm 1, t) = 0; \qquad a(x,0) = a_0(x), \qquad h(x,0) = h_0(x). \tag{1.1c}$$

Here a, h, $0 < \varepsilon \ll 1$, $D > 0$, and $\tau \geq 0$, represent the activator concentration, inhibitor concentration, activator diffusivity, inhibitor diffusivity, and reaction-time constant, respectively. The parameters $D > 0$ and $\tau \geq 0$ are assumed to be constant. The usual assumption on the exponents (p, q, m, s) (cf. [11]) are that they satisfy

$$p > 1, \qquad q > 0, \qquad m > 1, \qquad s \geq 0, \qquad \text{with} \qquad \zeta \equiv \frac{qm}{(p-1)} - (s+1) > 0. \tag{1.2}$$

To illustrate our analytical theory, we will give explicit stability results for the five different commonly used exponent sets (p, q, m, s) given by

$$(2, 1, 2, 0), \qquad (2, 1, 3, 0), \qquad (3, 2, 2, 0), \qquad (3, 2, 3, 1), \qquad (4, 2, 2, 0). \tag{1.3}$$

2

For the case $\tau = 0$ and $\varepsilon \ll 1$, the stability and existence of symmetric and asymmetric k-spike equilibria for (1.1) has been analyzed using formal asymptotic techniques in [14] and [30]. A rigorous framework for these stability analyses is given in [33]. A dynamical systems approach is used in [5] to construct multi-spike equilibrium solutions for (1.1). The existence of symmetric k-spike equilibria for (1.1) was proved in [28]. A formal asymptotic analysis of small amplitude solutions to activator-inhibitor systems was given in [15]. For the case $\tau = 0$, the dynamics of k-spike patterns to (1.1) was analyzed in [13]. In [27] various types of instabilities for the dynamics of one-spike solutions of the GM model with $D = O(1)$ and $\tau > 0$, and for a related reaction-diffusion system known as the Schnakenburg model (cf. [26]), were highlighted numerically. These instabilities include sudden oscillations of slowly drifting spikes.

For $\tau > 0$, there are only a few stability results for spike solutions to the GM system, and most of these results are for the shadow GM model obtained by letting $D \to \infty$ in (1.1b). For $\tau > 0$, the numerical results shown in [20] suggested that oscillatory instabilities can occur for a boundary spike solution to the shadow GM model. For $\tau > 0$, and D sufficiently large, the stability of a one-spike solution to (1.1) was analyzed rigorously in [21] under the condition that the exponents (p, q, m, s) in the model are such that $\zeta \to 0^+$ in (1.2). For the shadow GM model, it is proved in [3] that there are two eigenvalues in the spectrum of the linearization around a spike solution that are along the positive real axis when τ is sufficiently large, and a Hopf bifurcation as τ increases past some critical parameter is suggested. A combination of rigorous, asymptotic, and numerical, techniques is used in [31] to determine the conditions for the onset of oscillatory instabilities of an equilibrium one-spike solution to the shadow GM model in N spatial dimensions. The origin of the term "shadow system" first appeared in [22] in the context of examining bifurcation-theoretic properties of solutions to a general class of activator-inhibitor systems in the singularly perturbed limit where the diffusion coefficient of the inhibitor tends to infinity.

Our goal is to study the stability of symmetric k-spike patterns of (1.1) for finite D and for $\tau > 0$. Intuitively, for a fixed value of D, a spike pattern should become unstable as τ increases. This is because for large τ the inhibitor field responds slowly to small local fluctuations in the activator concentration. In addition, for a fixed $\tau \geq 0$ and for the shadow limit $D \to \infty$, multiple-spike solutions are unstable since the inhibitor field has no spatial variation to suppress the autocatalysis term a^p/h^q in (1.1) that is responsible for spike formation. Hence, we would expect that for sufficiently large values of D, multiple-spike solutions will be unstable even when τ is small. Our results characterize the onset of these instabilities precisely.

In our analysis, valid for $\varepsilon \to 0$, we linearize (1.1) around a symmetric k-spike equilibrium solution and use a Green's function method to derive a nonlocal eigenvalue problem that determines

the stability of this solution with respect to the $O(1)$ eigenvalues. These eigenvalues are referred to in [14] as the large eigenvalues. Our derivation of the nonlocal eigenvalue problem using Green's functions is related to the approach used in [23] to analyze the stability of transition layer solutions to the Fitzhugh-Nagumo model. For $k \geq 1$, we determine conditions on τ, D, and the exponent set (p, q, m, s), such that the spectrum of this eigenvalue problem is in the stable left half-plane $\text{Re}(\lambda) < 0$. The small eigenvalues of order $O(\varepsilon^2)$ in the spectrum of the linearization of (1.1) around a k-spike equilibrium solution are asymptotically independent of τ as $\varepsilon \to 0$. Thus, the spectral result of [14] still holds for the small eigenvalues.

The spectrum of the nonlocal eigenvalue problem is studied using a combination of functional-analytic, asymptotic, and numerical techniques. We first summarize some rigorous results for the case of a one-spike solution where $k = 1$. When $k = 1$, we prove in proposition 3.7 that there is a value $\tau_0(D) > 0$, such that when $\tau = \tau_0(D)$ there is a complex conjugate pair of eigenvalues on the imaginary axis $\text{Re}(\lambda) = 0$. We use a winding number approach to prove in propositions 3.3 and 3.4 that, when either $m = 2$ and $p > 1$ or when a certain monotonicity condition holds, the number of eigenvalues M in the unstable right half-plane is either $M = 0$ or $M = 2$ for any $\tau > 0$. In proposition 3.7, when either $m = 2$ and $p = 2$, or $m = p + 1$ and $1 < p \leq 5$, we prove that for any $D > 0$ there exists a value $\tau_c(D) > 0$ such that there are exactly two eigenvalues along the positive real axis $\text{Re}(\lambda) > 0$ for any $\tau > \tau_c(D)$. When $m = 2$ and $\tau > \tau_c(D)$ these are the only two eigenvalues in the right half-plane. Many additional results are obtained numerically. For $k = 1$, and for each of the exponent sets of (1.3), we compute the function $\tau_0(D)$ for which there is a complex conjugate pair of eigenvalues on the imaginary axis. We find that $\tau_0(D)$ is a decreasing function of D, with $\tau_0(D)$ tending to the shadow limit value $\tau_{0s} > 0$ as $D \to \infty$. For each of the exponent sets of (1.3), we show numerically that as τ increases past $\tau_0(D)$, these eigenvalues cross strictly into the right half-plane and that they merge onto the positive real axis at some critical value $\tau = \tau_c(D) > \tau_0(D)$. Hence, numerically we find that there are exactly two eigenvalues in the right half-plane for each $\tau > \tau_0(D)$. For $\tau > \tau_c(D)$, these eigenvalues remain on the positive real axis and their asymptotic behavior as $\tau \to \infty$ is given in propositions 3.8 and 3.9. The function $\tau_c(D)$ is computed numerically for each of the exponent sets of (1.3).

The stability properties of multi-spike solutions with $k \geq 2$ are more intricate. For $k \geq 2$, and for certain ranges of m and p, we prove in proposition 5.3 that a k-spike solution is unstable for any $\tau \geq 0$ when $D > D_k$, where $D_k > 0$ is the stability threshold for multi-spike solutions when $\tau = 0$ computed in [14] (see proposition 2.6 below). For $D > D_k$ and any $\tau \geq 0$, there is at least one eigenvalue of the spectrum of the linearization on the (unstable) positive real axis. For $0 < D < D_k$, we show that a k-spike solution is stable with respect to the $O(1)$ eigenvalues only

4

when $0 \le \tau < \tau_0(D; k)$. When τ increases past $\tau_0(D; k)$, an oscillatory instability is triggered. For the exponent sets of (1.3) and for $k \ge 2$, we show that $\tau_0(D; k)$ is a decreasing function of D with $\tau_0(D; k) \to \tau_{0k} > 0$ as $D \to D_k^-$. For $D \to 0$, we have that $\tau_0(D; k) \to \tau_{0u}$, where the value τ_{0u} depends on the exponent set (p, q, m, s), but is independent of k. Further qualitative features of the spectrum of the nonlocal eigenvalue problem for $k \ge 2$ are obtained.

To confirm our spectral results for $k = 1$, we compute full numerical solutions to (1.1) for values of τ near τ_0 and for values of τ well beyond τ_0. For the exponent sets of (1.3), we first verify that an oscillatory instability is triggered for τ slightly beyond τ_0. This is shown by computing the amplitude a_m of each spike as a function of t. The amplitude a_m of a spike is defined to be the value of the activator concentration a at the center of the spike. Numerical results are then shown for values of τ well beyond the critical value τ_0. For these values of τ, we show numerically that there can be a very complicated large-scale oscillatory motion in the amplitude of the spike. A qualitative explanation for these oscillations is given. For multi-spike solutions with $k \ge 2$, we also verify the stability results from full numerical computations of (1.1) near the threshold values.

To visually illustrate the types of instabilities that can occur, consider a four-spike solution to (1.1) for the exponent set $(p, q, m, s) = (2, 1, 3, 0)$ with $\varepsilon = 0.01$ (this is experiment 3 of §5). For three different parameter sets of D and τ we computed the solution to (1.1) numerically using the routine D03PCF from the NAG library [19]. The equilibrium solution a_e and h_e is shown in Fig. 1(a) when $D = 0.18$. In each case, for the initial condition for (1.1) we took a 2% localized perturbation off of a_e and h_e, with the perturbation chosen so that it is identical for the first and third, and for the second and fourth, spikes. The precise form for this perturbation is given in (5.19) below. The spike amplitudes a_{mn} are defined to be the values of a at the local maximum points. When $t = 0$ we have $a_{mn} = a(x_n, t)$ for $n = 1, .., 4$, where $x_n = -1 + (2n - 1)/4$ for $n = 1, .., 4$ are the equilibrium spike locations. We remark that for each of the three parameter sets of D and τ, the spike locations remained essentially at their equilibrium locations over the $O(1)$ time interval shown in the figures. On this $O(1)$ time interval, only the amplitudes of the spikes change appreciably. This is because the dynamics of the spatial locations of the spikes evolve on a much longer time-scale of order $O(\varepsilon^{-2})$ (cf. [13]). In Fig. 1(b) we show a competition instability that occurs when $D = 0.18$ and $\tau = 0.02$. For this value of D, which exceeds the critical threshold $D_4 = 0.1658$ discussed above, there is one eigenvalue of the linearization of the four-spike equilibrium solution on the positive real axis. The corresponding unstable eigenfunction introduces a competition between the spikes. When $D = 0.15 < D_4$, in Fig. 2(a) and Fig. 2(b) we plot the spike amplitudes when $\tau = 1.3$ and $\tau = 1.2$, respectively. For this value of D, the critical value of τ where a Hopf bifurcation occurs, as discussed above, is found to be $\tau_0(D; 4) = 1.275$. In Fig. 2(a), the spike amplitudes of the resulting

5

oscillatory instability are found to synchronize, so that as t increases the spikes eventually oscillate with a common amplitude and phase. In Fig. 2(b), τ is below the critical value. In this case, the spike amplitudes exhibit a slow oscillatory decay back to their equilibrium values. Our goal is to characterize explicitly the conditions for the onset of these instabilities, and to determine the mechanism that initiates both synchronous oscillatory instabilities and competition instabilities.

(a) The equilibrium solution

(b) a_m versus t
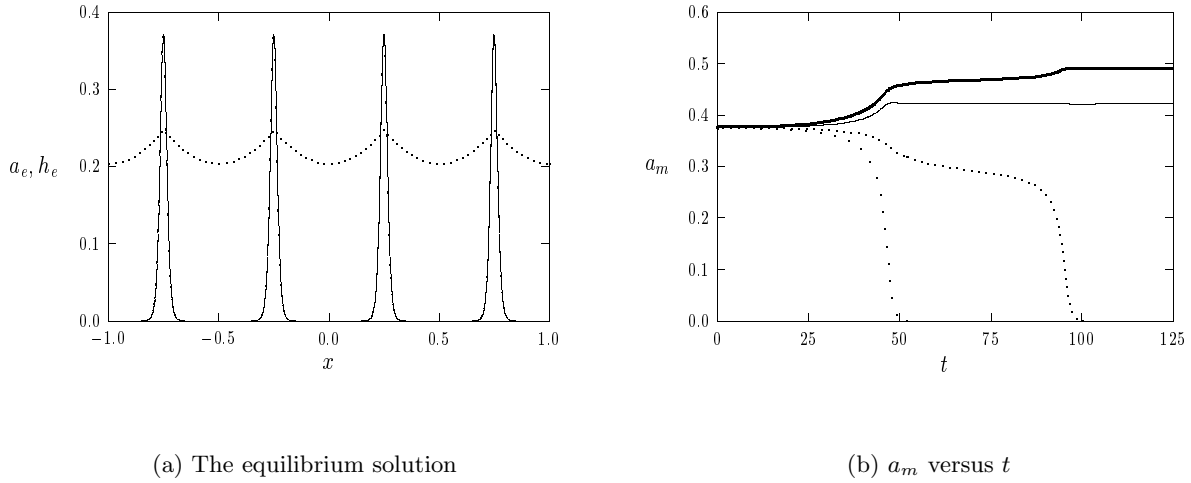
Figure 1: The parameters are $k = 4$, $(p, q, m, s) = (2, 1, 3, 0)$, $\varepsilon = 0.01$, and $D = 0.18$. Left figure: a_e (solid curve) and h_e (dashed curve). Right figure: The spike amplitudes when $\tau = 0.02$, with a_{m1} (solid curve), a_{m2} (widely space dots), a_{m3} (heavy solid curve), and a_{m4} (dashed curve).

Our study of the stability of symmetric k-spike patterns to (1.1) is related to the studies of the stability of pulse-patterns to the Gray-Scott model in [4], [6], and [7], and of spike patterns to a particular form of the GM model in [8]. As outlined in Appendix A, the form of the GM model studied in [8] corresponds precisely to taking $D = \varepsilon\tau$ in (1.1b) and replacing the finite domain in (1.1) by the infinite domain $-\infty < x < \infty$. Introducing μ by $\mu = 1/\tau$, it was shown in [8] (see page 491) that, for the exponent set $(p, q, m, s) = (2, 1, 2, 0)$, a one-spike solution undergoes a Hopf bifurcation when $\mu = 0.36$. Moreover, a complex conjugate pair of eigenvalues in the right half-plane merges onto the positive real axis when $\mu = 0.053$. As discussed in Remark 3.10 of §3, these previous results are consistent with our stability results for (1.1) when $D \ll 1$ and $\varepsilon \ll 1$.

There are three key qualitative differences between the analysis here and in [8]. Firstly, the GM model is studied on an unbounded spatial domain in [8], whereas we study (1.1) on a bounded

6
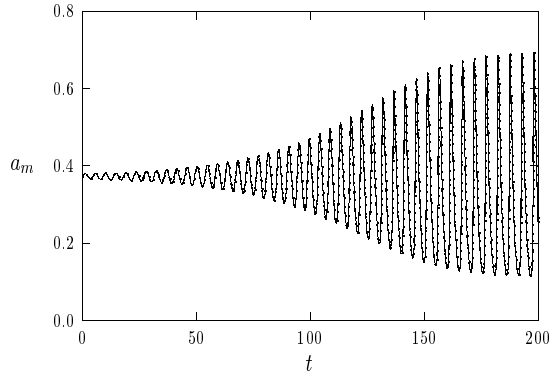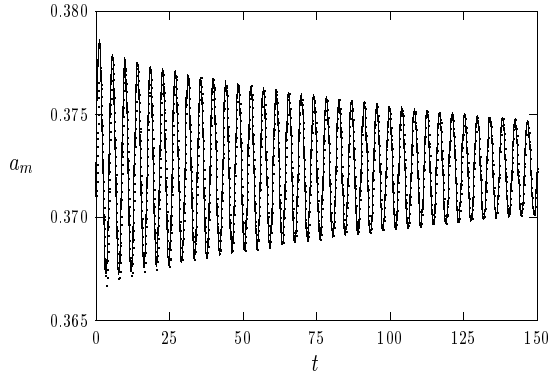
(a) a_m versus t (b) a_m versus t

Figure 2: Spike amplitudes for $k = 4$, $(p, q, m, s) = (2, 1, 3, 0)$, $D = 0.15$, and $\varepsilon = 0.01$. For the left figure $\tau = 1.3$, while for the right figure $\tau = 1.2$. In these figures the solid curve is both a_{m1} and a_{m3}, while the dashed curve is a_{m2} and a_{m4}.

domain with the Neumann boundary conditions (1.1c). This introduces an additional parameter into the analysis representing the length of the domain, or equivalently a finite $O(1)$ value of the inhibitor diffusivity D. Secondly, for the GM model of [8] on an infinite domain, a class of multi-spike equilibrium solutions corresponding to widely spaced pulses was constructed analytically. All of these solutions were found in [8] to be unstable. In contrast, in our analysis of (1.1) based on finite domain, we show that a k-spike solution with $k \geq 2$ is stable with respect to the $O(1)$ eigenvalues when $0 \leq \tau < \tau_0(D; k)$ and $0 < D < D_k$, and is unstable for any $\tau \geq 0$ when $D > D_k$. Finally, a key feature of the analysis in [8] is that the nonlocal eigenvalue problem is reduced to a transcendental equation for the eigenvalue parameter that involves certain generalized hypergeometric functions. In our study, we follow a PDE-based approach whereby we are able to give some rigorous proofs of qualitative features of the spectrum of the linearization in the unstable right half-plane, without requiring any numerical computations of special functions. Moreover, since our approach is not based on a dynamical systems framework as in [8], it should also be possible to extend our analysis to analyze spike stability in multi-dimensional spatial domains. In spite of these differences, the approach taken here and in [8] are complementary, and many of the qualitative features of the spectrum of the linearization of the GM model first discovered in [8], and found previously for the

7

Gray-Scott model in [4], [6], and [7], also hold for (1.1) on a finite domain.

There has been much recent work on the dynamics and stability of weakly interacting spikes and transition layers in reaction-diffusion systems on the infinite line (see [10] and [9] and the references therein). For this class of problems, the localized structures, representing homoclinic or heteroclinic connections for each of the chemical species, interact only via their exponential tail behavior. Moreover, because of the weak interaction, many of the spectral properties of the linearized operator for a multi-spike solution can be closely approximated by the spectral properties of the linearization around a one-spike solution. For the GM model (1.1), this type of weak interaction theory approach applies only to the case where $D = O(\varepsilon^2)$, so that both a and h are singularly perturbed. In this limit, pulse-splitting behavior is known to occur for (1.1) (see [27] and remark 6.2 of [25]). In addition, since a and h are both localized when $D \ll 1$, we may safely approximate the finite domain by an infinite domain provided that we are not examining any strong interaction properties, such as spike reflection off of a boundary. However, since we assume that $D = O(1)$ in (1.1), weak interaction theory is not relevant to our analysis of (1.1). When $D = O(1)$, the inhibitor field h does not decay to zero between neighboring spikes (see Fig. 1(a)), the finite domain plays a key role, and the spectrum of a multi-spike solution is very different from that of a one-spike solution.

The outline of this paper is as follows. In §2 we use the method of matched asymptotic expansions in the limit $\varepsilon \to 0$ to derive the nonlocal eigenvalue problem that determines the stability of a symmetric k-spike equilibrium solution to (1.1) with respect to the $O(1)$ eigenvalues of the linearization. This analysis is an extension of the work in [14] for the case $\tau = 0$. Some previous equilibrium and stability results of [14] for the case where $\tau = 0$ are summarized. In §3 the nonlocal eigenvalue problem is studied in detail for the case of a one-spike solution, and conditions for the onset of an oscillatory instability are derived. In §4, the results of §3 are compared favorably with full numerical results computed from (1.1). In addition, we also compute large-scale oscillatory motions that occur for a one-spike solution when $\tau > \tau_0$. In §5 we use many of the results in §3 to obtain the conditions for which a multi-spike solution with $k \geq 2$ is stable. The mechanism initiating synchronous oscillatory instabilities and competition instabilities are also discussed. Finally, in §6 we summarize our rigorous results for the prototypical exponent set $(2, 1, 2, 0)$, and we give a few open problems.

2 Derivation of the Nonlocal Eigenvalue Problem

In this section we summarize some previous results on spike equilibria, and on spike stability for the case where $\tau = 0$. In addition, for $\tau > 0$, we extend the analysis in [14] to derive the nonlocal eigenvalue problem associated with linearizing (1.1) around a symmetric k-spike equilibrium solution. This eigenvalue problem is central to the analysis in §3 and §5.

In [14], a k-spike equilibrium solution was constructed asymptotically in the limit $\varepsilon \to 0$ using the method of matched asymptotic expansions. The result is summarized below.

Proposition 2.1 (From [14]): *For $\varepsilon \to 0$, a symmetric k-spike equilibrium solution to (1.1), labeled by $a_e(x)$ and $h_e(x)$, is given asymptotically by*

$$a_e(x) \sim H^\gamma \sum_{n=1}^{k} w\left[\varepsilon^{-1}(x - x_n)\right] ; \qquad h_e(x) \sim \frac{H}{a_g} \sum_{n=1}^{k} G_0(x; x_n) . \tag{2.1}$$

Here $w(y)$ is the unique positive solution to

$$w'' - w + w^p = 0 , \qquad -\infty < y < \infty , \tag{2.2a}$$

$$w \to 0 \quad \text{as} \quad |y| \to \infty ; \qquad w'(0) = 0 , \quad w(0) > 0 . \tag{2.2b}$$

The Green's function $G_0(x; x_n)$ in (2.1) satisfies

$$DG_{0xx} - G_0 = -\delta(x - x_n) , \qquad -1 < x < 1 ; \qquad G_{0x}(\pm 1; x_n) = 0 . \tag{2.3}$$

The constants H, γ, and a_g in (2.1), for which $h_e(x_n) = H$ for all $n = 1, .., k$, are defined by

$$H^{\gamma m - (s+1)} \equiv \frac{1}{b_m a_g} , \qquad b_m \equiv \int_{-\infty}^{\infty} [w(y)]^m \, dy , \qquad \gamma \equiv \frac{q}{p - 1} , \tag{2.4a}$$

$$a_g \equiv \sum_{n=1}^{k} G_0(x_n; x_k) = \left[2\sqrt{D} \tanh\left(\frac{\theta_0}{k}\right)\right]^{-1} , \qquad \theta_0 \equiv D^{-1/2} . \tag{2.4b}$$

Finally, in (2.1) the spike locations satisfy

$$x_n = -1 + \frac{(2n - 1)}{k} , \qquad n = 1, .., k . \tag{2.5}$$

To determine the stability of this solution, we substitute

$$a = a_e + e^{\lambda t} \phi , \qquad h = h_e + e^{\lambda t} \eta , \tag{2.6}$$

9

into (1.1), where $\phi \ll 1$ and $\eta \ll 1$. This leads to the eigenvalue problem

$$\varepsilon^2 \phi_{xx} - \phi + \frac{pa_e^{p-1}}{h_e^q}\phi - \frac{qa_e^p}{h_e^{q+1}}\eta = \lambda\phi, \qquad -1 < x < 1, \tag{2.7a}$$

$$D\eta_{xx} - (1+\tau\lambda)\eta = -\varepsilon^{-1}\frac{ma_e^{m-1}}{h_e^s}\phi + \varepsilon^{-1}\frac{sa_e^m}{h_e^{s+1}}\eta, \qquad -1 < x < 1, \tag{2.7b}$$

$$\phi_x(\pm 1) = \eta_x(\pm 1) = 0. \tag{2.7c}$$

The spectrum of (2.7) contains two classes of eigenvalues. There are eigenvalues that are $O(1)$ as $\varepsilon \to 0$ and there are k eigenvalues that are $O(\varepsilon^2)$ as $\varepsilon \to 0$. We refer to these eigenvalues as the large and small eigenvalues, respectively.

In [14] the spectrum of (2.7) when $\tau = 0$ was analyzed in the limit $\varepsilon \to 0$. It was found that the eigenfunctions corresponding to the small eigenvalues are, asymptotically for $\varepsilon \to 0$, a linear combination of the translation modes $w'\left[\varepsilon^{-1}(x - x_n)\right]$. Moreover, the small eigenvalues can be determined in terms of the eigenvalues of a certain matrix eigenvalue problem. From an explicit calculation of the spectrum of this matrix eigenvalue problem, it was shown that, for $k \geq 2$, the small eigenvalues are real and, furthermore, are negative if and only if $D < D_k^*$, for some critical value D_k^*. Since $1 + \tau\lambda = 1 + O(\varepsilon^2)$ in (2.7b) when $\lambda = O(\varepsilon^2)$, the derivation and the leading order results for the small eigenvalues given in [14] also apply to the present case where $\tau \geq 0$ with $\tau = O(1)$. Thus, with this observation and with Proposition 11 of [14], we obtain the following stability result with respect to the small eigenvalues:

Proposition 2.2: *Assume that $0 < \varepsilon \ll 1$, $k \geq 2$, and $\tau \geq 0$ with $\tau = O(1)$. Consider the eigenvalues of (2.7) of order $\lambda = O(\varepsilon^2)$. Then, for $\varepsilon \to 0$, these eigenvalues are real and, furthermore, are negative if and only if $D < D_k^*$, where*

$$D_k^* \equiv \frac{1}{\left[k\ln(\sqrt{r} + \sqrt{r+1})\right]^2}, \qquad r \equiv \zeta^{-1}. \tag{2.8}$$

Here ζ is defined in (1.2). For the case of a one-spike solution with $k = 1$ and $\tau = 0$, it was found in [14] that the spike is stable with respect to the small eigenvalue for any $D > 0$. For the same reason as given above, a one-spike equilibrium solution is stable with respect to the small eigenvalues for any $\tau \geq 0$ with $\tau = O(1)$.

The spectrum of (2.7) is considerably more difficult to analyze for the large eigenvalues with $\lambda = O(1)$ as $\varepsilon \to 0$. We begin by deriving a nonlocal eigenvalue problem that governs the stability of a symmetric k-spike solution with respect to these eigenvalues.

10

To do so, it is convenient in (2.7) to introduce the new variables,

$$a_e = H^\gamma u \,, \qquad h_e = Hv \,, \qquad \phi = H^\gamma \bar\phi \,, \qquad \eta = H\bar\eta \,. \tag{2.9}$$

Substituting (2.9) into (2.7), and dropping the overbar notation, we obtain the eigenvalue problem

$$\varepsilon^2 \phi_{xx} - \phi + \frac{pu^{p-1}}{v^q} \phi - \frac{qu^p}{v^{q+1}} \eta = \lambda\phi \,, \qquad -1 < x < 1 \,, \tag{2.10a}$$

$$D\eta_{xx} - (1+\tau\lambda)\eta = -\varepsilon^{-1} \frac{mu^{m-1}}{b_m a_g v^s} \phi + \varepsilon^{-1} \frac{su^m}{b_m a_g v^{s+1}} \eta \,, \qquad -1 < x < 1 \,, \tag{2.10b}$$

$$\phi_x(\pm 1) = \eta_x(\pm 1) = 0 \,. \tag{2.10c}$$

In (2.10b), b_m and a_g are defined in (2.4).

As in [14], we look for a localized eigenfunction for ϕ in the form

$$\phi(x) \sim \sum_{n=1}^{k} c_n \Phi \left[\varepsilon^{-1}(x - x_n) \right] \,. \tag{2.11}$$

Since ϕ is localized near each x_n, both terms on the right-hand side of (2.10b) are multiples of Dirac masses near each $x = x_n$. Thus, for $\varepsilon \ll 1$, η satisfies

$$D\eta_{xx} - \left(1 + \tau\lambda + \frac{s}{a_g} \sum_{n=1}^{k} \delta(x - x_n) \right) \eta = -\frac{m}{b_m a_g} \left(\int_{-\infty}^{\infty} w^{m-1}\Phi \, dy \right) \sum_{n=1}^{k} c_n \delta(x - x_n) \,, \quad |x| < 1 \,, \tag{2.12a}$$

$$\eta_x(-1) = \eta_x(1) = 0 \,. \tag{2.12b}$$

This problem for η is equivalent to

$$D\eta_{xx} - (1+\tau\lambda)\, \eta = 0 \,, \qquad x_{n-1} < x < x_n \,, \quad n = 1, .., k+1 \,, \tag{2.13a}$$

$$[\eta]_n = 0 \,, \qquad n = 1, .., k \,, \tag{2.13b}$$

$$[D\eta_x]_n = -\omega_n + \frac{s}{a_g} \eta(x_n) \,, \qquad n = 1, .., k \,, \tag{2.13c}$$

$$\eta_x(-1) = \eta_x(1) = 0 \,. \tag{2.13d}$$

In (2.13), we have defined $x_0 \equiv -1$, $x_{k+1} \equiv 1$, $[v]_n \equiv v(x_{n+}) - v(x_{n-})$, and ω_n by

$$\omega_n \equiv \frac{mc_n}{b_m a_g} \int_{-\infty}^{\infty} w^{m-1}\Phi \, dy \,. \tag{2.13e}$$

11

To determine the eigenvalue problem for λ, we first need to compute $\eta(x_n)$ from (2.13). To do so, we solve (2.13a) on each subinterval and use the continuity condition (2.13b) and the jump condition (2.13c) to patch the solution across each subinterval. This calculation results in the matrix problem

$$\mathcal{B}_s \boldsymbol{\eta} = [(1 + \tau\lambda)D]^{-1/2} \boldsymbol{\omega} \,, \tag{2.14}$$

where

$$\boldsymbol{\omega} = \frac{m\boldsymbol{c}}{b_m a_g} \int_{-\infty}^{\infty} w^{m-1}\Phi \, dy \,. \tag{2.15}$$

Here we have defined

$$\boldsymbol{\eta} \equiv \begin{pmatrix} \eta(x_1) \\ \vdots \\ \eta(x_k) \end{pmatrix} \,, \qquad \boldsymbol{\omega} \equiv \begin{pmatrix} \omega_1 \\ \vdots \\ \omega_k \end{pmatrix} \,, \qquad \boldsymbol{c} \equiv \begin{pmatrix} c_1 \\ \vdots \\ c_k \end{pmatrix} \,. \tag{2.16}$$

The matrix $\mathcal{B}_s$ in (2.14) is given in terms of a tridiagonal matrix $\mathcal{B}$ by

$$\mathcal{B}_s = \mathcal{B} + \frac{s}{a_g\sqrt{(1+\tau\lambda)D}} I \,. \tag{2.17}$$

Here I is the $k \times k$ identity matrix, and B has the form

$$\mathcal{B} \equiv \begin{pmatrix} d_\lambda & f_\lambda & 0 & \cdots & 0 & 0 & 0 \\ f_\lambda & e_\lambda & f_\lambda & \cdots & 0 & 0 & 0 \\ 0 & f_\lambda & e_\lambda & \ddots & 0 & 0 & 0 \\ \vdots & \vdots & \ddots & \ddots & \ddots & \vdots & \vdots \\ 0 & 0 & 0 & \ddots & e_\lambda & f_\lambda & 0 \\ 0 & 0 & 0 & \cdots & f_\lambda & e_\lambda & f_\lambda \\ 0 & 0 & 0 & \cdots & 0 & f_\lambda & d_\lambda \end{pmatrix} \,, \tag{2.18a}$$

with matrix entries

$$d_\lambda \equiv \coth\left(\frac{2\theta_\lambda}{k}\right) + \tanh\left(\frac{\theta_\lambda}{k}\right) \,; \qquad e_\lambda \equiv 2\coth\left(\frac{2\theta_\lambda}{k}\right) \,; \qquad f_\lambda \equiv -\operatorname{csch}\left(\frac{2\theta_\lambda}{k}\right) \,. \tag{2.18b}$$

In (2.18b), θ_λ is the principal branch of the square root function defined by

$$\theta_\lambda \equiv \theta_0\sqrt{1 + \tau\lambda} \,, \qquad \theta_0 \equiv D^{-1/2} \,. \tag{2.18c}$$

12

Next, we substitute (2.14) and (2.11) into (2.10a). Since $v(x_n) = 1 + o(1)$ as $\varepsilon \to 0$, we obtain the following nonlocal problem for $\Phi(y)$, for $n = 1, .., k$:

$$c_n \left(\Phi'' - \Phi + pw^{p-1}\Phi \right) - \frac{qmw^p}{b_m a_g \sqrt{(1 + \tau\lambda)\, D}} \left(\int_{-\infty}^{\infty} w^{m-1}\Phi \, dy \right) \left(\mathcal{B}_s^{-1} c \right)_n = c_n \lambda\Phi \,, \qquad (2.19)$$

with $\Phi(y) \to 0$ as $|y| \to \infty$. Let κ and c be an eigenpair of the matrix eigenvalue problem

$$\mathcal{B}c = \kappa c \,. \qquad (2.20)$$

These eigenpairs were calculated explicitly in Proposition 2 of [14] as

$$\kappa_j = e_\lambda + 2f_\lambda \cos\left(\frac{\pi(j-1)}{k} \right) \,, \quad j = 1, .., k \,, \qquad (2.21a)$$

$$c_1^t = \frac{1}{\sqrt{k}} (1, .., 1) \,; \quad c_{l,j} = \sqrt{\frac{2}{k}} \cos\left(\frac{\pi(j-1)}{k} (l - 1/2) \right) \,, \quad j = 2, .., k \,, \qquad (2.21b)$$

with $c_j^t = (c_{1,j}, .., c_{k,j})$. Thus, from (2.17), the eigenvalues κ_s of $\mathcal{B}_s$ in (2.14) are related to κ by

$$\kappa_s = \kappa + \frac{s}{a_g \sqrt{(1 + \tau\lambda)\, D}} \,. \qquad (2.22)$$

Substituting (2.22), and $\mathcal{B}_s c = \kappa_s c$, into (2.19), we obtain the following problem for the $O(1)$ eigenvalues of (2.7):

Proposition 2.3: *Assume that $0 < \varepsilon \ll 1$ and $\tau \geq 0$. Then, with $\Phi = \Phi(y)$, the $O(1)$ eigenvalues of (2.7) satisfy the nonlocal eigenvalue problem*

$$L_0\Phi - \chi w^p \left(\frac{\int_{-\infty}^{\infty} w^{m-1}\Phi \, dy}{\int_{-\infty}^{\infty} w^m \, dy} \right) = \lambda\Phi \,, \qquad -\infty < y < \infty \,, \qquad (2.23a)$$

$$\Phi \to 0 \,, \quad as \quad |y| \to \infty \,. \qquad (2.23b)$$

Here the operator L_0, referred to as the local operator, and the multiplier χ are defined by

$$L_0\Phi \equiv \Phi'' - \Phi + pw^{p-1}\Phi \,; \qquad \chi \equiv \frac{qm}{s + a_g\kappa\sqrt{(1 + \tau\lambda)\, D}} \,, \qquad (2.24)$$

where κ, given in (2.21a), is an eigenvalue of B.

Using (2.18b), (2.4b) for a_g, and (2.21a) for κ_j, we can write the multiplier $\chi = \chi(z; j)$ in (2.24) as

$$\chi = \chi(z; j) \equiv qm \left(s + \frac{\sqrt{1+z}}{\tanh(\theta_0/k)} \left[\tanh(\theta_\lambda/k) + \frac{(1 - \cos[\pi(j-1)/k])}{\sinh(2\theta_\lambda/k)} \right] \right)^{-1} \,, \qquad (2.25a)$$

13

where

$$z \equiv \tau\lambda \,, \qquad \theta_\lambda \equiv \theta_0 \sqrt{1+z} \,, \qquad \theta_0 \equiv D^{-1/2} \,. \tag{2.25b}$$

The eigenvalue problem (2.23) is nonstandard since it is nonlocal and because the multiplier χ of the nonlocal term depends on λ. A nonlocal eigenvalue problem similar to (2.23) was studied in [4], [6], [7], [8] in regards to the stability of a one-spike solution to the Gray-Scott model and the GM model. For $\tau > 0$, the continuous spectrum for (2.23) is on the negative real axis with $\lambda < \max\left(-1, -\tau^{-1}\right)$, and is thus bounded away from the origin.

In §3 and §5 below, we require various limiting formulae for χ in different cases. When $D \ll 1$, we get to a first approximation from (2.25) that

$$\chi(z; j) \sim \frac{qm}{s + \sqrt{1+z}} \,, \qquad D \ll 1 \,. \tag{2.26}$$

Notice that, in this limit, $\chi(z; j)$ is independent of j and k. Alternatively for $D \gg 1$, we get from (2.25) that

$$\chi(z; j) \sim \begin{cases} qm \left[s + 1 + z\right]^{-1} \,, & j = 1 \,, \qquad D \gg 1 \,, \\ qm \left(\frac{Dk^2}{2} \left[1 - \cos\left(\pi(j-1)/k\right)\right]\right)^{-1} & j = 2, .., k \,, \quad D \gg 1 \,. \end{cases} \tag{2.27}$$

Next, we calculate the behavior of χ as $\tau \to \infty$. Assume that λ is real with $\lambda > 0$ and $\lambda = O(1)$ as $\tau \to \infty$. Then, from (2.25), we get

$$\chi(z; j) \sim \frac{qm}{\sqrt{z}} \tanh\left(\frac{\theta_0}{k}\right) \,, \qquad \tau \to \infty \,, \qquad \lambda = O(1) \,. \tag{2.28}$$

Thus, in this limit, $\chi = O\left(\tau^{-1/2}\right)$ as $\tau \to \infty$, independent of j.

For the case $\tau = 0$, the stability thresholds with respect to D were calculated in [14]. The following rigorous result, obtained in [32], was critical to the stability analysis of [14]:

Theorem 2.4 (From [32]): *Let $\alpha_0 > 0$ be real and L_0 be as defined in (2.24). Consider the following eigenvalue problem for $\Phi \in \mathcal{H}^1(R)$:*

$$L_0\Phi - \alpha_0(p-1)w^p \left(\frac{\int_{-\infty}^\infty w^{m-1}\Phi \, dy}{\int_{-\infty}^\infty w^m dy}\right) = \lambda\Phi \,, \qquad -\infty < y < \infty \,, \tag{2.29a}$$

$$\Phi \to 0 \quad \text{as} \quad |y| \to \infty \,, \tag{2.29b}$$

corresponding to eigenpairs for which $\lambda \neq 0$. Here w satisfies (2.2). Let $\lambda_0 \neq 0$ be the eigenvalue of (2.29) with the largest real part. Then, if $\alpha_0 < 1$, we conclude that

$$\mathrm{Re}(\lambda_0) > 0 \,. \tag{2.30}$$

14

Alternatively, if $\alpha_0 > 1$, and if either of the following two conditions hold

$$\text{(i)} \quad m = 2\,, \;\; 1 < p \le 5\,, \qquad \text{or} \qquad \text{(ii)} \quad m = p + 1\,, \;\; p > 1\,, \tag{2.31a}$$

then

$$\text{Re}(\lambda_0) < 0\,. \tag{2.31b}$$

Proof: The proof of (2.30) is given in Appendix E of [14]. The proof of (2.31) is given in Lemma A and Theorem 1.4 of [32], and is reproduced in Appendix F of [14]. ∎

For the special case $\alpha_0 = 0$, (2.29) reduces to the spectrum of the local operator L_0. This problem was first studied in [16], where the following result was obtained:

<u>Theorem 2.5</u> (From [16]): *Consider the local eigenvalue problem $L_0\phi_l = \nu\phi_l$ for $\phi_l \in \mathcal{H}^1(R)$. This problem admits the eigenvalues $\nu_0 > 0$, $\nu_1 = 0$, and $\nu_j < 0$ for $j > 1$. The eigenvalue ν_0 is simple, and the corresponding eigenfunction ϕ_{l0} has one sign.*

Notice that for any α_0 in (2.29), the translation mode $\Phi = w'$, which is an odd function, is an eigenfunction of (2.29) corresponding to the eigenvalue $\lambda = 0$. Since the eigenvalues of the local operator L_0 do not lead to oscillatory instabilities, we are only interested in the eigenvalues of (2.23) for which $\int_{-\infty}^{\infty} w^{m-1}\Phi\,dy \neq 0$.

To recover the stability results of [14] we set $\tau = 0$ in (2.25) to get $\chi(0; j)$. Let λ_0 be the eigenvalue with the largest real part of (2.23) with χ replaced by $\chi(0; j)$. Then, from the monotonicity result that $\chi(0; j-1) > \chi(0; j)$ for $j = 2, .., k$, it follows upon comparing (2.23) and (2.29) that, when condition (2.31a) is satisfied, we have $\text{Re}(\lambda_0) < 0$ for each $j = 1, .., k$ if and only if

$$\chi(0; k) > (p - 1)\,. \tag{2.32}$$

Thus, it is the smallest value of $\chi(0; j)$ for $j = 1, .., k$ that sets the stability threshold. By calculating $\chi(0; k)$, and substituting the result into (2.32), we recover proposition 7 of [14]:

Proposition 2.6 (From [14]): *Let $\tau = 0$ and $\varepsilon \ll 1$. Assume that condition (2.31a) holds. Then, the k-spike symmetric equilibrium solution of proposition 2.1 is stable with respect to the $O(1)$ eigenvalues if and only if*

$$D < D_k \equiv \mu_k^{-2}\,, \qquad k = 1, 2, ..\,, \tag{2.33a}$$

$$\mu_k \equiv \frac{k}{2}\ln\left[a_k + \sqrt{a_k^2 - 1}\right]\,, \qquad a_k \equiv 1 + \left[1 + \cos\left(\frac{\pi}{k}\right)\right]\zeta^{-1}\,. \tag{2.33b}$$

Here ζ is defined in (1.2). The critical values D_k are related to the critical values D_k^* in proposition 2.2, regarding the stability with respect to the small eigenvalues, by $D_k^* < D_k$ for $k \ge 2$.

15

From (2.33) we note that $D_1 = \infty$ when $k = 1$. Thus, when $\tau = 0$, a one-spike solution is stable with respect to the large eigenvalues for any $D > 0$, with D independent of ε. For the case where D is exponentially large as $\varepsilon \to 0$, the eigenvalue problem (2.23) must be modified slightly to incorporate the effect of the finite domain. A more refined analysis (see proposition 13 of [14]), based on this modified eigenvalue problem, has shown that when $\tau = 0$ a one-spike solution is stable when $D < D_*$, where $D_* = O\left(\varepsilon^2 e^{2/\varepsilon}\right)$ as $\varepsilon \to 0$.

The stability Theorem 2.4 easily yields the following instability result for $\tau \geq 0$:

Proposition 2.7: *Let $\tau \geq 0$, $\varepsilon \ll 1$, and $k \geq 2$. Assume that condition (2.31a) holds. Then, when D is sufficiently large, the k-spike symmetric equilibrium solution of proposition 2.1 is unstable with respect to the large eigenvalues.*

Proof: This result follows readily since from (2.27) we have $\chi(z; j) \to 0$ as $D \to \infty$ for any $j = 2, .., k$ and $\tau \geq 0$. By comparing the eigenvalue problems (2.23) and (2.29), we conclude that the eigenvalue λ_0 of (2.23) with the largest real part will satisfy $\mathrm{Re}(\lambda_0) > 0$. ∎

Finally, we reformulate (2.23) into a form more amenable to the analysis of §3 and §5. Let $\psi(y)$ be the solution to

$$L_0 \psi \equiv \psi'' - \psi + p w^{p-1} \psi = \lambda \psi + w^p; \qquad \psi \to 0 \quad \text{as} \quad |y| \to \infty. \tag{2.34}$$

Then, the eigenfunctions of (2.23) can be written as

$$\Phi = \chi(\tau\lambda; j)\psi J, \qquad J \equiv \frac{\int_{-\infty}^{\infty} w^{m-1} \Phi \, dy}{\int_{-\infty}^{\infty} w^m \, dy}. \tag{2.35}$$

We then multiply both sides of (2.35) by w^{m-1} and integrate over the domain. Assuming, as mentioned earlier that $\int_{-\infty}^{\infty} w^{m-1} \Phi \, dy \neq 0$, we then obtain a transcendental relation for the eigenvalues of (2.23) given by $g(\lambda) = 0$, where

$$g(\lambda) \equiv \frac{1}{\chi(\tau\lambda; j)} - f(\lambda), \qquad f(\lambda) \equiv \frac{\int_{-\infty}^{\infty} w^{m-1} \psi \, dy}{\int_{-\infty}^{\infty} w^m \, dy}, \qquad \psi = (L_0 - \lambda)^{-1} w^p. \tag{2.36}$$

3 The Stability of One-Spike Solutions

In this section we study the spectrum of (2.23) in detail for the case of a one-spike solution. The eigenvalues of (2.23) are the roots of $g(\lambda) = 0$ in (2.36). With this formulation we can obtain some qualitative, but rigorous, results on the spectrum of (2.23). Many of the results derived in this section are used in §5 to study the stability of multi-spike solutions. We remark that some of the

16

results in propositions 3.1 and 3.2 below were obtained previously in the analysis of [31] of spike oscillations for the shadow GM system in N-spatial dimensions.

We begin by separating (2.36) into real and imaginary parts by writing

$$g = g_R + ig_I \,, \qquad f = f_R + if_I \,, \qquad \lambda = \lambda_R + i\lambda_I \,, \qquad \psi = \psi_R + i\psi_I \,. \tag{3.1}$$

Substituting (3.1) into (2.36), and using the formula (2.25a) for χ with $j = k = 1$, we obtain

$$g_R(\lambda) = \mathrm{Re}\,[C(\lambda)] - f_R(\lambda) \,, \qquad f_R(\lambda) \equiv \frac{\int_{-\infty}^{\infty} w^{m-1}\psi_R \, dy}{\int_{-\infty}^{\infty} w^m \, dy} \,, \tag{3.2a}$$

$$g_I(\lambda) = \mathrm{Im}\,[C(\lambda)] - f_I(\lambda) \,, \qquad f_I(\lambda) \equiv \frac{\int_{-\infty}^{\infty} w^{m-1}\psi_I \, dy}{\int_{-\infty}^{\infty} w^m \, dy} \,. \tag{3.2b}$$

Here we have defined $C(\lambda)$ by

$$C(\lambda) \equiv \frac{1}{\chi(\tau\lambda; 1)} = \frac{s}{qm} + \frac{\sqrt{1+\tau\lambda}}{qm} \left[\frac{\tanh(\theta_\lambda)}{\tanh(\theta_0)} \right] \,, \qquad \theta_\lambda \equiv \theta_0\sqrt{1+\tau\lambda} \,, \quad \theta_0 = D^{-1/2} \,. \tag{3.2c}$$

In (3.2), the functions ψ_R and ψ_I, obtained from separating real and imaginary parts in (2.34), satisfy the coupled system

$$L_0\psi_R = \lambda_R\psi_R - \lambda_I\psi_I + w^p \,; \qquad L_0\psi_I = \lambda_R\psi_I + \lambda_I\psi_R \,, \tag{3.3}$$

with $\psi_R \to 0$ and $\psi_I \to 0$ as $|y| \to \infty$.

3.1 Critical Parameters for a Hopf Bifurcation

We first look for a pure imaginary eigenvalue of the form $\lambda = i\lambda_I$. Without loss of generality we may assume that $\lambda_I > 0$. Using (3.2) and (3.3), the eigenvalues of (2.23) along the positive imaginary axis $\lambda_I > 0$ are the roots of the coupled system $\tilde{g}_R = \tilde{g}_I = 0$, given by

$$\tilde{g}_R(\lambda_I) \equiv \tilde{C}_R(\lambda_I) - \tilde{f}_R(\lambda_I) \,, \qquad \tilde{g}_I(\lambda_I) \equiv \tilde{C}_I(\lambda_I) - \tilde{f}_I(\lambda_I) \,, \tag{3.4a}$$

where

$$\tilde{f}_R(\lambda_I) \equiv \frac{\int_{-\infty}^{\infty} w^{m-1} L_0 \left[L_0^2 + \lambda_I^2\right]^{-1} w^p \, dy}{\int_{-\infty}^{\infty} w^m \, dy} \,, \qquad \tilde{f}_I(\lambda_I) \equiv \frac{\lambda_I \int_{-\infty}^{\infty} w^{m-1} \left[L_0^2 + \lambda_I^2\right]^{-1} w^p \, dy}{\int_{-\infty}^{\infty} w^m \, dy} \,. \tag{3.4b}$$

Here we have defined

$$\tilde{C}_R(\lambda_I) \equiv \mathrm{Re}\,[C(i\lambda_I)] \,, \qquad \tilde{C}_I(\lambda_I) \equiv \mathrm{Im}\,[C(i\lambda_I)] \,. \tag{3.4c}$$

17

Some qualitative results on the spectrum along the imaginary axis can be obtained by first determining some analytical results on the functions $\tilde{f}_R$ and $\tilde{f}_I$. The following result holds for $\tilde{f}_R$:

Proposition 3.1: *The function $\tilde{f}_R$ in (3.4b) has the asymptotic behavior*

$$\tilde{f}_R(\lambda_I) \sim \frac{1}{p-1} - \kappa_c \lambda_I^2 + O(\lambda_I^4)\,, \quad \text{as} \quad \lambda_I \to 0\,; \qquad \tilde{f}_R(\lambda_I) = 0\left(\lambda_I^{-2}\right)\,, \quad \text{as} \quad \lambda_I \to \infty\,, \quad (3.5a)$$

where

$$\kappa_c \equiv \frac{\int_{-\infty}^{\infty} w^{m-1} L_0^{-3} w^p \, dy}{\int_{-\infty}^{\infty} w^m \, dy}\,. \tag{3.5b}$$

In the special case where $m = p+1$ and $p > 1$, we can calculate κ_c explicitly as

$$\kappa_c = \frac{(p+3)}{2(p+1)(p-1)^2}\left[\frac{1}{p-1} - \frac{1}{4}\right]\,, \quad \text{for} \quad m = p+1\,. \tag{3.5c}$$

In the special case where $m = 2$ and $p > 1$, we have,

$$\kappa_c = \frac{1}{(p-1)}\frac{\int_{-\infty}^{\infty} \left[L_0^{-1}w\right]^2 \, dy}{\int_{-\infty}^{\infty} w^2 \, dy} > 0\,. \tag{3.5d}$$

Furthermore, when $m = 2$ and $p > 1$ we have the global result that

$$\tilde{f}_R'(\lambda_I) < 0\,, \quad \text{for} \quad \lambda_I > 0\,. \tag{3.6}$$

Proof: The global result (3.6) was proved in [31]. For convenience, we reproduce the result here. The proof relies heavily on two explicit formulae for the local operator L_0 defined in (2.24). By a direct computation, we have

$$L_0^{-1} w^p = \frac{w}{p-1}\,; \qquad L_0^{-1} w = \frac{w}{p-1} + \frac{1}{2} y\, w'\,, \tag{3.7}$$

where w is defined in (2.2). Setting $m = 2$ in the expression for $\tilde{f}_R$ in (3.4b), we integrate by parts and use (3.7) for $L_0 w$, to get

$$\tilde{f}_R(\lambda_I) = (p-1)\frac{\int_{-\infty}^{\infty} w^p \left[L_0^2 + \lambda_I^2\right]^{-1} w^p \, dy}{\int_{-\infty}^{\infty} w^2 \, dy}\,. \tag{3.8}$$

Differentiating (3.8) with respect to λ_I, and integrating the resulting expression by parts, we obtain

$$\tilde{f}_R'(\lambda_I) = -2(p-1)\lambda_I \frac{\int_{-\infty}^{\infty} w^p \left[L_0^2 + \lambda_I^2\right]^{-2} w^p \, dy}{\int_{-\infty}^{\infty} w^2 \, dy} = -2(p-1)\lambda_I \frac{\int_{-\infty}^{\infty} \left(\left[L_0^2 + \lambda_I^2\right]^{-1} w^p\right)^2 \, dy}{\int_{-\infty}^{\infty} w^2 \, dy}\,. \tag{3.9}$$

18

Therefore, $\tilde{f}'_R < 0$ for $\lambda_I > 0$, which proves (3.6).

We now establish the local behavior (3.5) for $\tilde{f}_R$. The asymptotic behavior for $\tilde{f}_R$ as $\lambda_I \to \infty$ in (3.5a) is immediately clear. It remains to show the local behavior for $\tilde{f}_R$ as $\lambda_I \to 0$ given in (3.5). It is clear that all the odd derivatives of $\tilde{f}_R$ at $\lambda_I = 0$ are zero. Using (3.4b) for $\tilde{f}_R$, we calculate that

$$
\tilde{f}_R(0) = \frac{\int_{-\infty}^{\infty} w^{m-1} L_0^{-1} w^p \, dy}{\int_{-\infty}^{\infty} w^m \, dy} \,, \qquad \kappa_c = -\frac{\tilde{f}''_R(0)}{2} = \frac{\int_{-\infty}^{\infty} w^{m-1} L_0^{-3} w^p \, dy}{\int_{-\infty}^{\infty} w^m \, dy} \,. \tag{3.10}
$$

Using (3.7) for $L_0^{-1} w^p$, we obtain $\tilde{f}_R(0) = 1/(p-1)$. The formula for κ_c in (3.10) is precisely (3.5b). When $m = 2$, we can use (3.7) for $L_0^{-1} w^p$ to readily obtain (3.5d). When $m = p + 1$, we can use (3.7) for $L_0^{-1} w^p$ and $L_0^{-1} w$ to get

$$
\kappa_c \equiv \frac{1}{(p-1)} \frac{\int_{-\infty}^{\infty} w^p L_0^{-1} \left[\frac{w}{p-1} + \frac{1}{2} y w' \right] dy}{\int_{-\infty}^{\infty} w^{p+1} \, dy} \,. \tag{3.11}
$$

We then integrate by parts in (3.11) and use (3.7), to obtain

$$
\kappa_c \equiv \frac{1}{(p-1)} \frac{\int_{-\infty}^{\infty} \left(\frac{w}{p-1} + \frac{1}{2} y w' \right) L_0^{-1} w^p \, dy}{\int_{-\infty}^{\infty} w^m \, dy} = \frac{1}{(p-1)^2} \frac{\int_{-\infty}^{\infty} \left(\frac{w^2}{p-1} + \frac{1}{2} y w w' \right) dy}{\int_{-\infty}^{\infty} w^{p+1} \, dy} \,. \tag{3.12}
$$

Finally, integrating by parts in (3.12), we get

$$
k_c = \frac{1}{(p-1)^2} \left[\frac{1}{p-1} - \frac{1}{4} \right] \frac{\int_{-\infty}^{\infty} w^2 \, dy}{\int_{-\infty}^{\infty} w^{p+1} \, dy} \,. \tag{3.13}
$$

The ratio of the integrals in (3.13) was evaluated in Appendix B of [31], with the result

$$
\frac{\int_{-\infty}^{\infty} w^2 \, dy}{\int_{-\infty}^{\infty} w^{p+1} \, dy} = \frac{p+3}{2(p+1)} \,. \tag{3.14}
$$

Substituting (3.14) into (3.13), we obtain (3.5c). This completes the proof of proposition 3.1. ∎

Next, we establish some analytical results on the function $\tilde{f}_I$ in (3.4b). We summarize the result as follows:

Proposition 3.2: *The function $\tilde{f}_I$ in (3.4b) has the asymptotic behavior*

$$
\tilde{f}_I(\lambda_I) \sim \frac{\lambda_I}{p-1} \left[\frac{1}{p-1} - \frac{1}{2m} \right] + O(\lambda_I^3), \quad \text{as} \quad \lambda_I \to 0; \qquad \tilde{f}_I(\lambda_I) = 0 \left(\lambda_I^{-1} \right), \quad \text{as} \quad \lambda_I \to \infty. \tag{3.15}
$$

In the special case where either $m = p + 1$ and $p > 1$, or $m = 2$ and $1 < p \le 5$, we have the global result,

$$\tilde{f}_I(\lambda_I) > 0, \quad \text{for} \quad \lambda_I > 0. \tag{3.16}$$

Proof: We now prove this proposition. The asymptotic behavior for $\tilde{f}_I$ as $\lambda_I \to \infty$ in (3.15) is clear. To establish the local behavior (3.15) as $\lambda_I \to 0$, we use (3.4b) for $\tilde{f}_I$, and (3.7), to get

$$\tilde{f}_I'(0) = \frac{\int_{-\infty}^{\infty} w^{m-1} L_0^{-2} w^p \, dy}{\int_{-\infty}^{\infty} w^m \, dy} = \frac{1}{(p-1)} \frac{\int_{-\infty}^{\infty} w^{m-1} L_0^{-1} w \, dy}{\int_{-\infty}^{\infty} w^m \, dy} = \frac{1}{(p-1)} \frac{\int_{-\infty}^{\infty} w^{m-1} \left[\frac{w}{p-1} + \frac{1}{2} y w' \right] dy}{\int_{-\infty}^{\infty} w^m \, dy}. \tag{3.17}$$

The last integral in (3.17) is readily evaluated to obtain the local behavior (3.15).

We now prove the global result (3.16) for $m = p + 1$. Setting $m = p + 1$ in (3.4b), we write $\tilde{f}_I(\lambda_I)$ as

$$\tilde{f}_I(\lambda_I) = \lambda_I N(\lambda_I), \qquad N(\lambda_I) \equiv \frac{\int_{-\infty}^{\infty} w^p \left[L_0^2 + \lambda_I^2 \right]^{-1} w^p \, dy}{\int_{-\infty}^{\infty} w^{p+1} \, dy}. \tag{3.18}$$

We calculate

$$N'(\lambda_I) = -2\lambda_I \frac{\int_{-\infty}^{\infty} \left[\left(L_0^2 + \lambda_I^2 \right)^{-1} w^p \right]^2 dy}{\int_{-\infty}^{\infty} w^{p+1} \, dy} < 0, \qquad N(0) = \frac{1}{p-1} \left[\frac{1}{p-1} - \frac{1}{2(p+1)} \right]. \tag{3.19}$$

Thus, for $p > 1$, we have $N(0) > 0$, $N'(\lambda_I) < 0$ for $\lambda_I > 0$, and $N(\lambda_I) \to 0$ as $\lambda_I \to \infty$. Hence $N(\lambda_I) > 0$ for $\lambda_I > 0$. This establishes (3.16) when $m = p + 1$.

We now prove (3.16) for the more difficult case where $m = 2$. For the shadow GM model where $D = \infty$ this result was proved as a consequence of Theorem 2.3 of [31]. We can adapt the proof given there to our case where D is finite. Let $\tau = \tau_0$ and $\lambda_0 = i\lambda_I^0$, with $\lambda_I^0 > 0$, correspond to a root of $g(\lambda) = 0$. Then, repeating the proof as in [31], we can show for $1 < p \le 5$ that (see equation (2.29) of [31]),

$$0 < |\chi(\tau_0 \lambda_0; 1) - (p-1)|^2 \le -\text{Re} \left[\overline{\lambda_0} \chi(\tau_0 \lambda_0; 1) \right] \left(\frac{\int_{-\infty}^{\infty} w^2 \, dy}{\int_{-\infty}^{\infty} w^{p+1} \, dy} \right). \tag{3.20}$$

From the relation (3.2c) between χ and C, and using $\overline{\lambda_0} = -i\lambda_I^0$, we obtain from (3.20) that

$$0 < -\text{Re} \left[\overline{\lambda_0} \chi(\tau_0 \lambda_0; 1) \right] = \text{Re} \left[\frac{i\lambda_I^0}{C \left(i\lambda_I^0 \right)} \right] = \frac{\lambda_I^0 \tilde{C}_I(\lambda_I^0)}{|C(i\lambda_I^0)|^2}. \tag{3.21}$$

Thus, we have $\tilde{C}_I(\lambda_I^0) > 0$ and, consequently, $\tilde{f}_I(\lambda_I^0) > 0$. This proof does not require any explicit formula for λ_I^0. However, since $0 < \tilde{f}_R\left(\lambda_I^0\right) < 1/(p-1)$, $\tilde{C}_R(0) = (s+1)/(qm) < \tilde{f}_R(0)$, and $\tilde{g}_R = 0$

20

has exactly one root, we can get any value for λ_I^0 on $\lambda_I^0 > 0$, by choosing the ratio $(s+1)/(qm)$ accordingly. This gives an indirect proof that $\tilde{f}_I(\lambda_I) > 0$ when $m = 2$ and $1 < p \leq 5$, and completes the proof of proposition 3.2. $\blacksquare$

We now describe the numerical procedure used to compute the eigenvalues of (2.23) along the imaginary axis, and we give some numerical results. We first use the BVP solver COLSYS [1] to compute w satisfying (2.2). We then fix a large value of the inhibitor diffusivity D, and compute the value τ_0, λ_I^0 for which $\tilde{g}_R = \tilde{g}_I = 0$ in (3.4a). When $D = \infty$, which corresponds to the shadow GM model, a numerical value for τ_0 and for λ_I^0 were computed in [31]. Thus, we have a good initial guess for Newton's method when D is large. We then use Euler continuation and Newton's method to follow this root of $\tilde{g}_R = \tilde{g}_I = 0$ as D is decreased. At each step, ψ_R and ψ_I are computed from the coupled BVP system (3.3) with $\lambda_R = 0$ using COLSYS [1]. In this way, we obtain curves $\tau = \tau_0$ and $\lambda_I = \lambda_I^0$ as a function of D for which (2.23) has a complex conjugate pair of eigenvalues on the imaginary axis. The calculations are performed for the five different exponent sets (p, q, m, s) given in (1.3). In each case, we find numerically that τ_0 is a decreasing function of D with $\tau_0 \to \tau_0^* > 0$ as $D \to 0$, where τ_0^* is independent of D. This limiting behavior for τ_0 is a consequence of the independence of χ on D when $D \ll 1$, as seen from (2.26).

In Fig. 3(a) we plot τ_0 and λ_I^0 versus D for the exponent set $(2, 1, 2, 0)$. For this set, $\tau_0 \to 2.75$ as $D \to 0$, and $\tau_0 \to 0.771$ as $D \to \infty$. A similar plot is shown in Fig. 3(b) for the exponent set $(2, 1, 3, 0)$. For this case where $m = 3$, τ_0 is larger than in Fig. 3(a) where $m = 2$. In particular, $\tau_0 \to 5.4$ as $D \to 0$. In Fig. 4(a) and Fig. 4(b) we plot τ_0 and λ_I^0 versus D, respectively, for the other exponent sets of (1.3). These results, together with other numerical experiments we have performed, suggest that for each $D > 0$, τ_0 increases with m and decreases with p. Thus, oscillatory instabilities occur for smaller values of τ when p is larger, and are delayed as m increases. For the five exponent sets of (1.3), the small oscillation frequency λ_I^0 shows only a small variation with respect to D.

To determine the number of eigenvalues of (2.23) in the right half-plane, we calculate the winding number of $g(\lambda)$ in (3.2) over the counterclockwise contour composed of the imaginary axis $-iR \leq \text{Im}\lambda \leq iR$ and the semi-circle Γ_R, given by $|\lambda| = R > 0$, for $-\pi/2 \leq \arg\lambda \leq \pi/2$. Assuming that τ is chosen so that there are no zeros of $g(\lambda)$ on the imaginary axis, we let $R \to \infty$ and use the argument principle to determine the number of zeros of $g(\lambda)$ in the right half-plane. The function $g(\lambda)$ in (3.2) is analytic in the right half-plane, except at the simple pole $\lambda = \nu_0 > 0$, where ν_0 is the unique positive eigenvalue of the local operator L_0 (see Theorem 2.5 above). For any $\tau > 0$ and D finite, $C(\lambda) \sim b\sqrt{\lambda}$ as $|\lambda| \to \infty$ for some $b > 0$. Also, $f(\lambda) \to 0$ as $|\lambda| \to \infty$. Thus, for any $\tau > 0$,
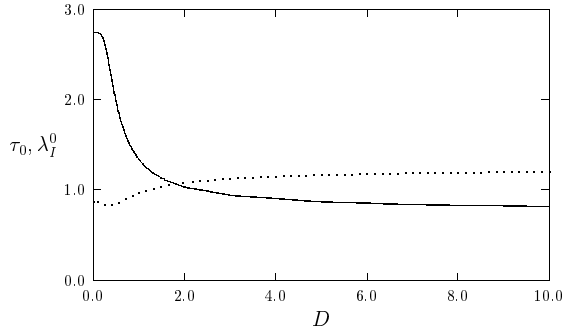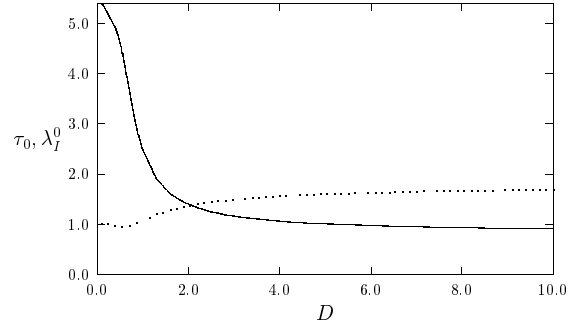
(a) $(p, q, m, s) = (2, 1, 2, 0)$ (b) $(p, q, m, s) = (2, 1, 3, 0)$

Figure 3: Plots of τ_0 (solid curve) and λ_I^0 (dashed curve) versus D for the exponent sets $(2, 1, 2, 0)$ and $(2, 1, 3, 0)$.
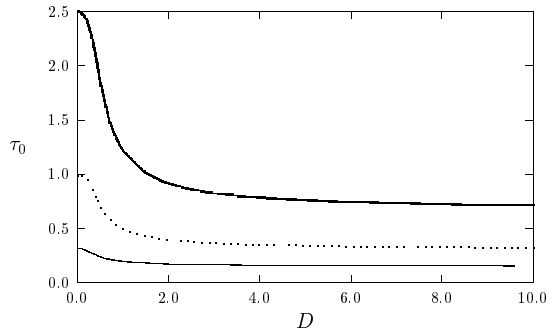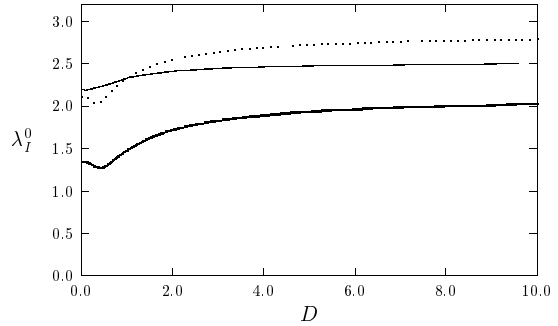
(a) τ_0 (b) λ_I^0

Figure 4: Plots of τ_0 and λ_I^0 versus D for three exponent sets. The solid curve is $(4, 2, 2, 0)$, the dashed curve is $(3, 2, 2, 0)$, and the heavy solid curve is $(3, 2, 3, 1)$.

the change in the argument of g over Γ_R as $R \to \infty$ is $\pi/2$. By using the argument principle, and $g(\overline{\lambda}) = \overline{g(\lambda)}$, we then obtain the following criterion:

Proposition 3.3: *Let $\tau > 0$ and assume that there are no zeros of $g(\lambda)$ on the imaginary axis. Then, the number of eigenvalues M of (2.23) in the right half-plane $Re(\lambda) > 0$ satisfies*

$$M = \frac{5}{4} + \frac{1}{\pi} \left[\arg g\right]_{\Gamma_I}, \qquad \tau > 0. \tag{3.22}$$

Here $\left[arg\, g\right]_{\Gamma_I}$ denotes the change in the argument of g along the semi-infinite imaginary axis $\Gamma_I = i\lambda_I$, $0 \le \lambda_I < \infty$, traversed in the downwards direction.

This criterion, together with proposition 3.1, leads to the following key result:

Proposition 3.4 *Assume that $\tau > 0$, $m = 2$, and $p > 1$. Then, for any $D > 0$, the number of eigenvalues M of (2.23) in the right half-plane is either $M = 0$ or $M = 2$. This result for M also holds whenever $\tilde{f}_R$ in (3.4b) is a monotonically decreasing function of λ_I.*

Proof: The proof of this result is simple. Define $\tilde{C}(\lambda_I) = C(i\lambda_I) = \tilde{C}_R + i\tilde{C}_I$. Then, for any $\tau > 0$, we have from (3.2c) that $\tilde{C} \sim b\sqrt{i\lambda_I}$ as $\lambda_I \to +\infty$ for some $b > 0$. Thus, since $\tilde{f}_R \to 0$ and $\tilde{f}_I \to 0$ as $\lambda_I \to +\infty$, we have $\tilde{g}_R/\tilde{g}_I \to 1$ as $\lambda_I \to +\infty$, with $\tilde{g}_R > 0$ and $\tilde{g}_I > 0$. Hence, the starting point for the argument of g on Γ_I is $\pi/4$ as $\lambda_I \to +\infty$. At $\lambda_I = 0$, we have from (3.2c) and (3.4c) that $\tilde{C}_R(0) = (s+1)/qm$ and $\tilde{C}_I(0) = 0$. The local behavior in (3.5a) and (3.15) gives $\tilde{f}_R(0) = 1/(p-1)$ and $\tilde{f}_I(0) = 0$. Hence, since $\tilde{f}_R(0) > \tilde{C}_R(0)$ holds from the condition (1.2) on the exponents, we have that $\tilde{g}_R(0) < 0$ and $\tilde{g}_I(0) = 0$. Thus, the ending point for the argument is on the negative real axis in the $\tilde{g}_R$ and $\tilde{g}_I$ plane. Next, a simple differentiation shows that $\tilde{C}_R(\lambda_I)$ is a monotonically increasing function of λ_I when $\tau > 0$ and D is finite. Hence, using the monotonicity result (3.6) on $\tilde{f}_R$ that holds for $m = 2$ and $p > 1$, the condition $\tilde{g}_R = 0$ is satisfied at only one value of λ_I for each $\tau > 0$. The sign of $\tilde{g}_I$ at this unique root of $\tilde{g}_R = 0$ determines whether the winding number is $3\pi/4$ or $-5\pi/4$. If $\tilde{g}_I > 0$ at the unique root of $\tilde{g}_R = 0$, we have $\left[\arg g\right]_{\Gamma_I} = 3\pi/4$. If $\tilde{g}_I < 0$ at this root, we get $\left[\arg g\right]_{\Gamma_I} = -5\pi/4$. Substituting this result into (3.22), we obtain proposition 3.4 for $m = 2$. ∎

The key condition in this proof is that $\tilde{g}_R = 0$ has exactly one root for each $\tau > 0$. Thus, proposition 3.4 will hold whenever $\tilde{f}_R$ in (3.4b) is a monotonically decreasing function of λ_I.

To illustrate these analytical results, in Fig. 5(a) and Fig. 5(b) we show a graphical determination of the zeros of $\tilde{g}_R$ and $\tilde{g}_I$ for the exponent set $(2,1,2,0)$ with $D = 1$. Since $m = 2$, we are guaranteed by proposition 3.1 that $\tilde{f}_R' < 0$, with $\tilde{f}_R > 0$. In Fig. 5(a) we plot $\tilde{f}_R$ together with $\tilde{C}_R$ at the critical value $\tau = \tau_0$ and $\lambda_I = \lambda_I^0$. In this figure, we have also plotted $\tilde{C}_R$ for three values of τ larger than τ_0. It is easy to show that when $\tau > 0$ and D is finite, we have $\tilde{C}_R' > 0$ for all

$\lambda_I > 0$. In addition, when D is finite and $\tau > 0$, $\tilde{C}_R$ is an increasing function of τ for each $\lambda_I > 0$. Thus, the unique root λ_I^* to $\tilde{g}_R = 0$ is a decreasing function of τ when D is finite, and it has the limiting behavior $\lambda_I^* \to 0^+$ as $\tau \to +\infty$. In Fig. 5(b), we plot $\tilde{f}_I$ and $\tilde{C}_I$ at the critical value $\tau = \tau_0$, together with $\tilde{C}_I$ at three values of $\tau > \tau_0$. Since $m = p = 2$, we have from proposition 3.2 that $\tilde{f}_I > 0$ for $\lambda_I > 0$. Again, it is easy to show that when D is finite, $\tilde{C}_I$ is an increasing function of λ_I when $\tau > 0$, and for each $\lambda_I > 0$ is an increasing function of τ. Hence, from the local behavior (3.15), it follows that at the root of $\tilde{g}_R = 0$, we have $\tilde{g}_I > 0$ when τ is sufficiently large. From the proof of proposition 3.4, we conclude that there are exactly two eigenvalues in the right half-plane when τ is sufficiently large.

(a) $\tilde{g}_R = 0$: plots of $\tilde{f}_R$ and $\tilde{C}_R$ (b) $\tilde{g}_I = 0$: plots of $\tilde{f}_I$ and $\tilde{C}_I$
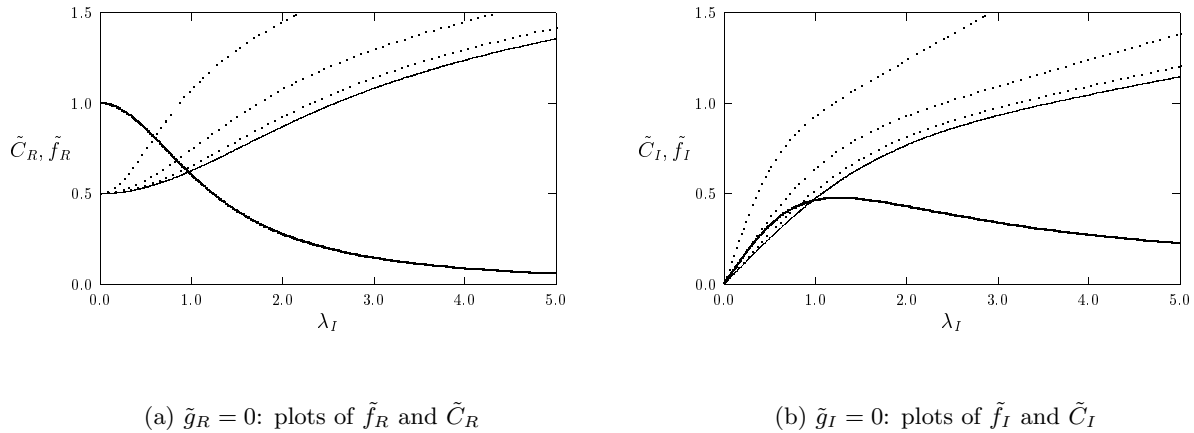
Figure 5: The roots of $\tilde{g}_R = \tilde{g}_I = 0$ shown graphically for the exponent set $(2, 1, 2, 0)$ with $D = 1$. The heavy solid curve in the left and right figures are $\tilde{f}_R$ and $\tilde{f}_I$, respectively. The solid curves are $\tilde{C}_R$ (left figure) and $\tilde{C}_I$ (right figure) at $\tau = \tau_0 = 1.343$. The top, middle, and bottom, dashed curves are $\tilde{C}_R$ (left figure) and $\tilde{C}_I$ (right figure) for $\tau = 4.0$, $\tau = 2.0$ and $\tau = 1.5$, respectively.

We have made plots similar to Fig. 5(a) and Fig. 5(b) for each of the exponent sets of (1.3). Although the monotonicity result (3.6) is proved only for $m = 2$ and $p > 1$, we have found numerically that $\tilde{f}_R' < 0$ for each exponent set of (1.3). Thus, $\tilde{g}_R = 0$ has a unique root. In addition, although $\tilde{f}_I > 0$ is proved in (3.16) only when $m = p + 1$, or when $m = 2$ and $1 < p \le 5$, we have found numerically that $\tilde{f}_I > 0$ for the exponent sets of (1.3). Thus, the results for the exponent sets of (1.3) are all qualitatively exactly the same as for the set $(2, 1, 2, 0)$. To illustrate this, in Fig. 6(a) and Fig. 6(b) we show the graphical determination of the root to $\tilde{g}_R = \tilde{g}_I = 0$ for

24

the exponent set $(2, 1, 3, 0)$ when $D = 1$. Once again, for $\tau > \tau_0$, with τ sufficiently large, there must be two eigenvalues in the right half-plane. Numerically, we used the winding number criterion (3.22) to verify that there are always two eigenvalues in the right half-plane for $\tau > \tau_0$ for each of the exponent sets in (1.3).

(a) $\tilde{g}_R = 0$: plots of $\tilde{f}_R$ and $\tilde{C}_R$ (b) $\tilde{g}_I = 0$: plots of $\tilde{f}_I$ and $\tilde{C}_I$
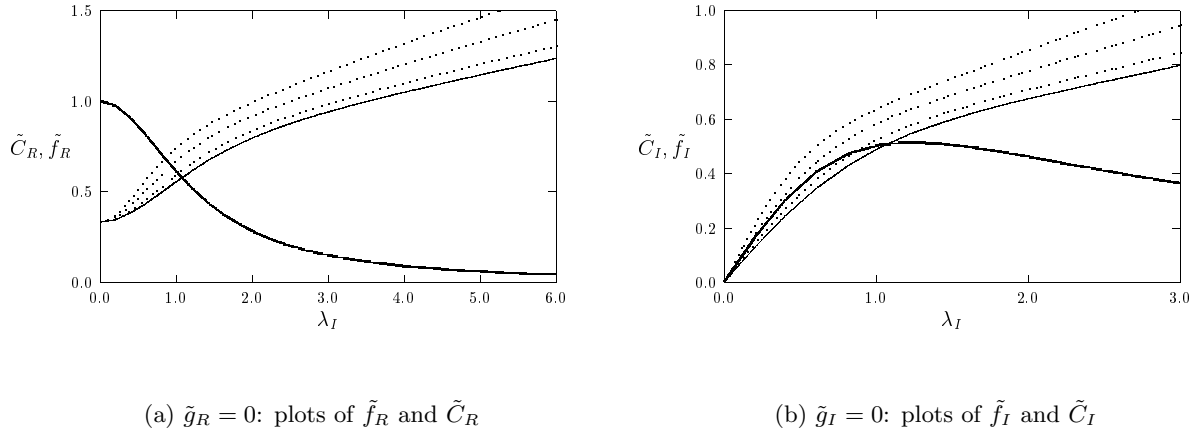
Figure 6: Same caption as in the previous figure except that here the exponent set is $(2, 1, 3, 0)$ and $D = 1$. The dashed curves are $\tilde{C}_R$ and $\tilde{C}_I$ for three values of $\tau > \tau_0 = 2.48$. The top, middle, and bottom, dashed curves are for $\tau = 4.3$, $\tau = 3.5$ and $\tau = 2.8$, respectively.

Finally, we make a few remarks. Firstly, the frequency of small oscillations, λ_I^0, is smaller for finite D than it is for the shadow GM model where $D = \infty$. This follows since $\tilde{C}_R(\lambda_I) \equiv (s + 1)/(qm)$ when $D = \infty$, and $\tilde{C}_R$ is an increasing function of both λ_I and τ when $\tau > 0$ and D is finite. Secondly, we note that the analysis is significantly more complicated for large values of p. When $p > 5$ and $m = p + 1$, the local behavior of proposition 3.1 proves that $\tilde{f}_R$ is locally increasing near $\lambda_I = 0$. The non-monotonicity of $\tilde{f}_R$ could change the winding number calculation and lead to more eigenvalues in the right half-plane. In addition, from the local behavior (3.15), we have that $\tilde{f}_I < 0$ in a neighborhood of the origin if $p > 1 + 2m$. However, $\tilde{f}_I$ tends to zero through positive values as $\lambda_I \to +\infty$. Thus, $\tilde{f}_I = 0$ at some point. This suggests that it is possible that $\tau_0 < 0$, implying that $M > 0$ when $\tau = 0$. We have not explored these different possibilities that can occur for large values of p since the previous numerical simulations have all had $p \leq 4$ (cf. [11], [12], [17], [18]).

3.2 Eigenvalues in the Right Half-Plane

Next, for a fixed value of D, we use Newton's method to track the roots of $g(\lambda) = 0$ for $\tau > \tau_0$ as they enter the right half-plane. At each step, the coupled BVP system (3.3) is solved using COLSYS [1]. This generates a path $\lambda(\tau) = \lambda_R(\tau) + i\lambda_I(\tau)$ as τ is increased past τ_0. For each of the exponent sets of (1.3), we have found numerically that this path converges monotonically, with $\lambda_R' > 0$ and $\lambda_I' < 0$, towards the positive real axis. For each exponent set of (1.3), we have found that the complex conjugate pair of eigenvalues merges onto the real axis at $\lambda_R = \lambda_R^0$, for some critical value $\tau = \tau_c(D) > \tau_0(D)$. As τ increases past $\tau_c(D)$, one eigenvalue tends to zero as $\tau \to \infty$, while the other eigenvalue tends to ν_0^- as $\tau \to \infty$. This path, and its conjugate, are plotted in Fig. 7(a) and Fig. 7(b) for the exponent sets $(2, 1, 2, 0)$ and $(3, 2, 2, 0)$ when $D = 1$. This numerical evidence supports the conjecture that there are exactly two eigenvalues in the right half-plane for any $\tau > \tau_0$. This type of path in the spectrum is qualitatively very similar to that found for the N-dimensional shadow GM problem studied in [31]. A similar spectral result was first shown to occur for the Gray-Scott model in one spatial dimension in [7]. It was also found in [8] in their analysis of (A.9) for the stability of a one-spike solution to the GM model on the infinite line.

(a) $(p, q, m, s) = (2, 1, 2, 0)$ (b) $(p, q, m, s) = (3, 2, 2, 0)$
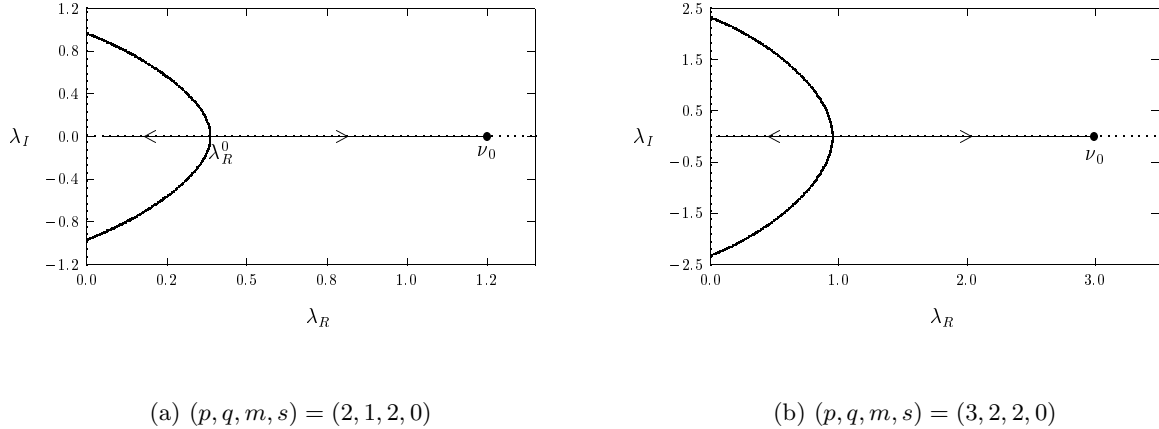
Figure 7: Plots of the path of $\lambda = \lambda_R \pm i\lambda_I$ for $D = 1$ as τ increases past $\tau_0(D)$. As τ increases, the paths converge monotonically onto the real axis at some critical value $\tau = \tau_c(D)$ with $\lambda_R = \lambda_R^0$. For $\tau > \tau_c(D)$, one eigenvalue tends to zero, and the other eigenvalue tends to the eigenvalue $\nu_0 > 0$ of the local operator L_0 as $\tau \to \infty$.

Our next goal is to prove rigorously that there exists a value $\tau = \tau_c(D)$, such that for each $\tau > \tau_c(D)$ there are exactly two eigenvalues on the real axis. To do so, we first look for eigenvalues $\lambda = \lambda_R$ on the positive real axis. From (3.2) and (3.3), they satisfy $g_R(\lambda_R) = 0$, where

$$g_R(\lambda_R) = C_R(\lambda_R) - f_R(\lambda_R)\,, \qquad f_R(\lambda_R) = \frac{\int_{-\infty}^{\infty} w^{m-1} (L_0 - \lambda_R)^{-1} w^p \, dy}{\int_{-\infty}^{\infty} w^m \, dy}\,. \tag{3.23}$$

Here $C_R(\lambda_R) \equiv C(\lambda_R)$, where $C(\lambda_R)$ is given in (3.2c). Clearly $f_R(\lambda_R) \to +\infty$ as $\lambda_R \to \nu_0^-$, where ν_0 is the principal eigenvalue of the local operator defined in (2.24). We need some analytical results on $f_R(\lambda_R)$. Our results are summarized as follows:

Proposition 3.5: *The function f_R in (3.23) has the asymptotic behavior*

$$f_R(\lambda_R) \sim \frac{1}{p-1} + \frac{\lambda_R}{p-1}\left[\frac{1}{p-1} - \frac{1}{2m}\right] + \kappa_c \lambda_R^2 + O(\lambda_R^3)\,, \quad \text{as} \quad \lambda_R \to 0\,, \tag{3.24}$$

with $f_R \to +\infty$ as $\lambda_R \to \nu_0^-$. Here κ_c is defined in (3.5b). Assume that either $m = p+1$ and $p > 1$, or $m = 2$ with $1 < p \le 5$. Then, we have the global result

$$f'_R(\lambda_R) > 0\,, \quad \text{for} \quad 0 < \lambda_R < \nu_0\,. \tag{3.25}$$

Furthermore, assume that either $m = p+1$ and $1 < p \le 5$, or $m = p = 2$. Then, we have convexity

$$f''_R(\lambda_R) > 0\,, \quad \text{for} \quad 0 < \lambda_R < \nu_0\,. \tag{3.26}$$

Finally, on the interval $\lambda_R > \nu_0$, we have

$$f_R(\lambda_R) < 0\,, \quad \text{for} \quad \lambda_R > \nu_0\,. \tag{3.27}$$

Proof: We now prove these results. To establish the local behavior (3.24) as $\lambda_R \to 0$, we use f_R in (3.23) to calculate

$$f_R(0) = \frac{\int_{-\infty}^{\infty} w^{m-1} L_0^{-1} w^p \, dy}{\int_{-\infty}^{\infty} w^m \, dy}\,, \quad f'_R(0) = \frac{\int_{-\infty}^{\infty} w^{m-1} L_0^{-2} w^p \, dy}{\int_{-\infty}^{\infty} w^m \, dy}\,, \quad f''_R(0) = \frac{2\int_{-\infty}^{\infty} w^{m-1} L_0^{-3} w^p \, dy}{\int_{-\infty}^{\infty} w^m \, dy}\,. \tag{3.28}$$

Using (3.7) for $L_0^{-1} w^p$, we get $f_R(0) = 1/(p-1)$. The integral for $f'_R(0)$ was calculated in (3.17). The integral for $f''_R(0)$ is $f_R''(0) = 2\kappa_c$, where κ_c was given in (3.5b)–(3.5d). This proves (3.24).

Next, we prove the global result (3.25) and (3.26) for the case $m = p+1$. When $m = p+1$, (3.23) for f_R becomes,

$$f_R(\lambda_R) = \frac{\int_{-\infty}^{\infty} w^p (L_0 - \lambda_R)^{-1} w^p \, dy}{\int_{-\infty}^{\infty} w^{p+1} \, dy}\,. \tag{3.29}$$

By differentiating (3.29) we obtain

$$f_R'(\lambda_R) = \frac{\int_{-\infty}^{\infty} w^p \, (L_0 - \lambda_R)^{-2} \, w^p \, dy}{\int_{-\infty}^{\infty} w^{p+1} \, dy} = \frac{\int_{-\infty}^{\infty} \left[(L_0 - \lambda_R)^{-1} \, w^p \right]^2 \, dy}{\int_{-\infty}^{\infty} w^{p+1} \, dy} > 0 \, . \tag{3.30}$$

This establishes (3.25) for $m = p+1$. To prove the convexity result, we first note that $f_R'''(\lambda_R) > 0$ on $0 \leq \lambda_R < \nu_0$. Thus, if $f_R''(0) \geq 0$, the result (3.26) follows. By differentiating (3.30), and comparing with (3.5b), we readily obtain that $f_R''(0) = 2\kappa_c$, where κ_c is given in (3.5c) when $m = p+1$. Hence,

$$f_R''(0) = \frac{(p+3)}{(p+1)(p-1)^2} \left[\frac{1}{p-1} - \frac{1}{4} \right] . \tag{3.31}$$

Thus, $f_R''(0) \geq 0$ when $1 < p \leq 5$. Therefore, by the remark above, $f_R''(\lambda_R) > 0$ on $0 < \lambda_R < \nu_0$ when $m = p + 1$ and $1 < p \leq 5$.

Next, we prove the global result (3.25) and (3.26) for the case $m = 2$. When $m = 2$, we use (3.7) to write f_R in (3.23) as

$$f_R(\lambda_R) = \frac{\int_{-\infty}^{\infty} w \, (L_0 - \lambda_R)^{-1} \, [(L_0 - \lambda_R) \, w + \lambda_R w] \, dy}{(p-1) \int_{-\infty}^{\infty} w^2 \, dy} = \frac{1}{(p-1)} + \frac{\lambda_R \int_{-\infty}^{\infty} w \, (L_0 - \lambda_R)^{-1} \, w \, dy}{(p-1) \int_{-\infty}^{\infty} w^2 \, dy} \, . \tag{3.32}$$

By differentiating (3.32) we obtain

$$f_R'(\lambda_R) = \frac{1}{(p-1)} \frac{\int_{-\infty}^{\infty} w \, (L_0 - \lambda_R)^{-1} \, w \, dy}{\int_{-\infty}^{\infty} w^2 \, dy} + \frac{\lambda_R}{(p-1)} \frac{\int_{-\infty}^{\infty} \left[(L_0 - \lambda_R)^{-1} \, w \right]^2 \, dy}{\int_{-\infty}^{\infty} w^2 \, dy} \, , \tag{3.33a}$$

and

$$f_R''(\lambda_R) = \frac{1}{(p-1)} \frac{\int_{-\infty}^{\infty} 2 \left[(L_0 - \lambda_R)^{-1} \, w \right]^2 \, dy}{\int_{-\infty}^{\infty} w^2 \, dy} + \frac{2\lambda_R}{(p-1)} \frac{\int_{-\infty}^{\infty} w \, (L_0 - \lambda_R)^{-3} \, w \, dy}{\int_{-\infty}^{\infty} w^2 \, dy} \, . \tag{3.33b}$$

To establish the sign of these terms, we need some properties for the auxiliary functions $h_1(\alpha)$ and $h_3(\alpha)$ defined by

$$h_1(\alpha) = \int_{-\infty}^{\infty} w \, (L_0 - \alpha)^{-1} \, w \, dy \, , \qquad h_3(\alpha) = \int_{-\infty}^{\infty} w \, (L_0 - \alpha)^{-3} \, w \, dy \, . \tag{3.34}$$

From (3.33a), the result $f_R'(\lambda_R) > 0$ follows if we can show that $h_1(\alpha) \geq 0$ on $0 \leq \alpha < \nu_0$. From differentiating $h_1(\alpha)$ in (3.34), it is clear that $h_1'(\alpha) > 0$. Next, we use (3.7) to calculate

$$h_1(0) = \int_{-\infty}^{\infty} w L_0^{-1} w \, dy = \int_{-\infty}^{\infty} \left(\frac{w^2}{p-1} + \frac{1}{2} y w w' \right) \, dy = \left(\frac{1}{p-1} - \frac{1}{4} \right) \int_{-\infty}^{\infty} w^2 \, dy \, . \tag{3.35}$$

28

Thus, when $1 < p \leq 5$ we have $h_1(0) \geq 0$. Since $h_1'(\alpha) > 0$, we obtain that $h_1(\alpha) > 0$ on $0 < \alpha < \nu_0$. This establishes (3.25) when $m = 2$ and $1 < p \leq 5$. From (3.33b) it is clear that a sufficient, but not necessary, condition for the convexity of f_R is that $h_3(\alpha) > 0$ for $0 < \alpha < \nu_0$. Since $h_3'(\alpha) > 0$, the result (3.26) is proved when $m = 2$ if we can show that $h_3(0) > 0$. This detailed calculation, which we give in Appendix B, shows that the determination of the sign of $h_3(0)$ can be reduced to a quadrature. From (B.4) of Appendix B, we get

$$h_3(0) = \left[\frac{1}{p-1} - \frac{1}{4}\right]\left(\frac{1}{(p-1)^2}\int_{-\infty}^{\infty} w^2\,dy - \frac{1}{2(p-1)}\int_{-\infty}^{\infty} w^2\,dy + \frac{1}{2}\int_{-\infty}^{\infty}\left(yw'\right)^2\,dy\right)$$
$$+ \frac{1}{4}\int_{-\infty}^{\infty}\left(w + yw'\right)L_0^{-1}\left(yw'\right)\,dy. \tag{3.36}$$

The function $L_0^{-1}\left(yw'\right)$ is given explicitly in (B.6) in terms of a quadrature. We cannot calculate $h_3(0)$ analytically, but (3.36) is readily evaluated numerically to give $h_3(0) = 2.7$ when $p = 2$. Thus, we have convexity of f_R when $m = 2$ and $p = 2$. However, for integer values of p with $p > 2$, we calculate $h_3(0) < 0$. Therefore, this method for proving the convexity of f_R fails when $p > 2$.

Finally, we prove the global result (3.27) for f_R on the interval $\lambda_R > \nu_0$. For this result we need the following technical lemma:

Lemma 3.6: *Let $\xi(y)$ be an even solution to*

$$(L_0 - \lambda_R)\xi = v, \qquad \text{for} \quad 0 \leq y < \infty, \tag{3.37}$$

satisfying $\xi'(0) = 0$, for which ξ decays exponentially to zero as $y \to \infty$. The function v is assumed to be even, smooth, and satisfies $v(y) > 0$ on $0 < y < \infty$, with $v \to 0$ exponentially as $y \to +\infty$. Let $\nu_0 > 0$ be the principal eigenvalue of L_0 as given in Theorem 2.5 of §2. Then, for any λ_R with $\lambda_R > \nu_0$, we have $\xi(y) \leq 0$ for $y \geq 0$.

The proof of this Lemma is given in Appendix C. By applying this result to $v = w^p$, we have $(L_0 - \lambda_R)^{-1}\,w^p \leq 0$ for $y \geq 0$ when $\lambda_R > \nu_0$. From the definition of f_R in (3.23), we then conclude $f_R(\lambda_R) \leq 0$ on $\lambda_R > \nu_0$, which proves (3.27). This completes the proof of proposition 3.5. ∎

Next, we derive a few key properties of the function $C_R(\lambda_R)$ in (3.23), given explicitly by

$$C_R(\lambda_R) = \frac{s}{qm} + \frac{\sqrt{1 + \tau\lambda_R}}{qm}\left(\frac{\tanh\theta_\lambda}{\tanh\theta_0}\right), \qquad \theta_\lambda \equiv \theta_0\sqrt{1 + \tau\lambda_R}, \qquad \theta_0 \equiv D^{-1/2}. \tag{3.38}$$

A simple calculation gives,

$$C_R'(\lambda_R) = \frac{\tau\theta_0}{2qm\tanh\theta_0}R(\xi), \tag{3.39a}$$

29

where $R(\xi)$ and ξ are defined by

$$R(\xi) \equiv \frac{\tanh \xi}{\xi} + \text{sech}^2\xi\,, \qquad \xi \equiv \theta_0 \sqrt{1 + \tau\lambda_R}\,. \tag{3.39b}$$

Since $R(\xi) > 0$ for $\xi > 0$ and $R(\xi) = O(\xi^{-1})$ as $\xi \to \infty$, it follows that $C_R' > 0$ for $\lambda_R > 0$, and $C_R' = O(\tau^{1/2})$ as $\tau \to \infty$ for any $\lambda_R > 0$. Moreover, for each value of $\tau > 0$ and $D > 0$ it follows that the function C_R is concave for $\lambda_R > 0$ if we can show that $R'(\xi) < 0$ for any $\xi > 0$. We calculate,

$$R'(\xi) = -\frac{\tanh \xi}{\xi^2} + \frac{\text{sech}^2\xi}{\xi} - 2\tanh\xi\,\text{sech}^2\xi\,. \tag{3.40}$$

This can be re-written more conveniently as

$$R'(\xi) = \frac{1}{2\xi^2 \cosh^2\xi}\left[2\xi - \sinh(2\xi)\right] - 2\tanh\xi\,\text{sech}^2\xi\,. \tag{3.41}$$

Since $z < \sinh(z)$ for $z > 0$, we have $R'(\xi) < 0$ for $\xi > 0$. From (3.39a), this proves that for any $D > 0$ and $\tau > 0$, the function $C_R(\lambda_R)$ is concave for $\lambda_R > 0$. This leads to the next proposition.

<u>Proposition 3.7</u>: *Suppose that either $m = 2$ and $p = 2$, or $m = p + 1$ and $1 < p \le 5$. Then, for any $D > 0$, there exists a value $\tau_c = \tau_c(D) > 0$, such that there are exactly two eigenvalues of (2.23) on the positive real axis for all $\tau > \tau_c$. These two roots are in the interval $0 < \lambda_R < \nu_0$. For $\tau > \tau_c$, and $m = 2$, these are the only two eigenvalues in the right half-plane. In the limit $\tau \to \infty$, one of these eigenvalues tends to zero, while the other eigenvalue tends to ν_0^-. This also proves the existence of a value $\tau_0(D) > 0$ such that there is a pair of complex conjugate eigenvalues on the imaginary axis when $\tau = \tau_0(D)$.*

    This result states that, under certain m and p, once the eigenvalues have merged onto the real axis, they remain on the real axis for all $\tau > \tau_c$.

<u>Proof:</u> We now prove this result. Firstly, any roots of $g_R(\lambda_R) = 0$ must satisfy $0 < \lambda_R < \nu_0$. This follows readily since $C_R(\lambda_R) > 0$ for $\tau > 0$ and $f_R(\lambda_R) < 0$ for $\lambda_R > \nu_0$ by (3.27) of proposition 3.5. On the interval $0 < \lambda_R < \nu_0$, and for these ranges of m and p, we have from proposition 3.5 that f_R is monotonically increasing, f_R is convex, and f_R has the limiting behavior $f_R \to +\infty$ as $\lambda_R \to \nu_0^-$. In addition, since $f_R(0) = 1/(p-1)$ and $C_R(0) = (s+1)/(qm)$, we have $f_R(0) > C_R(0)$ from condition (1.2). For $\tau = 0$, $C_R(\lambda_R) = C_R(0)$ for all $\lambda_R > 0$. Since, from (3.39a), $C_R'(\lambda_R) \to +\infty$ as $\tau \to \infty$, and C_R' is monotonic in τ, there will exist a value $\tau = \tau_c$ for which $g_R = 0$. For $\tau < \tau_c$, we have $g_R < 0$. Since f_R is convex and C_R is concave there will be exactly two roots to $g_R = 0$ for any $\tau > \tau_c$. This indirectly also proves the existence of a value $\tau_0(D)$ such that there is a pair of complex conjugate eigenvalues on the imaginary axis when $\tau = \tau_0(D)$. This follows, since by

proposition 2.6 we know that $\text{Re}(\lambda) < 0$ when $\tau = 0$ and by proposition 3.7 we know that there are two eigenvalues on the positive real axis when $\tau > \tau_c(D)$. Since $C_R(0)$ is independent of τ, eigenvalues cannot cross into the right half-plane along the real axis as τ is increased. Hence, by continuity they must have crossed into the right half-plane along the imaginary axis at some value $\tau_0(D) > 0$ (possibly non-unique). This completes the proof. $\blacksquare$

(a) $(p, q, m, s) = (2, 1, 2, 0)$ (b) $(p, q, m, s) = (3, 2, 2, 0)$
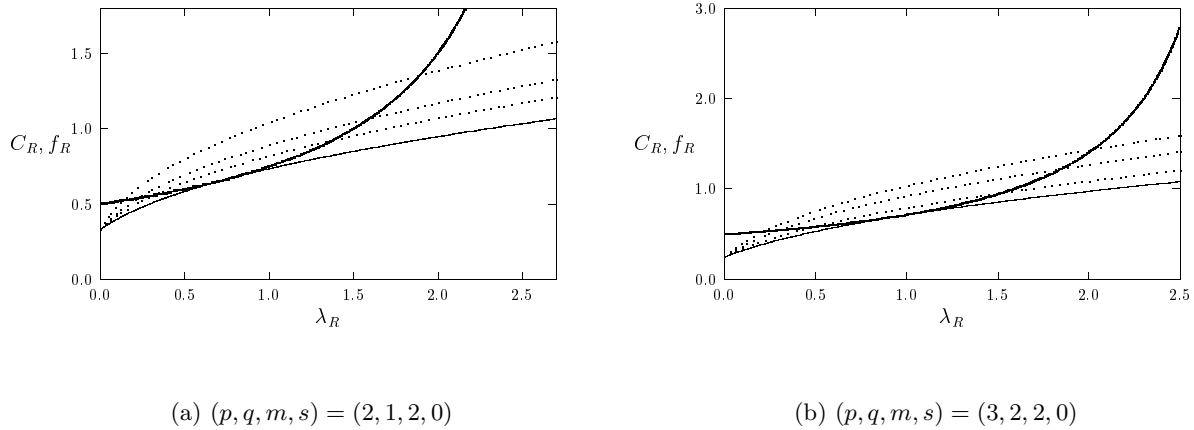
Figure 8: The roots of $g_R = 0$ are shown graphically for two exponent sets with $D = 1$. The heavy solid and solid curves are f_R and C_R, respectively, at the critical value $\tau = \tau_c$. For $(2, 1, 2, 0)$, $\tau_c = 10.25$, while for $(3, 2, 2, 0)$, $\tau_c = 3.97$, The top, middle, and bottom dashed curves in the left figure are C_R for $\tau = 30$, $\tau = 25$, and $\tau = 18$, respectively. The top, middle, and bottom dashed curves in the right figure are C_R for $\tau = 9$, $\tau = 7$, and $\tau = 5$, respectively.

In Fig. 8(a) we show graphically the determination of eigenvalues of (2.23) along the positive real axis for the exponent set $(2, 1, 2, 0)$ when $D = 1$. Since $p = m = 2$, the proposition 3.7 applies. In this figure, we plot f_R (heavy solid curve) and C_R (solid curve) versus λ_R when $\tau = \tau_c = 10.25$. The dashed curves in this figure are C_R for three values of $\tau > \tau_c$. For each $\tau > \tau_c$ there are exactly two roots to $g_R = 0$. The curve f_R is convex, while C_R is concave. For the exponent sets in (1.3), proposition 3.7 applies only to $(2, 1, 2, 0)$ and $(2, 1, 3, 0)$. Although, we do not have a proof that f_R is convex for the other exponent sets of (1.3), we have verified numerically that this is indeed the case. Thus, the determination of roots along the real axis will be qualitatively identical to that shown in Fig. 8(a). In particular, in Fig. 8(b) we plot f_R and C_R versus λ_R for the exponent set $(3, 2, 2, 0)$ when $D = 1$. For this set we find numerically that $\tau_c = 3.97$.

Next, we use Newton's method to compute the curves τ_c and λ_R^0 versus D for the exponent sets in (1.3). In Fig. 9(a) and Fig. 9(b), we plot τ_c and λ_R^0, respectively, for the exponent sets $(2,1,2,0)$ and $(2,1,3,0)$. We find that τ_c is a decreasing function of D, and that τ_c is larger when $m = 3$ than when $m = 2$. There is only a slight variation of λ_R^0 with respect to D. In Fig. 10(a) and Fig. 10(b), we plot τ_c and λ_R^0, respectively, for the other exponent sets of (1.3). In each case, we find that τ_c is a monotone decreasing function of D.

(a) τ_c versus D (b) λ_R^0 versus D
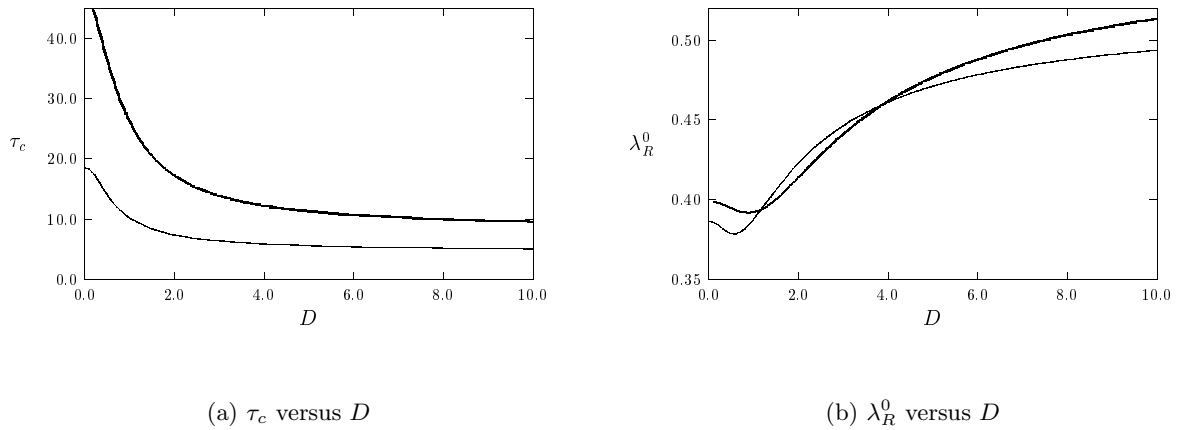
Figure 9: Plots of τ_c (left figure) and λ_R^0 (right figure) for two exponent sets when $D = 1$. The solid and heavy solid curves are for the exponent sets $(2,1,2,0)$ and $(2,1,3,0)$, respectively.

For each of the exponent sets of (1.3), we have verified numerically that there are two eigenvalues along the real axis for $\tau > \tau_c$. We now derive asymptotic formulae for these eigenvalues and their corresponding eigenfunctions in the limit $\tau \to \infty$. It is convenient here to write the eigenvalue relation (3.23) as

$$C_R(\lambda_R) = \frac{\int_{-\infty}^{\infty} w^{m-1} \psi_R \, dy}{\int_{-\infty}^{\infty} w^m \, dy} \,. \tag{3.42}$$

Here $C_R(\lambda_R)$ is given in (3.38), and ψ_R solves

$$(L_0 - \lambda_R) \, \psi_R = w^p \,. \tag{3.43}$$

As $\tau \to \infty$, one eigenvalue tends to zero and the other tends to the eigenvalue ν_0 of the local operator L_0. For this larger $O(1)$ eigenvalue, we have the following asymptotic result:

32
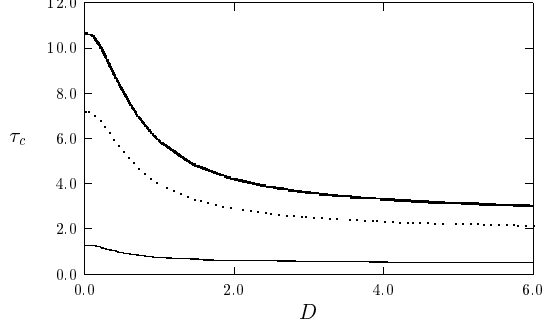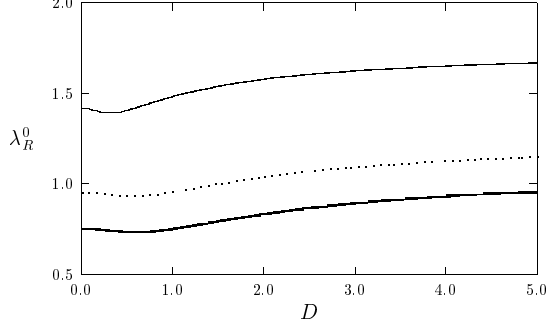
(a) τ_c versus D (b) λ_R^0 versus D

Figure 10: Plots of τ_c (left figure) and λ_R^0 (right figure) for three exponent sets when $D = 1$. The solid, dashed, and heavy solid curves are for the exponent sets $(4, 2, 2, 0)$, $(3, 2, 2, 0)$, and $(3, 2, 3, 1)$, respectively.

Proposition 3.8: *For $\tau \gg 1$, there is an eigenvalue of (2.23) with $\lambda_R = O(1)$ as $\tau \to \infty$. For $\tau \gg 1$, it has the asymptotic expansion,*

$$\lambda_R = \lambda_b \sim \nu_0 + \delta_1/\tau^{1/2} + \cdots ; \qquad \psi_R = \psi_b \sim \tau^{1/2} A_0 \phi_{l0} + O(1). \qquad (3.44)$$

The constants A_0 and δ_1 are given by,

$$A_0 = \frac{c_0 \int_{-\infty}^{\infty} w^m \, dy}{\int_{-\infty}^{\infty} w^{m-1} \phi_{l0} \, dy}, \qquad \delta_1 = -\frac{\left(\int_{-\infty}^{\infty} w^{m-1} \phi_{l0} \, dy\right)\left(\int_{-\infty}^{\infty} w^p \phi_{l0} \, dy\right)}{c_0 \int_{-\infty}^{\infty} w^m \, dy}, \qquad (3.45a)$$

where

$$c_0 = \frac{\sqrt{\nu_0}}{qm} \left(\tanh \theta_0\right)^{-1}. \qquad (3.45b)$$

Here ν_0 and ϕ_{l0} are the principal eigenpair of the local operator L_0 (see Theorem 2.5 in §2 above), with ϕ_{l0} normalized so that $\int_{-\infty}^{\infty} \phi_{l0}^2 \, dy = 1$.

Proof: To derive this result, for $\tau \gg 1$, we expand

$$\lambda_R = \lambda_b \sim \delta_0 + \delta_1/\tau^{1/2} + \cdots ; \qquad \psi_R = \psi_b \sim \tau^{1/2} \psi_{b0} + \psi_{b1} + \cdots . \qquad (3.46)$$

Substituting (3.46) into (3.43), and collecting powers of $\tau^{1/2}$, we obtain

$$L_0 \psi_{b0} - \delta_0 \psi_{b0} = 0 ; \qquad L_0 \psi_{b1} - \delta_0 \psi_{b1} = \delta_1 \psi_{b0} + w^p . \qquad (3.47)$$

33

Thus, $\delta_0 = \nu_0 > 0$ and $\psi_{b0} = A_0 \phi_{l0}$, where A_0 is an unknown constant. We normalize ϕ_{l0} by $\int_{-\infty}^{\infty} \phi_{l0}^2 \, dy = 1$. Then, the solvability condition for the equation for ψ_{b1} in (3.47) determines δ_1 as

$$\delta_1 = -A_0^{-1} \int_{-\infty}^{\infty} w^p \phi_{l0} \, dy \, . \tag{3.48}$$

To determine A_0, we substitute (3.46) into (3.42). This determines A_0 as

$$A_0 = \frac{c_0 \int_{-\infty}^{\infty} w^m \, dy}{\int_{-\infty}^{\infty} w^{m-1} \phi_{l0} \, dy} \, , \tag{3.49}$$

where c_0 is given in (3.45b). The constant c_0 is the leading coefficient in the expansion $C_R(\lambda_R) = c_0 \tau^{1/2} + O(1)$ as $\tau \to \infty$. Then, substituting (3.49) into (3.48), we determine δ_1 as in (3.45a). This completes the derivation of proposition 3.8. ∎

The asymptotic behavior of the eigenvalue that tends to zero as $\tau \to \infty$ is summarized as follows:

Proposition 3.9: *For $\tau \gg 1$, there is an eigenvalue of (2.23) with $\lambda_R = O\left(\tau^{-1}\right)$ as $\tau \to \infty$. For $\tau \gg 1$, it has the asymptotic expansion,*

$$\lambda_R = \lambda_s \sim \frac{\omega_0}{\tau} + \frac{\omega_1}{\tau^2} + \cdots ; \qquad \psi_R = \psi_s \sim \psi_{s0} + \frac{\psi_{s1}}{\tau} + \cdots . \tag{3.50}$$

The functions ψ_{s0} and ψ_{s1} are given by,

$$\psi_{s0} = \frac{w}{p-1} \, , \qquad \psi_{s1} = \frac{\omega_0}{p-1} \left[\frac{w}{p-1} + \frac{1}{2} y w' \right] \, , \tag{3.51}$$

where w satisfies (2.2). The positive constant ω_0 is the unique root of

$$\hat{C}_R(\omega_0) = \frac{1}{p-1} \, , \tag{3.52a}$$

and the constant ω_1 is

$$\omega_1 = \frac{\omega_0}{(p-1)\hat{C}_R'(\omega_0)} \left[\frac{1}{p-1} - \frac{1}{2m} \right] \, . \tag{3.52b}$$

Here the function $\hat{C}_R(\omega)$ is simply $\hat{C}_R(\omega) \equiv C_R\left(\omega/\tau\right)$.

Proof: To derive this result, we substitute (3.50) into (3.42) and (3.43). Collecting powers of τ, we obtain

$$L_0 \psi_{s0} = w^p \, , \qquad \hat{C}_R(\omega_0) = \frac{\int_{-\infty}^{\infty} w^{m-1} \psi_{s0} \, dy}{\int_{-\infty}^{\infty} w^m \, dy} \, , \tag{3.53a}$$

$$L_0 \psi_{s1} = \omega_0 \psi_{s0} \, , \qquad \omega_1 \hat{C}_R'(\omega_0) = \frac{\int_{-\infty}^{\infty} w^{m-1} \psi_{s1} \, dy}{\int_{-\infty}^{\infty} w^m \, dy} \, . \tag{3.53b}$$

Here $\hat{C}_R(\omega) \equiv C_R(\omega/\tau)$. By using (3.7), we readily obtain that the solutions ψ_{s0} and ψ_{s1} are as given in (3.51). By substituting these solutions into the integrals in (3.53), and by calculating the integrals explicitly, we obtain (3.52). Finally, we show that $\omega_0 > 0$ and is unique. Using (3.52a), and (3.38) for C_R, ω_0 can be written as the root of the transcendental equation

$$R(\omega_0) \equiv \sqrt{1 + \omega_0} \left(\frac{\tanh\left[\theta_0\sqrt{1 + \omega_0}\right]}{\tanh\theta_0} \right) - 1 = \zeta\,, \qquad \theta_0 = D^{-1/2}\,. \tag{3.54}$$

Here $\zeta > 0$ is the combination of exponents given in (1.2). Clearly $R(-1) = -1$, $R(0) = 0$, $R'(\omega) > 0$ for $\omega > -1$, with $R(\omega) \to \infty$. Hence, for any $\zeta > 0$ and D, (3.54) has a unique root ω_0, satisfying $\omega_0 > 0$. Since $\omega_0 > 0$, the small eigenvalue of (3.50) approaches the origin through positive real values as $\tau \to \infty$, but it cannot cross through the origin into the left half-plane. This completes the derivation of proposition 3.9. ■

The results in propositions 3.8 and 3.9 apply to all m and p satisfying the basic condition (1.2). In Fig. 11(a) and Fig. 11(b), we compare the asymptotic formulae, given in propositions 3.8 and 3.9, with the corresponding numerically computed values when $D = 1$. The exponent sets for Fig. 11(a) and Fig. 11(b) are $(2, 1, 2, 0)$ and $(4, 2, 2, 0)$, respectively. These plots show that the asymptotic results (3.44) and (3.50) are quite accurate, even for only moderately large values of τ.
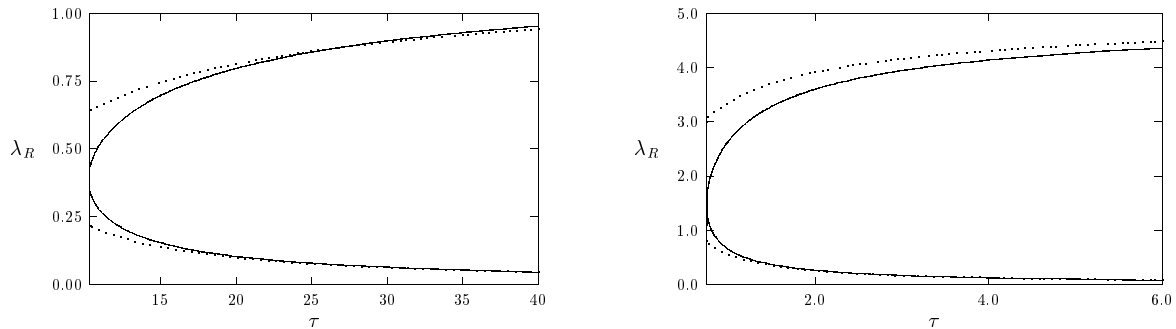
(a) $(p, q, m, s) = (2, 1, 2, 0)$ (b) $(p, q, m, s) = (4, 2, 2, 0)$

Figure 11: Plot of the eigenvalues on the real axis for two exponent sets when $D = 1$ and $\tau > \tau_c$. The solid curves are the numerical results, and the dashed curves are the asymptotic approximations of propositions 3.8 and 3.9. One eigenvalue tends to zero and the other tends to ν_0^- as $\tau \to \infty$.

35

An open problem is to prove a transversal crossing condition that ensures that whenever there is a pair of complex conjugate eigenvalues on the imaginary axis at some value $\tau = \tau_0(D)$, then they remain inside the right-half plane for $\tau > \tau_0(D)$. This condition would also imply that $\tau_0(D)$ is unique. If we write the eigenvalue path as $\lambda(\tau) = \lambda_R(\tau) + i\lambda_I(\tau)$, the transversal crossing condition is equivalent to proving that $\lambda'_R(\tau_0) > 0$ whenever $\lambda_R(\tau_0) = 0$. A simple calculation shows that $\lambda'_R(\tau_0) > 0$ for a root $\lambda = i\lambda_I^0$ on the imaginary axis if and only if

$$\text{Im}\left[\frac{dC}{dz}f'(\lambda)\right] < 0 \qquad \text{when} \quad z = i\lambda_I^0\tau_0\,, \quad \lambda = i\lambda_I^0\,. \tag{3.55}$$

Here we have written $C = C(z)$, where $z = \tau\lambda$. In [31], we were able to prove a transversal crossing condition for the N-dimensional shadow GM model, since in that case the root of $\tilde{C}_R(\lambda_I) = \tilde{f}_R(\lambda_I)$ remained fixed as τ increased. We have not been able to give a rigorous proof of the sign in (3.55).

Remark 3.10 When $D \ll 1$, the key parameter in (1.1) is τ. As discussed in Appendix A, our spectral results for a one-spike solution when $D \ll 1$ should correspond to the spectral results obtained in [8] for the GM system (A.9) of Appendix A, provided we identify $\mu = 1/\tau$ in (A.9b). For the parameter set $(p, q, m, s) = (2, 1, 2, 0)$, it was shown in [8] (see page 491) that there is a Hopf bifurcation when $\mu = 0.36$. The corresponding value of λ_I on the positive imaginary axis computed in [8] is $\lambda_I = 0.86$. From the data used to generate Fig. 3(a) with $D \ll 1$, our numerical values for the Hopf bifurcation point are $\tau = 2.75$ and $\lambda_I = 0.867$, which are consistent with those of [8]. In addition, it was shown in [8] (see page 491) that the complex conjugate pair of eigenvalues in the right half-plane merge onto the positive real axis at $\lambda_R = 0.38$ when $\mu = 0.053$. From the data used to generate Fig. 9(a) and Fig. 9(b) with $D \ll 1$, our corresponding values are $\lambda_R = 0.386$ and $\tau = 18.7$. These results are again consistent with those of [8].

4   Numerical Validation: Small and Large-Scale Oscillations

We now confirm numerically our predictions for the onset of an oscillatory instability as τ increases past τ_0. We also give numerical results for the large-scale oscillations that occur when τ is well beyond τ_0. To do so, we solve the GM model (1.1) numerically using the NAG library routine D03PCF [19] with 2000 uniformly spaced meshpoints and stringent control on the accuracy of local time-steps. The initial condition for the GM model (1.1) is taken to be

$$a(x, 0) = a_e\left[1 + 0.02\cos\left(\frac{\pi x}{\varepsilon}\right)e^{-x^2/(2\varepsilon^2)}\right]\,, \qquad h(x, 0) = h_e(x)\,, \tag{4.1}$$

where a_e and h_e are the one-spike equilibrium solutions given in proposition 2.1. The initial condition for a_e represents a 2% localized perturbation. To show the oscillatory behavior, in each

of the figures below we plot $a_m \equiv a(0, t)$, referred to as the amplitude of the spike, versus t.

In Fig. 12(a) we plot a_m versus t for two values of τ for the exponent set $(4, 2, 2, 0)$ with $D = 1$, and $\varepsilon = 0.03$. For this data, the critical value τ_0 for the onset of an oscillatory instability as predicted by the spectral analysis in §3 is $\tau_0 = 0.197$. From Fig. 12(a), we note that when $\tau = 0.19$ the oscillations generated by the initial perturbation are damped out, whereas when $\tau = 0.2$, the oscillations grow. A similar plot is shown in Fig. 12(b) for the exponent set $(3, 2, 2, 0)$ with $D = 1$, and $\varepsilon = 0.01$. For this data, we compute $\tau_0 = 0.497$. The oscillations are seen to decay when $\tau = 0.485$, and they grow when $\tau = 0.5$. We have performed many other numerical simulations for different exponent sets and for different values of D to confirm our spectral results for the onset of an oscillatory instability.

Next, we plot a_m versus t for values of τ near τ_0, and for values well beyond τ_0. In Fig. 13(a) we plot a_m versus t, showing small-scale oscillations for the exponent set $(2, 1, 2, 0)$ with $D = 1$ and $\varepsilon = 0.01$. For this data, $\tau_0 = 1.343$. From Fig. 13(a), the oscillations die out when $\tau = 1.3$ and they grow when $\tau = 1.35$. In Fig. 13(b) we increase τ to $\tau = 1.38$. For this value, we observe a very intricate large-scale motion in the spike amplitude. In Fig. 14(a), we increase τ to $\tau = 1.5$. For this value, the amplitude of the spike exhibits a few large transient oscillations, but then eventually collapses to zero. Similar spike collapse behavior occurs for this exponent set at even larger values of τ. When $\tau > \tau_c$, the eigenvalues of the linearized analysis are on the real axis. In this case, we have found that $a_m \to 0$ as $t \to \infty$ monotonically, without any oscillations. The behavior for τ near τ_0 suggests that the resulting Hopf bifurcation at $\tau = \tau_0$ is probably subcritical, since we have found numerically that the emerging small-scale oscillations are unstable. In particular, in Fig. 14(b) we plot a_m versus t for the exponent set $(3, 2, 3, 1)$ with $\tau = 1.3$, $D = 1$, and $\varepsilon = 0.02$. For this set, the critical value τ_0 is predicted to be $\tau_0 = 1.22$. For the value $\tau = 1.3$, it is shown in Fig. 14(b) that $a_m \to 0$ as $t \to \infty$.

These numerical results suggest that when τ is only slightly beyond τ_0, there can be a large-scale oscillation that persists for long time intervals, such as that shown in Fig. 13(b). However, for larger values of τ, the numerical evidence suggests that the amplitude a_m of the spike should eventually tend to zero as t increases. It is beyond our scope here to give an analysis of these large-scale oscillations. However, we now derive a heuristic criterion for the stability of the degenerate, uniform solution $a \equiv 0$ and $h \equiv 0$. What we now show is that the uniform solution is linearly stable when $\tau > \tau^* = q/(p-1)$.

Consider a one-spike time-dependent solution to the GM model (1.1), where the spike is located at $x = 0$. We construct a solution by the method of matched asymptotic expansions. In the inner region near $x = 0$, we introduce $y = \varepsilon^{-1}x$, and we expand $a = a_0(y, t) + \varepsilon a_1(y, t) + \cdots$, and
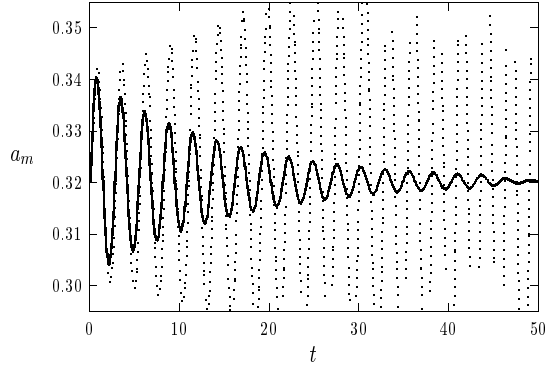
(a) $(p, q, m, s) = (4, 2, 2, 0)$ with $\varepsilon = 0.03$
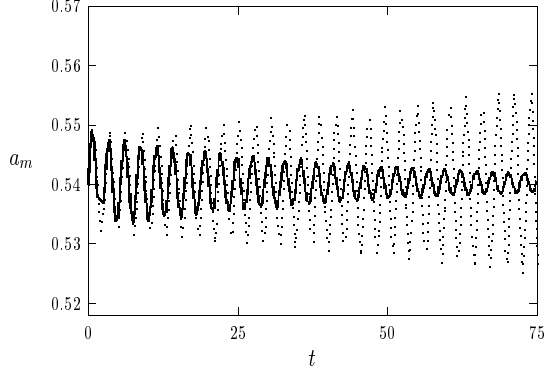
(b) $(p, q, m, s) = (3, 2, 2, 0)$ with $\varepsilon = 0.01$

Figure 12: Plots of a_m versus t for two exponent sets when $D = 1$. In the left figure, $\tau = 0.19$ (heavy solid curve), and $\tau = 0.2$ (dashed curve). In the right figure, $\tau = 0.485$ (heavy solid curve), and $\tau = 0.5$ (dashed curve). The critical values are $\tau_0 = 0.197$ (left), and $\tau_0 = 0.497$ (right).
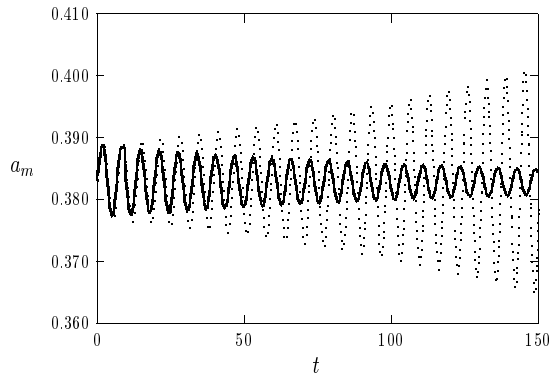
(a) $\tau = 1.3$ and $\tau = 1.35$.
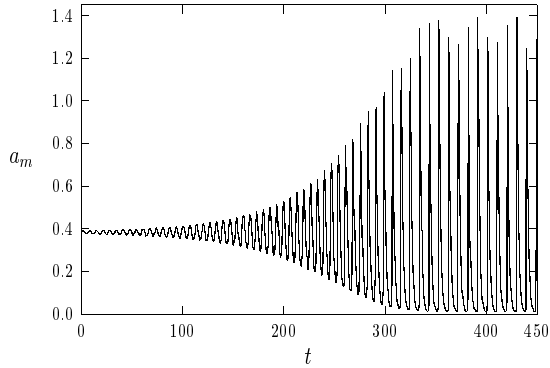
(b) $\tau = 1.38$

Figure 13: Plots of a_m versus t for several values of τ for the exponent set $(2, 1, 2, 0)$ with $\varepsilon = 0.01$ and $D = 1.0$. In the figure on the left, the heavy solid curve is for $\tau = 1.3$ and the dashed curve is for $\tau = 1.35$. In the figure on the right, $\tau = 1.38$. The critical value τ_0 is $\tau_0 = 1.343$.

38
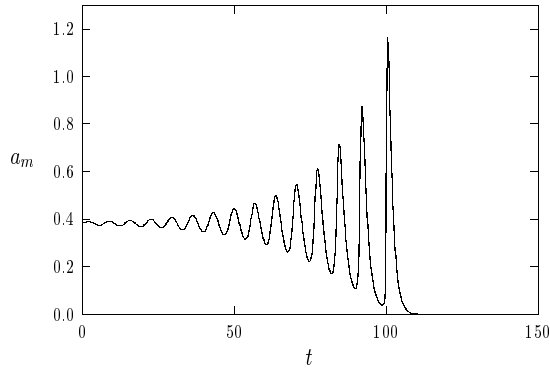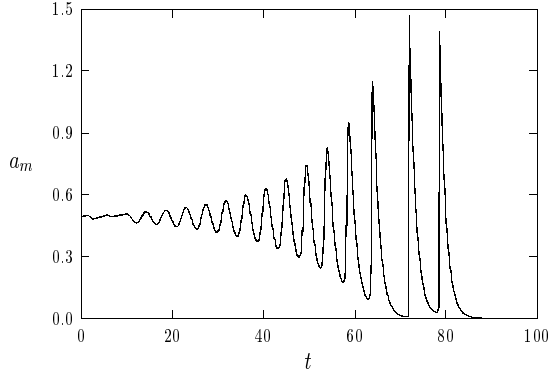
(a) $(p, q, m, s) = (2, 1, 2, 0)$ with $\tau = 1.5$ (b) $(p, q, m, s) = (3, 2, 3, 1)$ with $\tau = 1.3$

Figure 14: In the figure on the left we plot a_m versus t for the exponent set $(2, 1, 2, 0)$ with $\tau = 1.5$, $D = 1$, and $\varepsilon = 0.01$. The figure on the right corresponds to the exponent set $(3, 2, 3, 1)$ with $\tau = 1.3$, $D = 1$, and $\varepsilon = 0.02$. In both cases, $a_m \to 0$ as t increases.

$h = h_0(y, t) + \varepsilon h_1(y, t) + \cdots$. Substituting this expansion into (1.1), we obtain that $h_0 = H(t)$, and that a_0 satisfies

$$a_{0t} = a_{0yy} - a_0 + \frac{a_0^p}{H^q}, \qquad -\infty < y < \infty; \qquad a_0 \to 0 \quad \text{as} \quad |y| \to \infty. \qquad (4.2)$$

Here $H(t)$ is a function to be determined. In (4.2), we introduce the new variable v defined by $a = H^\gamma v$, where $\gamma = q/(p-1)$. From (4.2), we obtain that v satisfies

$$v_t = v_{yy} - \left(1 + \gamma \frac{H'}{H}\right) v + v^p; \qquad -\infty < y < \infty, \qquad v \to 0 \quad \text{as} \quad |y| \to \infty. \qquad (4.3a)$$

In the outer region, a is exponentially small, and $h = O(1)$. Since the term $\varepsilon^{-1} a^m / h^s$ in (1.1b) is localized near $x = 0$, we obtain from (1.1b), that for $\varepsilon \ll 1$, h satisfies

$$\tau h_t = D h_{xx} - h + H^{\zeta+1} \left(\int_{-\infty}^{\infty} [v(y, t)]^m \, dy\right) \delta(x), \qquad -1 < x < 1; \qquad h_x(\pm 1, t) = 0. \quad (4.3b)$$

Here $\zeta > 0$ is defined in (1.2), and $\delta(x)$ is the Delta function. The matching condition of the inner and outer solutions for h provides the coupling between (4.3a) and (4.3b). This condition requires

39

that

$$h(0, t) = H(t). \tag{4.3c}$$

In the v, h formulation of (4.3), we can investigate the stability of the zero solution to small localized perturbations in a. For $0 < \sigma \ll 1$, suppose that $h(x, 0) = \sigma h_0(x) > 0$ on $|x| \leq 1$, and $v(y, 0) = \sigma v_0(y) > 0$, with $v_0(y) \to 0$ exponentially as $|y| \to \infty$. Since $\zeta > 0$ in (4.3b), the linearization of (4.3) for $\sigma \ll 1$ is

$$v_t = v_{yy} - \left(1 + \gamma \frac{H'}{H}\right) v, \qquad -\infty < y < \infty; \qquad v \to 0, \quad \text{as} \quad |y| \to \infty, \tag{4.4a}$$

$$\tau h_t = D h_{xx} - h, \qquad -1 < x < 1; \qquad h_x(\pm 1, t) = 0, \tag{4.4b}$$

with $v(y, 0) = v_0(y)$, $h(x, 0) = h_0(x)$, and $h(0, t) = H(t)$. The problem (4.4a) for v is readily solved by Fourier transforms to get

$$v(y, t) = \left(\frac{U(0)}{U(t)}\right)^\gamma e^{-(1-\gamma/\tau)t} g(y, t), \qquad g(y, t) = \frac{1}{2\sqrt{\pi t}} \int_{-\infty}^{\infty} v_0(s) e^{-(y-s)^2/4t} \, ds. \tag{4.5}$$

Here $U(0) = h_0(0)$, and $U(t)$ is to be determined from

$$\tau u_t = D u_{xx}, \qquad -1 < x < 1; \qquad u_x(\pm 1, t) = 0; \qquad u(x, 0) = u_0(x); \qquad U(t) = u(0, t). \tag{4.6}$$

For $t \gg 1$, we readily calculate that

$$U(t) \sim \frac{1}{2} \int_{-1}^{1} u_0(x) \, dx + e^{-D\pi^2 t/\tau} b_0 \cos(\pi x) + \cdots, \qquad b_0 \equiv \int_{-1}^{1} u_0(x) \cos(\pi x) \, dx. \tag{4.7}$$

From (4.5), we predict that the zero solution is stable when $\tau > \tau^* \equiv \gamma$, where $\gamma = q/(p-1)$, and is unstable when $\tau < \tau^*$. As a remark, if we took an initial condition with $v(y, 0) = O(1)$ and $h(x, 0) = \sigma h_0(x)$, with $\sigma \ll 1$, then the linearization would have (4.4b) for h, and (4.3a) for v. The resulting equation for v, with the v^p term retained, is highly unstable when $v = O(1)$ since it closely approximates the nonlinear heat equation for which the linearized operator is the local operator L_0 of Theorem 2.5. Thus, v should grow exponentially with a growth rate close to ν_0, where $\nu_0 > 0$ is the principal eigenvalue of the local operator L_0 in Theorem 2.5. However, if v does increase exponentially, then the integral term in the h equation (4.3b) that is proportional to $H^{\xi+1}$ becomes significant. This term has the effect of limiting the growth in v by introducing a large positive coefficient H'/H in (4.3a). This type of self-limiting growth is presumably a very

rough outline of the mechanism of the large-scale oscillations found in the numerical simulations above.

For the exponent sets $(2, 1, 2, 0)$, $(2, 1, 3, 0)$, and $(3, 2, 3, 1)$, we have computed numerically that $\tau_0 > \tau^*$ when $D = 1$. Therefore, to test our prediction of the stability of the zero solution, we take the exponent set $(3, 2, 2, 0)$ with $D = 1$, for which $\tau^* = 1$. For this data set, $\tau_0 = 0.497$ and $\tau_c = 3.97$. Thus, if we choose $\tau > 1$, we should expect that if a_m gets close enough to the basin of attraction of the zero solution, it will approach the zero solution as t increases. Alternatively, if we take a value of τ with $0.497 < \tau < 1$ then the one-spike equilibrium solution is unstable and the zero solution is unstable. In this case, we should observe a very intricate oscillatory motion that persists over long time intervals. In Fig. 15(a) we plot $\log_{10}(1 + a_m)$ versus t for the exponent set $(3, 2, 2, 0)$ with $\tau = 1.05$, $D = 1$, and $\varepsilon = 0.02$. In Fig. 15(b) we plot $\log_{10}(1 + v_m)$ versus t, where $v_m = a_m(t)/[h(0, t)]$. This definition of v_m is motivated by the analysis leading to (4.3) above. For this value of τ, which exceeds $\tau^* = 1$, we do indeed observe that a_m and v_m tend to zero as $t \to \infty$. However, since the amplitude of a_m can become very large during the transient process, the plot has been done on a logarithmic scale. Alternatively, in Fig. 16(a) and Fig. 16(b) we plot $\log_{10}(1 + a_m)$ and $\log_{10}(1 + v_m)$ versus t for the same data, but now with $\tau = 0.65$. For this case, where both the one-spike solution and the zero solution are unstable, we do indeed observe a persistent, large-scale oscillation punctuated by sudden, and large, peaks in the amplitude a_m. Notice that, in agreement with the qualitative analysis above, v_m does become very small, but the zero solution seems unstable. The ultimate fate of this solution as $t \to \infty$ is unknown. A related type of intermittent behavior was computed numerically in [31] for the shadow GM model, under certain parameter regimes. In [24] it was shown that the Gray-Scott model can exhibit various types of chaotic pulse dynamics in certain parameter regimes when the two diffusion coefficients in the model are both asymptotically small. The irregular behavior observed above is significantly different in that it occurs for an $O(1)$ inhibitor diffusivity and an $O(\varepsilon^2)$ activator diffusivity.

5   The Stability of Multi-Spike Solutions

In this section we study the stability of multi-spike solutions. From (2.36), the eigenvalues of (2.23) are the union of the zeros of the functions $g_j(\lambda) = 0$ for $j = 1, .., k$, where

$$g_j(\lambda) \equiv C_j(\lambda) - f(\lambda), \qquad f(\lambda) \equiv \frac{\int_{-\infty}^{\infty} w^{m-1} \left(L_0 - \lambda\right)^{-1} w^p \, dy}{\int_{-\infty}^{\infty} w^m \, dy}. \tag{5.1}$$
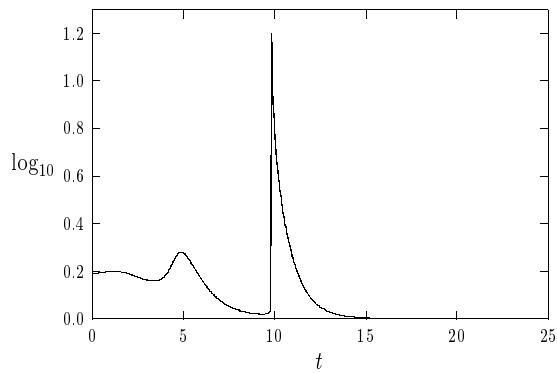
(a) $\log_{10}(1 + a_m)$ versus t
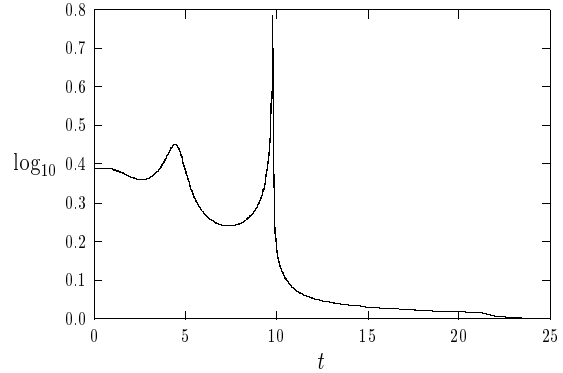
(b) $\log_{10}(1 + v_m)$ versus t

Figure 15: Plots of a_m and v_m versus t for the exponent set $(3, 2, 2, 0)$ with $\tau = 1.05$, $D = 1$, and $\varepsilon = 0.02$. Here $v_m(t) \equiv a_m(t)/h(0, t)$. Notice that there is one very large peak in a_m, but that a_m and v_m tend to zero as t increases.
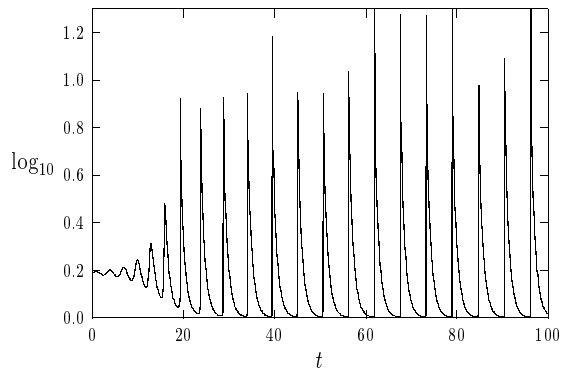
(a) $\log_{10}(1 + a_m)$ versus t
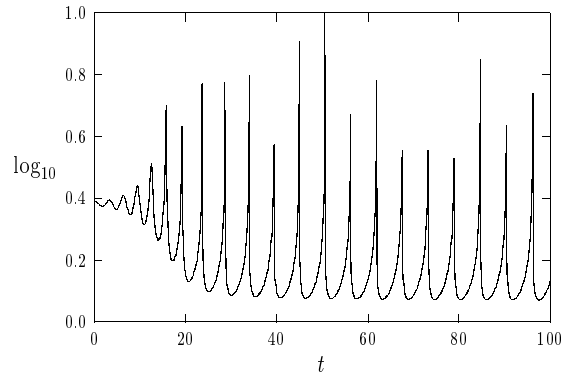
(b) $\log_{10}(1 + v_m)$ versus t

Figure 16: Plots of a_m and v_m versus t for the exponent set $(3, 2, 2, 0)$ with $\tau = 0.65$, $D = 1$, and $\varepsilon = 0.02$. The large-scale oscillation persists for long time intervals.

42

Here we have defined $C_j(\lambda) \equiv [\chi(\tau\lambda; j)]^{-1}$, where from (2.25a),

$$C_j(\lambda) = \frac{s}{qm} + \frac{\sqrt{1 + \tau\lambda}}{qm \tanh(\theta_0/k)} \left[\tanh(\theta_\lambda/k) + \frac{(1 - \cos[\pi(j-1)/k])}{\sinh(2\theta_\lambda/k)} \right], \tag{5.2}$$

with $\theta_\lambda = \theta_0\sqrt{1 + \tau\lambda}$ and $\theta_0 = D^{-1/2}$.

As we will explain below, there is one main difference between the spectrum of (2.23) for a one-spike solution and for a multi-spike solution with $k \geq 2$. In order to explain this difference precisely, we need a few properties of $C_j(\lambda_R)$, when λ_R is real with $\lambda_R \geq 0$.

Proposition 5.1: *For any fixed $\tau > 0$ and $D > 0$, we have a monotonicity result for $\lambda_R \geq 0$ that*

$$C_k(\lambda_R) > C_{k-1}(\lambda_R) > ... > C_1(\lambda_R) > 0, \qquad C_k'(\lambda_R) < C_{k-1}'(\lambda_R) < ... < C_1'(\lambda_R). \tag{5.3a}$$

For any fixed $D > 0$ and $\tau > 0$, and for each $j = 1, .., k$, we have for $\lambda_R > 0$ that

$$C_j'(\lambda_R) > 0, \qquad C_j''(\lambda_R) < 0, \qquad C_j'(\lambda_R) = O(\tau^{1/2}), \quad \text{as} \quad \tau \to +\infty. \tag{5.3b}$$

Define the functions $B_j(D) = C_j(0)$ for $j = 1, .., k$. These functions are independent of τ, and for $D > 0$ and $j = 2, .., k$, they are monotonically increasing in D. For $j = 1$, $B_1(D)$ is independent of D. We have

$$B_j'(D) > 0, \quad \text{for} \quad D > 0, \quad \text{and} \quad j = 2, .., k; \qquad B_1(D) = \frac{s+1}{qm}. \tag{5.3c}$$

Finally, for $j = 2, .., k$, we have $B_j(D) = 1/(p-1)$ when $D = \tilde{D}_j$, where

$$\tilde{D}_j \equiv \frac{4}{k^2 \left[\log\left(a_j + \sqrt{a_j^2 - 1} \right) \right]^2}, \qquad a_j \equiv 1 + \left[1 - \cos\left(\frac{\pi(j-1)}{k} \right) \right] \zeta^{-1}. \tag{5.3d}$$

Here ζ is defined in (1.2), and the relation $\tilde{D}_{j-1} > \tilde{D}_j$ holds for $j = 3, .., k$.

Proof: We now prove this result. To prove (5.3a), we use (5.2) to calculate for $j = 1, .., k-1$ that

$$C_{j+1}(\lambda_R) - C_j(\lambda_R) = \frac{2\sqrt{1 + \tau\lambda_R}}{qm \tanh(\theta_0/k)} \frac{\sin[\pi(j-1/2)/k] \sin[\pi/k]}{\sinh(2\theta_\lambda/k)} > 0. \tag{5.4}$$

This proves $C_{j+1}(\lambda_R) > C_j(\lambda_R)$ for $j = 1, .., k-1$. Clearly, $C_j(\lambda_R) > 0$ for $\lambda_R > 0$. By differentiating (5.4), we obtain for $j = 1, .., k-1$ that

$$C_{j+1}'(\lambda_R) - C_j'(\lambda_R) = \frac{\sin[\pi(j-1/2)/k] \sin[\pi/k]}{qm \tanh(\theta_0/k)} \left(\frac{2\theta_0\tau}{k\xi} \right) \frac{(\tanh\xi - \xi)}{\sinh^2\xi \cosh\xi}, \tag{5.5}$$

43

where $\xi \equiv 2\theta_\lambda/k$. Since $\tanh \xi < \xi$ for $\xi > 0$, we have $C'_{j+1}(\lambda_R) < C'_j(\lambda_R)$ for $j = 1, .., k-1$, which proves (5.3a).

Next, we prove (5.3b). Here it is convenient to define $\xi \equiv \theta_\lambda/k \geq 0$. We then differentiate $C_j(\lambda_R)$ in (5.2), and rearrange the resulting equation, to obtain

$$C'_j(\lambda_R) = \frac{\tau \theta_0}{2kqm \tanh (\theta_0/k)} R_j(\xi) \,. \tag{5.6}$$

Here $R_j(\xi)$ is defined by

$$R_j(\xi) \equiv \frac{1}{2\xi \cosh^2 \xi} \left[\sinh(2\xi) + 2(1 - \gamma_j)\xi\right] + \frac{\gamma_j}{\xi \sinh^2(2\xi)} \left[\sinh(2\xi) - 2\xi\right] \,, \tag{5.7a}$$

$$\gamma_j \equiv 1 - \cos\left[\pi(j-1)k\right] \,, \qquad j = 1, .., k \,. \tag{5.7b}$$

Since $0 \leq \gamma_j < 2$ for $j = 1, .., k$, it follows that $R_j(\xi) > 0$ for $\xi > 0$, since both terms in the square brackets in (5.7a) are positive when $\xi > 0$. Therefore, $C'_j(\lambda_R) > 0$ for $\lambda_R > 0$ and $j = 1, .., k$. To prove that $C_j(\lambda_R)$ is concave, we must show that $R'_j(\xi) < 0$ when $\xi > 0$ for $j = 1, .., k$. The proof of this is straightforward, but lengthy, and we leave the details to the reader. For $\tau \to \infty$, we have $\xi \to \infty$ and $R_j(\xi) = O(1/\xi)$. Therefore, for any $\xi > 0$ we have $R_j(\xi) = O(\tau^{-1/2})$ as $\tau \to \infty$. From (5.6), we conclude that $C'_j(\lambda_R) = O(\tau^{1/2})$ as $\tau \to \infty$ for any $\lambda_R > 0$. This proves (5.3b).

Next, we prove (5.3c). Defining $B_j(D) \equiv C_j(0)$, we calculate from (5.2) that

$$B_j(D) = \frac{(s+1)}{qm} + \frac{\gamma_j}{2qm \sinh^2(\theta_0/k)} \,, \qquad \theta_0 = D^{-1/2} \,. \tag{5.8}$$

Here γ_j is defined in (5.7b). For $j = 1$, we have $\gamma_1 = 0$, and $B_1(D) = (s+1)/qm < 1/(p-1)$. By differentiating (5.8), we get $B'_j(D) > 0$ for $j = 2, .., k$. This proves (5.3c). Finally, by setting $B_j(D) = 1/(p-1)$ for $j = 2, .., k$, and using (5.8), we obtain after a little algebra that $D = \tilde{D}_j$, where $\tilde{D}_j$ is given in (5.3d). A simple calculation shows that $\tilde{D}_{j-1} > \tilde{D}_j$ for $j = 3, .., k$. This completes the proof. ∎

We now use these properties of $C_j(\lambda_R)$ to determine the spectrum of (2.23) on the positive real axis. When $\lambda = \lambda_R$, we have from (5.1) that the eigenvalues of (2.23) are the union of the roots of $C_j(\lambda_R) = f_R(\lambda_R)$, for $j = 1, .., k$, where $f_R(\lambda_R) \equiv f(\lambda_R)$. The properties of $f_R(\lambda_R)$ were given previously in proposition 3.5. This leads to the proposition.

Proposition 5.2: *Let $k \geq 2$, and suppose that either $m = p + 1$ and $p > 1$, or $m = p = 2$. Then, when $D > \tilde{D}_2$, and for any $\tau \geq 0$, the number of eigenvalues M of (2.23) on the positive real axis satisfies*

$$k - 1 \leq M \leq k + 1 \,. \tag{5.9}$$

44

These eigenvalues are all located in the interval $0 < \lambda_R < \nu_0$, where ν_0 is the principal eigenvalue of the local operator L_0 in Theorem 2.5. Moreover, suppose that $0 < D < D_k$, where D_k is given in (2.33) of proposition 2.6, and $\tau > 0$ is sufficiently large. Then, there are exactly $2k$ eigenvalues on the positive real axis.

<u>Proof:</u> We now prove this result. Suppose that $D > \tilde{D}_2$. Then, by (5.3a) and (5.3c), we have that $C_j(0) > 1/(p-1)$ for $j = 2, .., k$. Moreover, $C_j(\lambda_R)$ is increasing and concave from (5.3b). By proposition 3.5, $f_R(0) = 1/(p-1)$ and f_R is increasing and convex on the interval $0 < \lambda_R < \nu_0$ when either $m = p + 1$ and $p > 1$, or $m = p = 2$. The function f_R tends to $+\infty$ as $\lambda_R \to \nu_0^-$, and by (3.27), we have $f_R < 0$ for $\lambda_R > \nu_0$. Thus, for each $j = 2, .., k$, there is exactly one root to $g_j(\lambda_R) = 0$ for any $\tau > 0$ on the interval $0 < \lambda_R < \nu_0$. Therefore, we have at least $k - 1$ eigenvalues on the real axis when $D > \tilde{D}_2$. For $j = 1$, $C_1(0) < f_R(0)$, and hence for τ sufficiently small there will be no roots to $g_1(\lambda_R) = 0$. The concavity of C_1 and the convexity of f_R, together with the fact that $C_1' \to \infty$ as $\tau \to \infty$, proves that there will be exactly two roots to $g_1(\lambda_R) = 0$ when τ is sufficiently large. Thus, the total number of roots on the real axis is at most $k + 1$. Next, we prove the second conclusion of this proposition. By comparing (5.3d) for $\tilde{D}_j$ and (2.33) for D_k, we have that $D_k = \tilde{D}_k$. When $D < D_k$, we are guaranteed from proposition 5.1 that $C_j(0) < 1/(p-1)$ for $j = 1, .., k$. The curves C_j are concave for $j = 1, .., k$, f_R is convex, and $C_j = O(\tau^{1/2})$ as $\tau \to \infty$, uniformly in λ_R. Hence, for τ sufficiently large, each of the curves $C_j(\lambda_R)$ will intersect $f_R(\lambda_R)$ exactly twice, yielding exactly $2k$ roots on the positive real axis. This completes the proof of proposition 5.2. ∎

As a remark, in the limit $\tau \to \infty$, we can readily extend propositions 3.8 and 3.9 to determine the explicit asymptotic behavior of each pair of roots of $g_j = 0$ for $j = 1, .., k$. We leave the details to the reader.

When $D = \infty$ and $\tau = 0$, it is well known that a multi-spike solution with $k \geq 2$ is unstable for the shadow GM model as a result of having $k - 1$ eigenvalues of the linearization on the positive real axis (cf. [32]). Proposition 5.2 proves that a multi-spike solution to the full GM model (1.1) for any $\tau > 0$ has a very similar type of instability as for the shadow GM model with $\tau = 0$ until D is decreased to the value $\tilde{D}_2$. For the exponent set $(2, 1, 2, 0)$ we calculate from (5.3d) that $\tilde{D}_2 = 0.5766$ when $k = 2$, $\tilde{D}_2 = 0.4798$ when $k = 3$, and $\tilde{D}_2 = 0.4470$ when $k = 4$. Since these values are numerically rather small, it is clear that the shadow GM model instability result holds for a wide range of D.

We now use the numerical method of §3 to graphically illustrate the conclusions of propositions 5.2 for a three-spike solution to (1.1) for the exponent set $(2, 1, 2, 0)$. In Fig. 17(a) we take $D =$

45

$0.52 > \tilde{D}_2 = 0.4798$. For the value $\tau = 2.0$ chosen in Fig. 17(a), there are exactly two eigenvalues of (2.23) on the positive real axis. In Fig. 17(b) we we take take the values $\tau = 12.5$ and $D = 0.134 < D_3 = 0.181$. For this value of τ, each of the curves $C_j(\lambda_R)$, for $j = 1, 2, 3$, intersects $f_R(\lambda_R)$ exactly twice. Thus, we have six positive real eigenvalues. As a remark, for each of the exponent sets of (1.3) we verified numerically in §3 that $f_R(\lambda_R)$ is monotone increasing and convex. Thus, although we are unable to give a rigorous proof, the results of proposition 5.2 should hold for all of the exponent sets of (1.3).

(a) $D > \tilde{D}_2$ (b) $D < D_k$
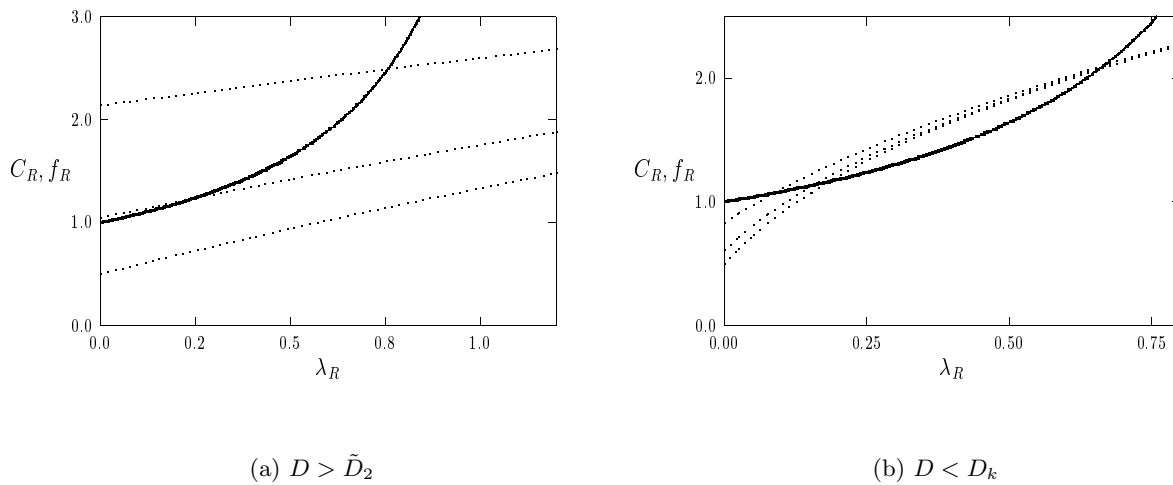
Figure 17: Plots of $f_R(\lambda_R)$ (heavy solid curve) and $C_j(\lambda_R)$ (dashed curves) for $j = 1$ (bottom curve), $j = 2$ (middle curve), and $j = 3$ (top curve), for a three-spike solution for the exponent set $(2, 1, 2, 0)$. In the left figure $\tau = 2.0$ and $D = 0.52 > \tilde{D}_2$, so that proposition 5.2 guarantees at least two roots. In the right figure $D = 0.13 < D_3 = 0.181$ and $\tau = 12.5$. In this case there are six roots.

The main difference between the spectrum of (2.23) for one-spike and multi-spike solutions is that for a multi-spike solution eigenvalues can cross through the origin along the real axis $\mathrm{Im}(\lambda) = 0$ as D is varied. Since $C_j(0)$ is independent of τ, the eigenvalues of (2.23) can never cross through the origin along the real axis for any fixed D as τ is increased. Thus, instabilities as τ is increased can only occur from Hopf bifurcations, whereas instabilities that occur as D is increased can occur from real eigenvalues entering the right half-plane. As D is increased, eigenvalues can cross between the left and right half-planes in either direction. To see this, suppose that $\tau > 0$ is sufficiently small and $D < D_k$. Then, $g_k(\lambda_R) < 0$ for $\lambda_R > 0$. Keeping the value of τ fixed, we then increase D

slightly past the value D_k. When $D > D_k$ there is a root of $g_k(\lambda_R) = 0$ in $\lambda_R > 0$, and hence an eigenvalue of (2.23) has crossed through the origin into the positive real axis. Next, suppose that $D < D_k$, but that τ is sufficiently large so that $g_k(\lambda_R) = 0$ has exactly two roots in $0 < \lambda_R < \nu_0$. For this value of τ, as D is increased past D_k one of these roots crosses from the right to the left half-plane, since when $D > D_k$ there is exactly one root to $g_k(\lambda_R) = 0$ in $0 < \lambda_R < \nu_0$.

We now determine eigenvalues on the imaginary axis. Setting $\lambda = i\lambda_I$ in (5.1) and defining $g_j(i\lambda_I) = \tilde{g}_{Rj}(\lambda_I) + i\tilde{g}_{Ij}(\lambda_I)$, we obtain that the eigenvalues of (2.23) along the imaginary axis are the union of the roots of the coupled systems $\tilde{g}_{Rj} = \tilde{g}_{Ij} = 0$, given by

$$\tilde{g}_{Rj}(\lambda_I) \equiv \tilde{C}_{Rj}(\lambda_I) - \tilde{f}_R(\lambda_I), \qquad \tilde{g}_{Ij}(\lambda_I) \equiv \tilde{C}_{Ij}(\lambda_I) - \tilde{f}_I(\lambda_I), \qquad j = 1, .., k. \tag{5.10a}$$

Here we have defined $\tilde{C}_{Rj}$ and $\tilde{C}_{Ij}$ by

$$\tilde{C}_{Rj}(\lambda_I) = \operatorname{Re}\left[C_j(i\lambda_I)\right], \qquad \tilde{C}_{Ij}(\lambda_I) = \operatorname{Im}\left[C_j(i\lambda_I)\right], \tag{5.10b}$$

where C_j is given in (5.2). The functions $\tilde{f}_R$ and $\tilde{f}_I$ are as defined in (3.4b), and their properties were given in propositions 3.1 and 3.2 of §3, respectively.

We can readily generalize the winding number criterion given in proposition 3.3. Suppose that $\tau > 0$, and that there are no zeros of $g_j(\lambda)$ on the imaginary axis for $j = 1, .., k$. Then, for $k \geq 1$, the number of eigenvalues M of (2.23) in the right half-plane is

$$M = \frac{5k}{4} + \frac{1}{\pi} \sum_{j=1}^{k} [\arg g_j]_{\Gamma_I}, \quad \text{for} \quad \tau > 0. \tag{5.11}$$

Here $[\arg g_j]_{\Gamma_I}$ denotes the change in the argument of g_j along the semi-infinite imaginary axis $\Gamma_I = i\lambda_I$, $0 \leq \lambda_I < \infty$, traversed in the downwards direction.

Our next result gives conditions for the stability and instability of a multi-spike solution to the GM model (1.1).

Proposition 5.3: *Let $k \geq 2$ and suppose that either $m = p+1$ and $p > 1$, or $m = 2$ and $1 < p \leq 5$. Then, a multi-spike solution is unstable for any $\tau \geq 0$ when $D > D_k$, where D_k is given in (2.33) of proposition 2.6. Next, suppose that $0 < D < D_k$, with $m = 2$ and $1 < p \leq 5$. Then, a multi-spike solution is stable on an $O(1)$ time-scale for $0 \leq \tau < \tau_0$, where $\tau_0 > 0$ is sufficiently small.*

Proof: We now prove this result. As noted in the proof of proposition 5.2 we have $D_k = \tilde{D}_k$. When $D > D_k$, we are guaranteed from (5.3c) that $C_k(0) > 1/(p-1)$. Under the conditions on m and p given in proposition 5.3, we have from (3.25) of proposition 5.3 that $f'_R(\lambda_R) > 0$ and $f_R \to \infty$ as $\lambda_R \to \nu_0^-$. Hence $g_k(\lambda_R) = 0$ has a root in $0 < \lambda_R < \nu_0$. Therefore, a k-spike solution is unstable

47

for any $\tau > 0$ when $D > D_k$. Next, suppose that $D < D_k$. Then, since $C_j(0) < 1/(p-1)$ for $j = 1, .., k$, the curves $C_j(\lambda_R)$ and $f_R(\lambda_R)$ will not intersect when τ is sufficiently small. Hence, for τ small, there are no eigenvalues of (2.23) on the real axis. We now show that for τ sufficiently small, there are also no eigenvalues on the imaginary axis. When $\tau = 0$ we have $\tilde{C}_{Rj}(\lambda_I) = \tilde{C}_{Rj}(0)$ for $j = 1, .., k$. For $\tau > 0$, we can readily verify from (5.2) and (5.10b) that $\tilde{C}_{Rj}$ is an increasing function of λ_I for $j = 1, .., k$ with $\tilde{C}_{Rj}(0) > 0$. Since for $m = 2$ and $p > 1$, we know that $\tilde{f}_R$ is monotone decreasing from (3.6) of proposition 3.1, we have that $\tilde{g}_{Rj} = 0$ has a unique root for each $j = 1, .., k$. As in the proof of proposition 3.4, we will have that $[\arg g_j]_{\Gamma_I} = -5\pi/4$ for each j if we can show that $\tilde{g}_{Ij} < 0$ at the root of $\tilde{g}_{Rj} = 0$. This is clear, since for $m = 2$ and $1 < p \le 5$, we have $\tilde{f}_I > 0$ from (3.16) of proposition 3.2, together with $\tilde{C}_{Ij}(0) = 0$ and $\tilde{C}_{Ij} = O(\tau)$ as $\tau \to 0$ for finite λ_I. Hence, for $j = 1, .., k$, there exists a $\tau_0 > 0$ such that $[\arg g_j]_{\Gamma_I} = -5\pi/4$ for all τ satisfying $0 \le \tau < \tau_0$. Substituting this result into the winding number criterion (5.11), we get $M = 0$. This proves stability on an $O(1)$ time-scale. To ensure stability on an $O(\varepsilon^{-2})$ time-scale, recall that the additional criterion in proposition 2.2 needs to be satisfied. This completes the proof of proposition 5.3. ∎

Therefore, when $0 < D < D_k$, we will have stability on an $O(1)$ time-scale until τ increases past some value $\tau_0 > 0$. We now determine this critical value. First, we claim that for each $j = 1, .., k$, there exists a value $\lambda_I = \lambda_{Ij}^0(D)$ and $\tau = \tau_{0j}(D) > 0$ such that $\tilde{g}_{Rj} = \tilde{g}_{Ij} = 0$ in (5.10a). This follows since by proposition 2.6, the eigenvalues of (2.23) are in the left half-plane when $\tau = 0$, and by proposition 5.2 each g_j has two roots on the positive real axis when τ is sufficiently large. Hence, since eigenvalues cannot enter into the right half-plane along the real axis as τ is increased, by continuity of the eigenvalue branch with respect to τ they must have entered the right half-plane at some points $\lambda_I = \lambda_{Ij}^0(D)$ and $\tau = \tau_{0j}(D) > 0$ for $j = 1, .., k$. Even without the existence of a transversal crossing condition to ensure that $\tau = \tau_{0j}(D)$ is uniquely determined, we still have the result that for $0 < D < D_k$, a k-spike solution for (1.1) will be stable on an $O(1)$ time-scale when

$$0 \le \tau < \tau_0(D; k) \equiv \mathrm{Min}\left(\tau_{0j}(D)\,;\, j = 1, .., k\right). \tag{5.12}$$

This defines a function $\tau_0(D; k)$.

The numerical method of §3 is used to compute the curves $\tau_{0j}(D)$ for $j = 1, .., k$ for each of the exponent sets of (1.3). The value $\tau_0(D; k)$ is then computed from (5.12). For each of the exponent sets of (1.3) we have found numerically that there is a strict transversal crossing condition in that for any $\tau > \tau_{0j}(D)$, the function g_j contributes exactly two eigenvalues to the right half-plane. Moreover, for the exponent sets of (1.3), we have found that for each value of k and D, with $0 < D < D_k$, the criterion (5.12) yields $\tau_0(D; k) = \tau_{01}(D)$. Moreover, there is an ordering principal

of the form $\tau_{0j}(D) < \tau_{0j+1}(D)$ for $j = 1, .., k - 1$. Thus, the numerical evidence suggests that the $j = 1$ mode determines the stability threshold for $0 < D < D_k$.

In Fig. 18(a), we plot the curves $\tau_0(D; k)$ for $k = 2, 3, 4$, for the exponent set $(2, 1, 2, 0)$. The critical values D_k are labeled in the figure. In Fig. 18(b) we also plot the curves $\tau_{0j}(D)$ for $2 \leq j \leq k$. These curves represent the values of τ where additional pairs of complex conjugate eigenvalues first enter the right half-plane. For $k = 1, 2, 3$ we have found numerically that $\tau_{0j}(D) < \tau_{0j+1}(D)$. In Fig. 19(a) and Fig. 19(b) we plot $\tau_0(D; k)$ for the exponent sets $(2, 1, 3, 0)$ and $(3, 2, 2, 0)$, respectively. Similarly, in Fig. 20(a) and Fig. 20(b) we plot $\tau_0(D; k)$ for the exponent sets $(3, 2, 3, 1)$ and $(4, 2, 2, 0)$. As seen from these figures, the threshold curves $\tau_0(D; k)$ are all qualitatively quite similar. For a given exponent set, there is a universal limit $\tau_0(D; k) \to \tau_{0u}$ as $D \to 0$, where τ_{0u} is independent of k. This results from the asymptotic independence of $\chi(\tau\lambda; j)$ on k when $D \ll 1$, as seen from (2.26).

(a) $\tau_0(D; k)$ versus D (b) τ_{0j}
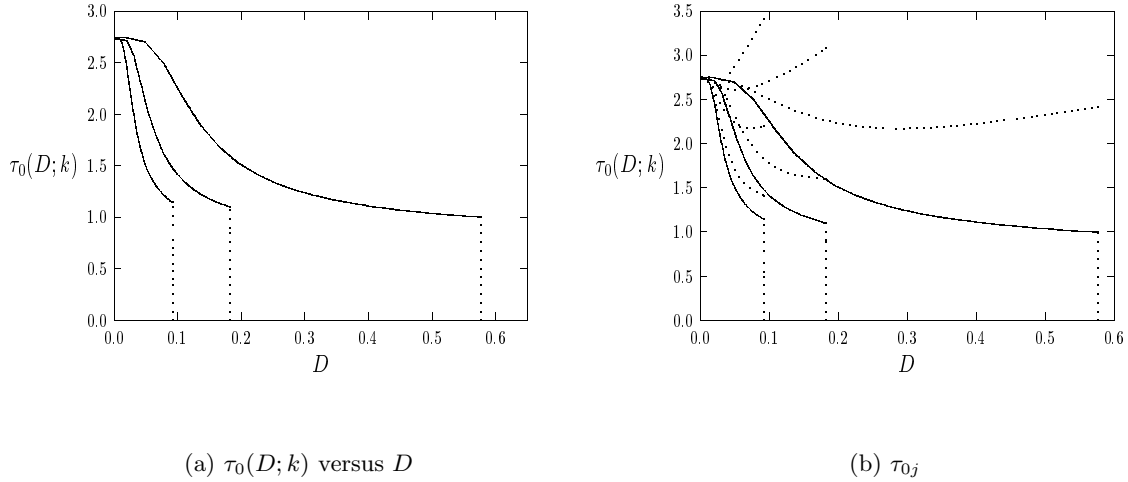
Figure 18: Left figure: we plot $\tau_0(D; k)$ (solid lines), for $k = 2, .., 4$, for the exponent set $(2, 1, 2, 0)$. The values of D_k (vertical dashed lines) are $D_2 = 0.5767$, $D_3 = 0.1810$, and $D_4 = 0.0915$. Right figure: we also plot $\tau_{0j}(D)$ (dashed curves) for $2 \leq j \leq k$ and $k = 2, 3, 4$. These dashed curves are the values of τ, where more pairs of complex conjugate eigenvalues first enter the right half-plane.

Next, we suggest an explanation to support the conclusion that the $j = 1$ mode corresponds to the minimum in the stability criterion (5.12). We begin by trying to establish an ordering principle

for $\tilde{C}_{Rj}$ and $\tilde{C}_{Ij}$. From (5.10b) and (5.2), we readily calculate for $j = 1, .., k-1$ that

$$\tilde{C}_{Rj+1} - \tilde{C}_{Rj} = \beta_j \text{Re}\,[E(\xi)] \,, \qquad \tilde{C}_{Ij+1} - \tilde{C}_{Ij} = \beta_j \text{Im}\,[E(\xi)] \,. \qquad (5.13a)$$

Here β_j and $E(\xi)$ are defined by

$$\beta_j \equiv \left(\frac{k}{\theta_0 qm} \right) \left(\frac{\sin\,[\pi(j-1/2)/k] \sin\,[\pi/k]}{\tanh\,(\theta_0/k)} \right) > 0 \,, \qquad E(\xi) \equiv \frac{\xi}{\sinh \xi} \,, \qquad (5.13b)$$

with

$$\xi \equiv \frac{2\theta_0}{k} \sqrt{1 + i\tau\lambda_I} \,. \qquad (5.13c)$$

(a) $(p, q, m, s) = (2, 1, 3, 0)$ (b) $(p, q, m, s) = (3, 2, 2, 0)$
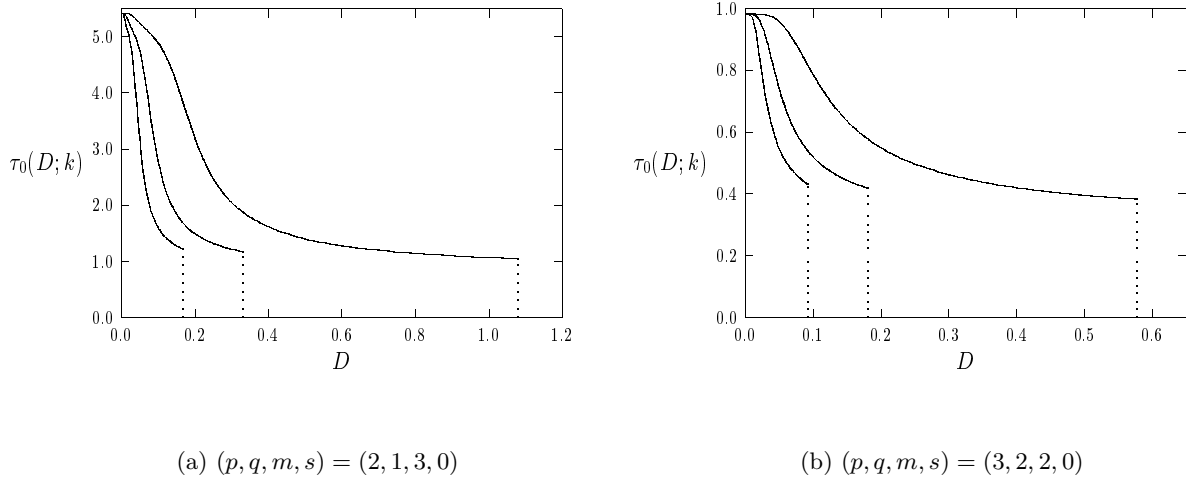
Figure 19: Plots of $\tau_0(D; k)$ (solid curves) for the exponent sets $(2, 1, 3, 0)$ (left figure) and $(3, 2, 2, 0)$ (right figure). For $(2, 1, 2, 0)$, the critical values are $D_2 = 1.080$, $D_3 = 0.3310$, and $D_4 = 0.1658$. For $(3, 2, 2, 0)$, the critical values are $D_2 = 0.5767$, $D_3 = 0.1810$, and $D_4 = 0.0915$.

Let $\xi = \xi_R + i\xi_I$. When $\lambda_I = 0$ we have $\xi_R = 2\theta_0/k > 0$ and $\xi_I = 0$. With the principal value of the square root, we have $\xi_R > 0$ and $\xi_R > \xi_I$ for $\lambda_I > 0$. As $\lambda_I \to \infty$, we have $\xi_R \sim \xi_I \sim |\xi|e^{i\pi/4}$. Thus, to establish an ordering principle as λ_I ranges from $0 \leq \lambda_I < \infty$, we must determine the signs of the real and imaginary parts of $E(\xi)$ in the region $\xi_R \geq 2\theta_0/k > 0$ with $0 \leq \xi_I \leq \xi_R$. By calculating $E(\xi)$ explicitly in (5.13b), it is easy to see that $\text{Re}\,[E(\xi)] > 0$ for $0 \leq \xi_I < \pi/2$, and that $\text{Im}\,[E(\xi)] < 0$ for some range $0 \leq \xi_I < \xi_c$. The value $\xi_c > 0$ is tedious to determine. Thus, for

λ_I sufficiently small, we have from (5.13a) that there is an ordering principle for any $D > 0$ and $\tau > 0$ of the form

$$\tilde{C}_{Rj+1}(\lambda_I) > \tilde{C}_{Rj}(\lambda_I), \qquad \tilde{C}_{Ij+1}(\lambda_I) < \tilde{C}_{Ij}(\lambda_I). \tag{5.14}$$

This ordering principle only holds for λ_I sufficiently small. For λ_I sufficiently large, it is easy to see that the signs of the real and imaginary parts of E will change.
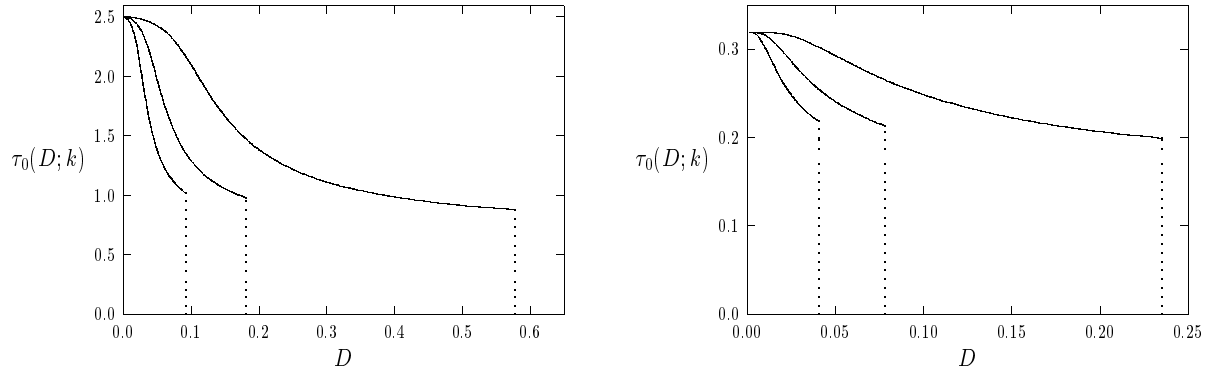
(a) $(p, q, m, s) = (3, 2, 3, 1)$ (b) $(p, q, m, s) = (4, 2, 2, 0)$

Figure 20: Plots of $\tau_0(D; k)$ (solid curves) for the exponent sets $(3, 2, 3, 1)$ (left figure) and $(4, 2, 2, 0)$ (right figure). For $(3, 2, 3, 1)$, the critical values are $D_2 = 0.5767$, $D_3 = 0.1810$, and $D_4 = 0.0915$. For $(4, 2, 2, 0)$, the critical values are $D_2 = 0.2349$, $D_3 = 0.0778$, and $D_4 = 0.0410$.

We now argue that if the ordering principle (5.14) holds up until beyond the values of λ_I where $\tilde{C}_{Rj}$ and $\tilde{C}_{Ij}$ intersect $\tilde{f}_R$ and $\tilde{f}_I$, then we are guaranteed that the stability threshold in (5.12) is set by the $j = 1$ mode. This implies that $\tau_0(D; k) = \tau_{01}(D)$. For each of the exponent sets of (1.3), we have verified numerically that this ordering assumption is satisfied. To illustrate graphically this analysis, in Fig. 21(a) we plot the numerically computed functions $\tilde{f}_R$ and $\tilde{C}_{Rj}$ for $j = 1, 2, 3$ for a three-spike solution for the exponent set $(2, 1, 2, 0)$ with $D = 0.1465$. From proposition 3.1 we know that $\tilde{f}_R$ is monotone decreasing, and hence since $\tilde{C}_{Rj}$ is increasing, there is exactly one crossing point for each j in Fig. 21(a). Similarly, in Fig. 21(b) we plot the corresponding $\tilde{f}_I$ and $\tilde{C}_{Ij}$ for $j = 1, 2, 3$. From these figures we notice that the ordering principle (5.14) holds until, at least, after the crossing points. The plots in Fig. 21(a) and Fig. 21(b) correspond to the numerically computed value $\tau = \tau_{01} = 1.18$. From Fig. 21(a) and Fig. 21(b), we see that the implication of

this ordering principle is that when $\tilde{g}_{Rj} = 0$ for $j = 2, 3$, we will have $\tilde{g}_{Ij} < 0$. Repeating the steps in the proof of proposition 3.4, we calculate that the contribution of g_j for $j = 2, 3$ to the winding number is $[\arg g_j]_{\Gamma_I} = -5\pi/4$. Thus, when $\tau = \tau_{01}$, there are no zeros of g_j for $j = 2, 3$ in the right half-plane. Hence, the complex conjugate pair for g_1 when $\tau = \tau_{01}$ is the first pair to cross into the right half-plane. For each of the exponent sets in (1.3), we found numerically that $\tau_0(D; k) = \tau_{01}(D)$. The discussion above suggests the underlying mechanism behind this result. The ordering principal (5.14) for small λ_I, also suggests why $\tau_{0j} < \tau_{0j+1}$ for $j = 1, .., k - 1$.

(a) $\tilde{f}_R$; $\tilde{C}_{Rj}$ for $j = 1, 2, 3$ (b) $\tilde{f}_I$; $\tilde{C}_{Ij}$ for $j = 1, 2, 3$
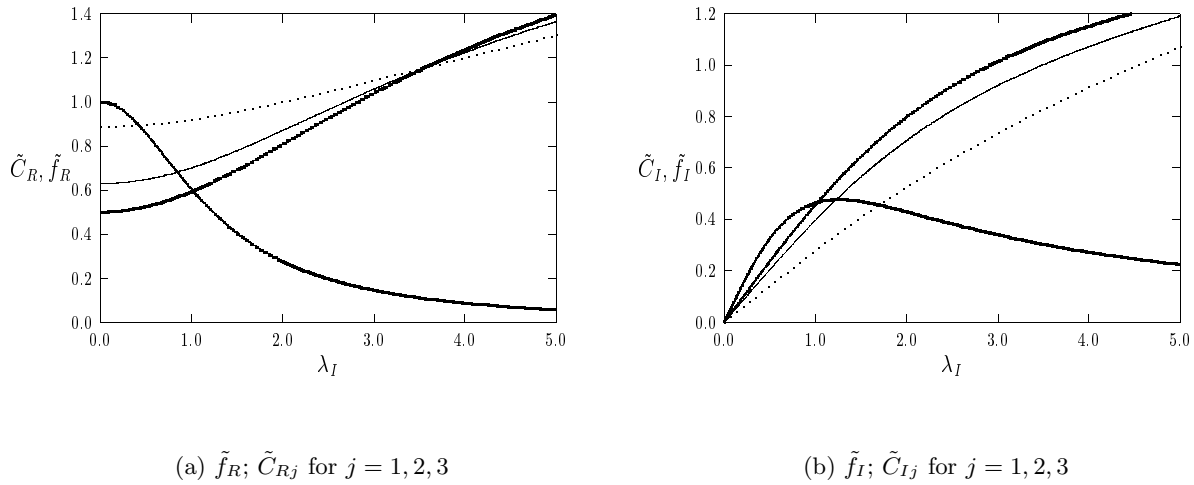
Figure 21: Left figure: Plots of $\tilde{f}_R$ and $\tilde{C}_{Rj}$ for $j = 1$ (heavy solid), $j = 2$ (solid), and $j = 3$ (dashed). Right figure: Plots of $\tilde{f}_I$ and $\tilde{C}_{Ij}$ (same labels) for $j = 1, 2, 3$. The exponent set is $(2, 1, 2, 0)$ with $k = 3$, $D = 0.1465$. The plot is for $\tau = \tau_{01} = 1.18$ at which $g_1 = 0$. Notice that at the roots of $\tilde{g}_{Rj} = 0$ for $j = 2, 3$, we have $\tilde{g}_{Ij} < 0$.

Next, we consider the limit $D \to D_k^-$. In this limit, the complex conjugate roots of $\tilde{g}_{Rk} = 0$ approach the real axis. This occurs since $C_k(0) \to 1/(p - 1)$ from below. When $D = D_k$ we have a double root at the origin. For $D > D_k$ the roots split, with one root moving along the real axis into the right half-plane. Thus, as discussed earlier, it is the $j = k$ mode that determines the instability of a k-spike solution for $D > D_k$. We now characterize the merger of this complex conjugate pair onto the real axis as $D \to D_k^-$. We define $\delta = D_k - D$ with $0 \le \delta \ll 1$. We then look for a solution $\lambda = i\lambda_I$ and $\tau = \tau_{0k}$ to

$$C_k(\tau\lambda; D) = f(\lambda), \qquad f(i\lambda_I) = \tilde{f}_R(\lambda_I) + i\tilde{f}_I(\lambda_I). \tag{5.15}$$

Here we have indicated the explicit dependence of C_k on $z = \tau\lambda$ and on D. Since $\lambda_I \to 0$, the local behaviors of $\tilde{f}_R$ and $\tilde{f}_I$ given in (3.5a) and (3.15) of propositions 3.1 and 3.2 are central to the calculation. Performing a Taylor expansion of C_k in both D and λ, we substitute the expansion into the left-hand side of (5.15) and use the local behaviors (3.5a) and (3.15) to calculate the right-hand side of (5.15). Equating real and imaginary parts, we obtain the local scaling result for $\delta \ll 1$ that

$$\lambda \sim i\delta^{1/2} \left(\kappa_c^{-1} \frac{\partial C_k}{\partial D}(0:D_k) \right)^{1/2}, \tag{5.16a}$$

$$\tau_{0k} \sim \tau_{0k}^* + o(1), \qquad \tau_{0k}^* \equiv \frac{1}{p-1}\left(\frac{1}{p-1} - \frac{1}{2m} \right)\left[\frac{\partial C_k}{\partial z}(0; D_k) \right]^{-1}. \tag{5.16b}$$

In (5.16a), we need to assume that κ_c, defined in proposition 3.1, is positive. From (3.5c) and (3.5d) this occurs for $m = p + 1$ with $p > 1$, and $m = 2$ with $p > 1$. This condition implies that $\tilde{f}_R$ is locally decreasing for λ_I small. This local behavior yields the scaling law $\lambda_I = O\left(\sqrt{D_k - D}\right)$ as $D \to D_k^-$ for the $j = k$ mode.

5.1 Competition Instabilities and Synchronous Oscillations

Finally, we illustrate the physical manifestations of the different types of unstable modes that give rise to the initial instability. As discussed above, and verified numerically, the oscillatory instability for $0 < D < D_k$ is a result of the $j = 1$ mode. The corresponding eigenfunction has the form given in (2.11) with coefficients given in (2.21b). Thus, from (2.9), (2.11), (2.21b), and from (2.35) which relates Φ to ψ, we conclude that the initial instability for $0 < D < D_k$ has the form

$$a = a_e + \delta e^{i\lambda_I^0 t}\phi + \text{c.c}, \quad \phi(x) = \sum_{n=1}^{k} c_n\psi\left[\varepsilon^{-1}(x - x_n)\right], \quad c_n = 1, \quad n = 1, .., k. \tag{5.17}$$

Here c.c denotes complex conjugate, $\delta << 1$, and $\psi(y)$ is the solution to $(L_0 - \lambda)\psi = w^p$ at the value $\lambda = i\lambda_I^0$, $\tau = \tau_0(D; k)$ corresponding to the zero of $g_1(\lambda) = 0$. The key point here is that, since $c_n = 1$ for $n = 1, .., k$, the initial form of the instability is to synchronize the amplitudes of the spikes. In contrast, suppose that $D_k < D < \tilde{D}_{k-1}$ and that τ is sufficiently small. We have shown above that the instability that occurs here is a result of only the $j = k$ mode. For this mode there is exactly one eigenvalue λ_R on the positive real axis. Therefore, using (2.21b) with $j = k$, the initial instability has the different form

$$a = a_e + \delta e^{\lambda_R t}\phi, \quad \phi(x) = \sum_{n=1}^{k} c_n\psi\left[\varepsilon^{-1}(x - x_n)\right], \quad c_n = \cos\left(\frac{\pi(k-1)}{k}(n - 1/2)\right) \quad n = 1, .., k. \tag{5.18}$$

Here $\psi(y)$ is the solution to $(L_0 - \lambda_R)\psi = w^p$, at the value $\lambda = \lambda_R$ for which $g_k(\lambda_R) = 0$. Since $\sum_{n=1}^{k} c_n = 1$, this type of initial instability conserves the sum of the amplitudes of the spikes. However, it introduces a spike competition as it increases the amplitude of some of the spikes while decreasing the amplitude of others. As shown in the numerical experiments below, this instability has the effect of annihilating spikes.

5.2 Numerical Validation: Small and Large-Scale Oscillations

We now illustrate numerically the rigorous and formal asymptotic results given above for the stability of multi-spike solutions. As in §4, we solve the GM model (1.1) numerically using the NAG library routine D03PCF [19] with 2000 uniformly spaced meshpoints and stringent control on the accuracy of local time-steps. The initial condition for the GM model (1.1) is now taken to be a localized perturbation off of a_e in the form

$$a(x,0) = a_e \left[1 + 0.02 \sum_{n=1}^{k} b_n \cos\left(\frac{\pi(x - x_n)}{\varepsilon} \right) e^{-(x-x_n)^2/(2\varepsilon^2)} \right], \qquad h(x,0) = h_e(x). \qquad (5.19)$$

Here $b_n \equiv 1$ if n is odd and $b_n \equiv -1$ if n is even. The functions a_e and h_e are the k-spike equilibrium solutions given in proposition 2.1. In each of the figures below we plot the amplitude a_{mn} of each spike, defined by $a_{mn} \equiv a(x_n, t)$, versus t. To illustrate the theory, we consider three experiments. In each of these experiments the time-scale chosen was much smaller than $O(\varepsilon^{-2})$. Therefore, the spike locations remained essentially frozen at their equilibrium values.

Experiment 1: Consider a two-spike solution to (1.1) for the exponent set $(2, 1, 2, 0)$ with $\varepsilon = 0.01$. In Fig. 22(a), we plot the equilibrium solution a_e and h_e when $D = 0.59$. Notice that the initial perturbation (5.19) is different for the two spikes. Since $D > D_2 = 0.5766$, this solution is unstable as a result of one eigenvalue of the linearization on the positive real axis. In Fig. 22(b), we plot the amplitudes a_{m1} and a_{m2} of the spikes when $\tau = 0.02$. As t increases, one of the spikes is annihilated, but there is no oscillatory instability. This instability, whereby one spike is annihilated in a competition, is suggested by (5.18). In Fig. 23(a) and Fig. 23(b) we plot the spike amplitudes when $D = 0.5472$. For this value of D, the critical threshold, $\tau_0(D; 2)$, for an instability is $\tau_0(D; 2) = 1.012$ as obtained from Fig. 18(a). For the value $\tau = 0.99 < 1.012$, we show in Fig. 23(a) that the initial perturbations in the spike amplitudes die out as t increases. However, this only shows that we have stability on an $O(1)$ time-scale. The threshold for stability with respect to the small $O(\varepsilon^2)$ eigenvalues in the spectrum is that $D < D_2^*$, where D_2^* is as given in proposition 2.2. For the data given, we calculate $D_2^* = 0.3218$. Since $D = 0.5472 > D_2^*$, we would expect to see another instability that is only triggered after a much longer time-scale

$t = O(\varepsilon^{-2}) \approx 1.0 \times 10^4$. In Fig. 23(b), we take $D = 0.5472$ and $\tau = 1.1 > \tau_0(D; 2)$. For this value we observe that an oscillatory instability is triggered. As t increases, the phase and amplitudes of the two spikes become synchronous as suggested, at least near the onset of the instability, by (5.17). As shown in Fig. 23(b), when $\tau = 1.1$, the long-time behavior of the solution appears to be a synchronous periodic oscillation of the amplitudes of the two spikes.

(a) a_e and h_e

(b) a_m versus t
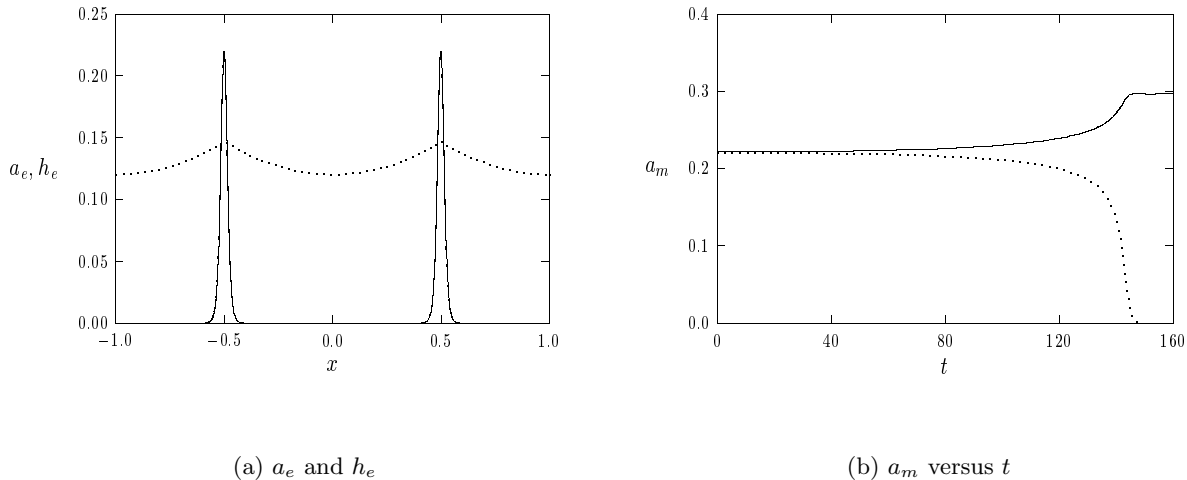
Figure 22: Experiment 1: The left figure is a_e (solid curve) and h_e (dashed curve) for $k = 2$ with $D = 0.59$. In the right figure we plot the spike amplitudes versus t when $\tau = 0.02$ and $D = 0.59$. The solid curve is a_{m1} and the dashed curve is a_{m2}. As t increases the second spike is annihilated.

Experiment 2: Next, we consider a three-spike solution to (1.1) for the exponent set $(2, 1, 2, 0)$ with $\varepsilon = 0.01$. In Fig. 24(a) we plot the equilibrium solution a_e and h_e when $D = 0.19$. Notice that from (5.19), the initial perturbation is the same for the first and third spikes, but is different for the second spike. Since $D > D_3 = 0.1811$, but $D < \tilde{D}_2 = 0.4798$, there is exactly one eigenvalue on the positive real axis. In Fig. 24(b), where we plot the spike amplitudes when $\tau = 0.02$, we observe that the middle spike is annihilated as t is increased, and there is no oscillatory instability. This type of competition instability is again suggested by (5.18), since the unstable eigenvector from (5.18) is $c_1 = c_3 = 1/2$ and $c_2 = -1$. For other initial perturbations of the spike amplitudes, we were able to obtain solutions where the first and third spikes were annihilated leaving only the middle spike. In Fig. 25(a) and Fig. 25(b), we plot the spike amplitudes when $D = 0.1695$. For this value of D, the critical threshold for an instability is $\tau_0(D; 3) = 1.128$ from Fig. 18(a). When $\tau = 1.05 < 1.128$, we

(a) $\tau = 0.99$ (b) $\tau = 1.1$
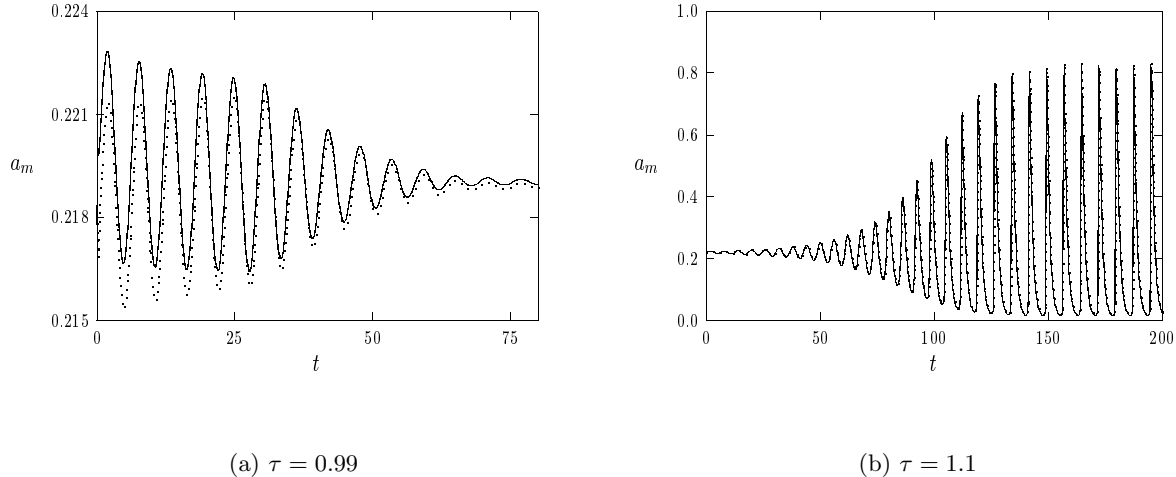
Figure 23: Experiment 1: In the left figure we plot the spike amplitudes a_{m1} (solid curve) and a_{m2} (dashed curve) for $k = 2$, $D = 0.5472$, and $\tau = 0.99$. In the right figure a similar plot is made for $D = 0.5472$ and $\tau = 1.1$. The critical value is $\tau_0 = 1.012$.

show in Fig. 25(a) that the initial perturbations in the spike amplitudes die out as t is increased. However, as in experiment 1, this only shows stability on an $O(1)$ time-scale. From proposition 2.2 we require $D < D_3^* = 0.143$ to obtain stability on an $O(\varepsilon^{-2})$ time-scale. Finally, in Fig. 25(b) we take $\tau = 1.15$ and $D = 0.1695$. An oscillatory instability is triggered, the oscillations synchronize near the onset of the instability, and the numerical evidence suggests that the final pattern is a synchronous periodic oscillation of the amplitudes of the three spikes.

Experiment 3: Finally, we consider the four-spike example mentioned in §1 for the exponent set $(p, q, m, s) = (2, 1, 3, 0)$ with $\varepsilon = 0.01$. For this exponent set, the critical value of D is $D_4 = 0.1658$. Since $D = 0.18 > D_4$ in Fig. 1(b), and $\tau = 0.02$ is small, there is only one eigenvalue of the linearization in the right half-plane and it is on the positive real axis. The resulting competition instability was shown in Fig. 1(b). From the data used to generate Fig. 19(a), we calculate $\tau_0(D; 4) = 1.275$ when $D = 0.15$. For the value $\tau = 1.3$ and $D = 0.15$, we predict the onset of an oscillatory instability that synchronizes as t increases. This was precisely the behavior shown in Fig. 2(a). When $\tau = 1.2$ and $D = 0.15$, there are two complex conjugate eigenvalues of the linearization that have small negative real parts. The resulting slowly decaying oscillation in the spike amplitudes was shown in Fig. 2(b). Finally, consider the parameter set $D = 0.18$ with $\tau = 1.75$. Since $D > D_4$

56
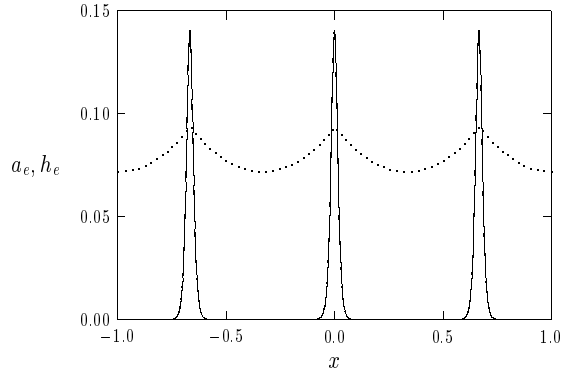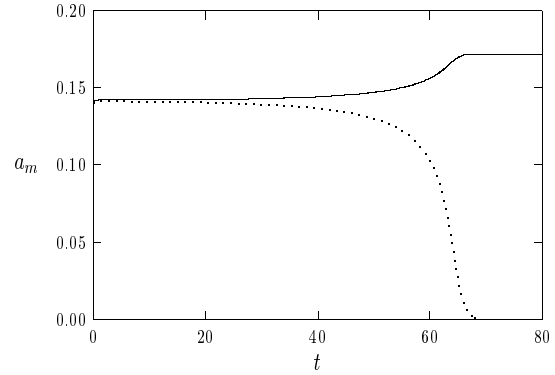
(a) a_e and h_e

(b) a_m versus t

Figure 24: Experiment 2: The left figure is a_e (solid curve) and h_e (dashed curve) for $k = 3$ with $D = 0.19$. In the right figure we plot the spike amplitudes versus t for $\tau = 0.02$ and $D = 0.19$. The solid curve is a_{m1} and a_{m3}, and the dashed curve is a_{m2}. As t increases a_{m2} is annihilated.
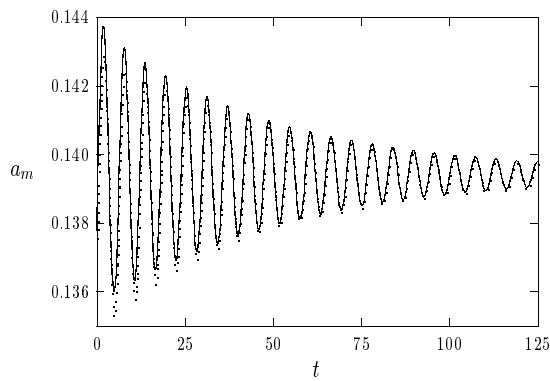
(a) $\tau = 1.05$
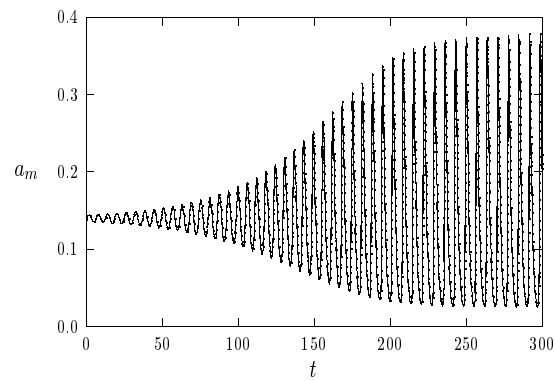
(b) $\tau = 1.15$

Figure 25: Experiment 2: In the left figure the solid curve is the spike amplitudes a_{m1} and a_{m3}. The dashed curve is a_{m2}. The parameter values are $k = 2$, $D = 0.1695$, and $\tau = 1.05$. In the right figure a similar plot is made for $D = 0.1695$ and $\tau = 1.15$. The critical value is $\tau_0 = 1.128$.

there is an eigenvalue on the positive real axis. In addition, for these values of τ and D there is also a pair of complex conjugate eigenvalues that have small positive real parts. The threshold value of τ, where this additional unstable mode entered the right half-plane is computed to be $\tau = 1.72$. Therefore, we predict that the onset of the instability will be, approximately, a superposition of a synchronous oscillation and a competition instability. In Fig. 26(a) we plot the resulting spike amplitudes. The oscillations indeed becomes synchronized after a short time period. However, near $t = 30$, the spikes a_{m2} and a_{m4} are annihilated. This annihilation behavior is shown more clearly on the magnified time interval of Fig. 26(b). This type of oscillatory competition is to be contrasted with the monotone behavior shown previously in Fig. 1(b) for the same parameter values, but with $\tau = 0.02$.

(a) a_{mn} versus t (b) a_{mn} versus t
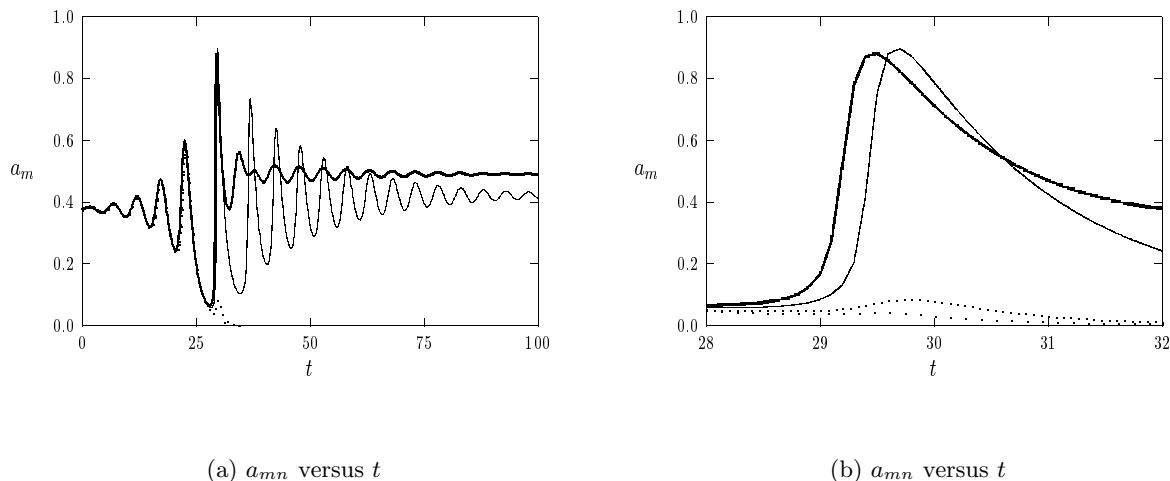
Figure 26: Experiment 3: The spike amplitudes when $k = 4$, $(p, q, m, s) = (2, 1, 3, 0)$, $\varepsilon = 0.01$, $D = 0.18$, and $\tau = 1.75$. Here a_{m1} (solid curve), a_{m2} (widely spaced dots), a_{m3} (heavy solid curve), and a_{m4} (dashed curve). The time interval for the right figure is near when a_{m2} and a_{m4} are annihilated.

6   Conclusions

We have analyzed the stability of one-spike and multi-spike equilibrium solutions for (1.1) in the limit $\varepsilon \to 0$ for different ranges of D and τ. The analysis was a blend of rigorous, asymptotic,

and numerical methods. The results given in the propositions have been proved rigorously. Let us summarize the rigorous results established for the prototypical exponent set $(2, 1, 2, 0)$. In proposition 3.4 we proved that there are either zero or two eigenvalues in the right half-plane for any $\tau > 0$. In proposition 3.7 we proved that there is a value $\tau_c(D) > 0$, such that when $\tau > \tau_c(D)$ there are exactly two eigenvalues on the positive real axis on the interval $0 < \lambda_R < \nu_0$. In proposition 3.7, we proved that these eigenvalues must have entered the right half-plane as a complex conjugate pair at some value $\tau = \tau_0(D) > 0$. The asymptotic behavior of the eigenvalues on the real axis for $\tau > \tau_c(D)$ is given in propositions 3.8 and 3.9. In proposition 5.3 we prove that a multi-spike solution with $k > 2$ is unstable for any $\tau \geq 0$ when $D > D_k$, where D_k was given in proposition 2.6. In proposition 5.2, we prove that when $D > \tilde{D}_2$ (see (5.3d)), then there are at least $k - 1$ eigenvalues on the positive real axis. Moreover, in proposition 5.2, we prove that when $0 < D < D_k$, there are exactly $2k$ eigenvalues on the positive real axis for τ sufficiently large. In proposition 5.3, we prove that there exists a $\tau_0 \geq 0$, such that a k-spike solution is stable on an $O(1)$ time-scale when $0 < D < D_k$ and $0 \leq \tau < \tau_0$.

For a one-spike solution, and for certain exponent sets, we have shown in Fig. 12(a), Fig. 12(b), and Fig. 13(a), that small-scale oscillations in the spike amplitude occur when τ increases past the critical value τ_0. We conjecture that this behavior occurs for all exponent sets satisfying (1.2). Large-scale oscillations in the spike amplitude for τ well beyond τ_0, that await a mathematical understanding, were shown in Fig. 13(b), Fig. 14(a), Fig. 14(b), Fig. 15(a), Fig. 15(b), Fig. 16(a), and Fig. 16(b). For multi-spike solutions, our analysis has suggested two different instability mechanisms for different ranges of D and τ: competition instabilities and synchronous oscillations in the spike amplitudes. The conditions for the onset of these instabilities were predicted in §5. In the figures corresponding to Experiments 1–3 in §5.2 we have illustrated these instabilities numerically.

We now list several interesting open problems. We begin with the technical problems that await rigorous proof. A central problem is to establish analytically the transversal crossing condition (3.55) that guarantees that eigenvalues enter the right half-plane at some $\tau = \tau_0$ and remain in the right half-plane for $\tau > \tau_0$. A second technical problem is to establish more general conditions on the exponent set (p, q, m, s) under which $\tilde{f}_R(\lambda_I)$ in proposition 3.1 is monotone decreasing. This condition is key to the winding number criterion that guarantees that each g_j for a k-spike solution contributes, exactly, either zero or two eigenvalues to the right half-plane. Finally, it would be interesting to prove that the stability threshold for a multi-spike solution for the range $0 < D < D_k$ is set by the $j = 1$ mode, as was found numerically and suggested analytically for the exponent sets of (1.3). From (5.17), the existence of such a threshold mode is the mechanism that leads to the onset of a synchronicity for the amplitude and phase of the spike oscillations.

59

Another open problem suggested by the numerical computations is to investigate the nature of the small and large-scale oscillations computed in §4 and §5. One problem is to determine analytically whether the Hopf bifurcation is subcritical or supercritical. Another problem is to investigate rigorously the stability of the degenerate zero solution studied asymptotically in §4. In §4, we argued that the zero solution is stable only when $\tau > q/(p-1)$. However, for certain exponent sets, such as for $(3, 2, 2, 0)$, the threshold τ_0 for an oscillatory instability for a one-spike solution can satisfy $\tau_0 < q/(p-1)$. Hence, if one chooses τ in the range $\tau_0 < \tau < q/(p-1)$, then the zero solution is unstable and a one-spike equilibrium solution is unstable. The resulting oscillation shown in Fig. 16(a) and Fig. 16(b) is intricate and has large dramatic peaks in the amplitude. These peaks become even more pronounced as D is increased. In particular, for the shadow limit $D \to \infty$, an extremely large amplitude, and irregular, oscillation was shown numerically in [31] to occur for the shadow GM model in N-dimensions. It would be interesting to study this problem analytically. Finally, for a multi-spike solution on the range $0 < D < D_k$, it would be interesting to study analytically the large-scale synchronous oscillations computed in §5 for values of τ slightly beyond $\tau_0(D; k)$. These oscillations that occur for $k \geq 2$ seem much more regular than the oscillatory instabilities that occur for a one-spike solution.

It would also be of interest to extend the framework of the analysis given here to include other reaction-diffusion systems that have localized spike patterns, such as the Schnakenburg model (cf. [26]) and the Gray-Scott model (cf. [7]). In addition, it should be possible to analyze a modified GM system that includes a saturation effect on the activator autocatalysis term a^p/h^q in (1.1a). A qualitative discussion of such saturation mechanisms is described in [18] (see section 2.4), and a preliminary mathematical analysis of the resulting modified GM system is given in [23]. Finally, since our framework for studying spike stability has not relied on dynamical systems techniques, it should also be possible to extend this framework to analyze spike stability in a multi-dimensional spatial domain.

Acknowledgements

A   Nondimensionalizing the GM Model

The dimensional Gierer-Meinhardt model is

$$A_T = D_1 A_{yy} - \alpha A + \beta \frac{A^p}{H^q} \,, \tag{A.1a}$$

$$H_T = D_2 H_{yy} - \xi H + \sigma \frac{A^m}{H^s} \,, \tag{A.1b}$$

where α, β, ξ, and σ, are positive constants. The exponents (p, q, m, s) satisfy (1.2). We assume that D_2/D_1 is large, and so we introduce a small parameter ε by

$$\frac{D_2}{D_1} = \varepsilon^{-2} K_0 \,, \tag{A.2}$$

where $K_0 > 0$ is $O(1)$ as $\varepsilon \to 0$. In this limit, (A.1) supports spike solutions that are localized in A. We introduce dimensionless variables a, h, t and x, by

$$T = \omega t \,, \qquad x = y/L \,, \qquad A = \varepsilon^{-\nu_a} a_0 a \,, \qquad H = \varepsilon^{-\nu_h} h_0 h \,, \tag{A.3}$$

where a_0 and h_0 are constants. Substituting (A.3) into (A.1), we get

$$\frac{1}{\omega} a_t = \frac{D_1}{L^2} a_{xx} - \alpha a + \beta \varepsilon^{\nu_a(1-p)+\nu_h q} \left(\frac{a_0^{p-1}}{h_0^q} \right) \frac{a^p}{h^q} \,, \tag{A.4a}$$

$$\frac{1}{\omega} h_t = \frac{D_2}{L^2} h_{xx} - \xi h + \sigma \varepsilon^{-\nu_a m + \nu_h(1+s)} \left(\frac{a_0^m}{h_0^{s+1}} \right) \frac{a^m}{h^s} \,. \tag{A.4b}$$

To ensure that the amplitude of a spike is $O(1)$ as $\varepsilon \to 0$, we must make the coefficients of a^p/h^q and a^m/h^s be $O(1)$ and $O(\varepsilon^{-1})$ as $\varepsilon \to 0$, respectively. This condition yields that

$$\nu_a = \frac{q}{p-1} \zeta^{-1} \,, \qquad \nu_h = \zeta^{-1} \,, \tag{A.5}$$

where ζ was defined in (1.2). To eliminate as many parameters as possible in (A.4), we choose ω and L by $\omega = 1/\alpha$ and $L^2 = D_1 \varepsilon^{-2}/\alpha$. The constants a_0 and h_0 are taken to be

$$h_0 = \left[\frac{\xi}{\sigma} \left(\frac{\beta}{\alpha} \right)^{\frac{m}{p-1}} \right]^{\frac{1}{\zeta}} \,, \qquad a_0 = \left(\frac{\alpha}{\beta} \right)^{\frac{1}{p-1}} \left[\frac{\xi}{\sigma} \left(\frac{\beta}{\alpha} \right)^{\frac{m}{p-1}} \right]^{\frac{q}{(p-1)\zeta}} \,. \tag{A.6}$$

Then, (A.4) becomes

$$a_t = \varepsilon^2 a_{xx} - a + \frac{a^p}{h^q} \,, \tag{A.7a}$$

$$\tau h_t = \tau \varepsilon^2 \left(\frac{D_2}{D_1} \right) h_{xx} - h + \varepsilon^{-1} \frac{a^m}{h^s} \,. \tag{A.7b}$$

61

Finally, substituting (A.2) for D_2/D_1 into (A.7b), we obtain the dimensionless system (1.1), where τ and D in (1.1) are defined by

$$\tau \equiv \alpha/\xi \qquad D \equiv \tau K_0 . \tag{A.8}$$

In [8] spectral results are proved for the following reaction-diffusion system (see equation (1.2) of [8]) on the infinite line $-\infty < y < \infty$:

$$V_t = \hat{\varepsilon}^2 V_{yy} - V + \gamma_2 U^{\alpha_2} V^{\beta_2} , \tag{A.9a}$$

$$U_t = U_{yy} - \mu U + \gamma_1 U^{\alpha_1} V^{\beta_1} . \tag{A.9b}$$

Here $\hat{\varepsilon} \ll 1$, while γ_1 and γ_2 are positive $O(1)$ constants. In the GM model of (1.1) we identify $\alpha_1 = -s$, $\alpha_2 = -q$, $\beta_1 = m$, and $\beta_2 = p$. The usual assumptions (1.2) on the exponents are assumed to hold. To compare our form (1.1) of the GM system with (A.9), we set $D = \varepsilon\tau$ in (1.1b), with $\varepsilon \ll 1$, and consider (1.1) on the infinite domain $-\infty < x < \infty$. When $D \ll 1$, the inhibitor field decays exponentially away from a spike core. Therefore, in this limit it is reasonable to replace the finite domain in (1.1) with an infinite domain. Introducing the new variable y by $x = \varepsilon^{1/2}y$, we transform (1.1) to

$$a_t = \varepsilon a_{yy} - a + a^p/h^q , \tag{A.10a}$$

$$h_t = h_{yy} - h/\tau + \varepsilon^{-1} a^m/(\tau h^s) . \tag{A.10b}$$

Next, we introduce the new variables U and V by $a = a_0 V$ and $h = h_0 U$, where a_0 and h_0 satisfy

$$a_0^{p-1}/h_0^q = \gamma_2 , \qquad \varepsilon^{-1} a_0^m/(\tau h_0^{s+1}) = \gamma_1 . \tag{A.11}$$

In terms of U and V, (A.10) becomes

$$V_t = \varepsilon V_{yy} - V + \gamma_2 V^p/U^q , \tag{A.12a}$$

$$U_t = U_{yy} - U/\tau + \gamma_1 V^m/U^s . \tag{A.12b}$$

This system is precisely (A.9) if we identify $\hat{\varepsilon} = \varepsilon^{1/2}$ and $\mu = 1/\tau$.

Therefore, we conclude that our results in the limit $D \ll 1$ for the spectrum of the linearization of (1.1) around a one-spike equilibrium solution should correspond to the spectral results obtained in [8] provided we identify $\tau = 1/\mu$. This correspondence is compared quantitatively in Remark 3.10 of §3.

62

B   Calculation of an Integral

A sufficient condition for the convexity result (3.26) when $m = 2$ is that $h_3(0) > 0$, where $h_3(\alpha)$ is defined in (3.34). Using (3.7) for $L_0^{-1}w$ and (3.34), we calculate

$$h_3(0) \equiv \int_{-\infty}^{\infty} w L_0^{-3} w \, dy = \frac{1}{(p-1)} \int_{-\infty}^{\infty} w L_0^{-2} w \, dy + \frac{1}{2} \int_{-\infty}^{\infty} w L_0^{-2} \left(y w' \right) dy \,. \tag{B.1}$$

Integrating by parts on the second term in (B.1), and using (3.7) for $L_0^{-1}w$, we get

$$h_3(0) = \frac{1}{(p-1)} \int_{-\infty}^{\infty} w L_0^{-1} \left(\frac{w}{p-1} + \frac{1}{2} y w' \right) dy + \frac{1}{2} \int_{-\infty}^{\infty} \left[\frac{w}{p-1} + \frac{1}{2} y w' \right] L_0^{-1} \left(y w' \right) dy \,. \tag{B.2}$$

Integrating by parts on the second term in (B.2), we get

$$h_3(0) = \frac{1}{(p-1)^2} \int_{-\infty}^{\infty} w L_0^{-1} w \, dy + \frac{1}{(p-1)} \int_{-\infty}^{\infty} w L_0^{-1} \left(y w' \right) dy + \frac{1}{4} \int_{-\infty}^{\infty} y w' L_0^{-1} \left(y w' \right) dy \,. \tag{B.3}$$

Finally, we integrate by parts on the middle term in (B.3), and calculate $\int_{-\infty}^{\infty} w L_0^{-1} w \, dy$ explicitly. This gives the main formula,

$$h_3(0) = \left[\frac{1}{p-1} - \frac{1}{4} \right] \left(\frac{1}{(p-1)^2} \int_{-\infty}^{\infty} w^2 \, dy - \frac{1}{2(p-1)} \int_{-\infty}^{\infty} w^2 \, dy + \frac{1}{2} \int_{-\infty}^{\infty} \left(y w' \right)^2 dy \right)$$
$$+ \frac{1}{4} \int_{-\infty}^{\infty} \left(w + y w' \right) L_0^{-1} \left(y w' \right) dy \,. \tag{B.4}$$

In (B.4) we must calculate the function $\xi \equiv L_0^{-1}(y w')$. This function changes sign, but since it it is even, we consider only the domain $0 \le y < \infty$. To calculate ξ, it is convenient to first find an even function that satisfies $L_0 \psi_e = 0$. A simple calculation gives

$$\psi_e = b_e \left[\frac{1}{w} + \frac{5}{3} - \frac{10}{3} \left(w + \frac{1}{2} y w' \right) \right] \,, \qquad \text{when} \quad p = 2 \,, \tag{B.5a}$$

$$\psi_e = b_e \left[\frac{1}{w} - \frac{3}{2} \left(w + y w' \right) \right] \,, \qquad \text{when} \quad p = 3 \,. \tag{B.5b}$$

Here b_e is a constant chosen so that $\psi_e(0) = 1$. A formula for ψ_e for arbitrary p can be written in terms of a quadrature. The function ψ_e is even, it grows exponentially as $y \to \infty$, and there is a unique y^* where $\psi_e(y^*) = 0$. Since ξ is even, we look for a solution for ξ in the form $\xi = v \psi_e$. This gives the following formula for ξ

$$\xi(y) = \psi_e(y) v(y) \,, \qquad v'(y) = \frac{1}{[\psi_e(y)]^2} \int_{y^*}^{y} s w'(s) \psi_e(s) \, ds \,. \tag{B.6}$$

63

We must choose the lower limit to be y^* in the integral in (B.6) to obtain a removable singularity for v' at y^*. Next, we multiply the equation $L_0\xi = yw'$ by w', and integrate over the domain $0 < y < \infty$ to get

$$\xi(0) = \frac{1}{w''(0)} \int_0^\infty y \left[w'(y)\right]^2 dy. \tag{B.7}$$

Since $\psi_e(0) = 1$, this implies that $v(0) = \xi(0) < 0$. We then integrate (B.6) with this initial value and determine $v(y)$, which yields $\xi(y)$. We can then evaluate the integrals in (B.4) numerically. When $p = 2$, we use $w = \frac{3}{2}\mathrm{sech}^2(y/2)$. In this way we calculate that $h_3(0) = 2.7$ when $p = 2$. However, our computations show that $h_3(0) < 0$ when $p = 3, 4$.

C   The Proof of Lemma 3.6

In this appendix we prove Lemma 3.6. The proof is by contradiction. Assume that there exists a $y_0 > 0$ with $\xi(y_0) > 0$. Then, by continuity, it follows that $\xi(y) > 0$ on $y \in (y_1, y_2)$, with either: (i) $\xi(y_1) = \xi(y_2) = 0$, with $\xi'(y_1) \geq 0$ and $\xi'(y_2) \leq 0$, where $0 < y_1 < y_2 \leq \infty$, or (ii) $y_1 = 0$ with $\xi(0) \geq 0$, $\xi'(0) = 0$, $\xi(y_2) = 0$, and $\xi'(y_2) \leq 0$, where $y_2 \leq \infty$.

Let ν_0, ϕ_{l0} be the principal eigenpair of L_0 as in Theorem 2.5. Since ϕ_{l0} has constant sign, we can assume that $\phi_{l0} > 0$ for $y \geq 0$. We then multiply (3.37) by ϕ_{l0}, and integrate by parts over the interval $y_1 < y < y_2$, to get

$$(\nu_0 - \lambda_R) \int_{y_1}^{y_2} \phi_{l0}\xi \, dy + \phi_{l0}\xi'|_{y_1}^{y_2} = \int_{y_1}^{y_2} \phi_{l0}v \, dy. \tag{C.1}$$

In both cases (i) and (ii) we obtain that $\phi_{l0}\xi'|_{y_1}^{y_2} \leq 0$. Therefore, since $\lambda_R > \nu_0$, the left-hand side of (C.1) is negative, whereas the right-hand side of (C.1) is positive. This is a contradiction, and hence $\xi(y) \leq 0$ on $y \geq 0$ when $\lambda_R > \nu_0$. This proves Lemma 3.6.

References

[1] U. Ascher, R. Christiansen, R. Russell, *Collocation Software for Boundary Value ODE's*, Math. Comp., **33**, (1979), pp. 659-679.

[2] M. Cross, P. Hohenburg, *Pattern Formation Outside of Equilibrium*, Rev. Mod. Physics, **65**, (1993), pp. 851-1112.

[3] E. N. Dancer, *On Stability and Hopf Bifurcations for Chemotaxis Systems*, Methods and Appl. of Analysis, Vol. 8, No. 2, (2001), pp. 245-256.

[4] A. Doelman, T. J. Kaper, P. Zegeling, *Pattern Formation in the One-Dimensional Gray-Scott Model*, Nonlinearity, **10**, (1997), pp. 523-563.

[5] A. Doelman, T. Kaper, H. van der Ploeg, *Spatially Periodic and Aperiodic Multi-Pulse Patterns in the One-Dimensional Gierer-Meinhardt Model*, Methods and Appl. of Analysis, Vol. 8, No. 3, (2001), pp. 387-414.

[6] A. Doelman, R. A. Gardner, T. J. Kaper, *Stability Analysis of Singular Patterns in the 1D Gray-Scott Model: A Matched Asymptotics Approach*, Physica D, **122**, (1998), pp. 1-36.

[7] A. Doelman, R. A. Gardner, T. Kaper, *A Stability Index Analysis of 1-D Patterns of the Gray Scott Model*, Memoirs of the AMS, **155**, No. 737, (2002).

[8] A. Doelman, R. A. Gardner, T. Kaper, *Large Stable Pulse Solutions in Reaction-Diffusion Equations*, Indiana U. Math. Journ., Vol. 50, No. 1, (2001), pp. 443-507.

[9] S. Ei, Y. Nishiura, K. Ueda, 2^n *Splitting or Edge Splitting?: A Manner of Splitting in Dissipative Systems*, Japan. J. Indust. Appl. Math., **18**, (2001), pp. 181-205.

[10] S. Ei, *The Motion of Weakly Interacting Pulses in Reaction-Diffusion Systems*, J. Dynam. Differential Equations, **14**, No. 1, (2002), pp. 85-137.

[11] A. Gierer, H. Meinhardt, *A Theory of Biological Pattern Formation*, Kybernetik, **12**, (1972), pp. 30–39.

[12] L. Harrison, D. Holloway, *Order and Localization in Reaction-Diffusion Pattern*, Physica A, **222**, (1995), pp. 210-233.

[13] D. Iron, M. J. Ward, *The Dynamics of Multi-Spike Solutions to the One-Dimensional Gierer-Meinhardt Model*, SIAM J. Appl. Math., **62**, No. 6, (2002), pp. 1924-1951. (electronic)

[14] D. Iron, M. J. Ward, J. Wei, *The Stability of Spike Solutions to the One-Dimensional Gierer-Meinhardt Model*, Physica D, **150**, No. 1-2, (2001), pp. 25-62.

[15] J. Keener, *Activators and Inhibitors in Pattern Formation*, Stud. Appl. Math., **59**, (1978), pp. 1-23.

[16] C. S. Lin, W. M. Ni, I. Takagi, *Large Amplitude Stationary Solutions to a Chemotaxis System*, J. Diff. Eq., **72**, (1988), pp. 1-27.

[17] H. Meinhardt, *Models of Biological Pattern Formation*, Academic Press, London, (1982).

[18] H. Meinhardt, *The Algorithmic Beauty of Sea Shells*, Springer-Verlag, Berlin, (1995).

[19] NAG Fortran library Mark 17, routine D03PCF, Numerical Algorithms Group Ltd., Oxford, United Kingdom (1995).

[20] W. Ni, *Diffusion, Cross-Diffusion, and Their Spike-Layer Steady-States*, Notices of the AMS, Vol. **45**, No. 1, (1998), pp. 9-18.

[21] W. Ni, I. Takagi, E. Yanagida, *Stability Analysis of Point-Condensation Solutions to a Reaction-Diffusion System Proposed by Gierer and Meinhardt*, to appear, Tohoku Math J., (2002).

[22] Y. Nishiura, *Global Structure of Bifurcating Solutions of Some Reaction-Diffusion Systems*, SIAM J. Math. Anal., **13**, No. 4, (1982), pp. 555-593.

[23] Y. Nishiura, *Coexistence of Infinitely Many Stable Solutions to Reaction-Diffusion Equations in the Singular Limit*, in Dynamics Reported: Expositions in Dynamical Systems Volume 3 (editors: C. K. R. T. Jones, U. Kirchgraber), Springer-Verlag, New York, (1995).

[24] Y. Nishiura, D. Ueyama, *Spatio-Temporal Chaos for the Gray-Scott Model*, Physica D, **150**, (2001), pp. 137-162.

[25] Y. Nishiura, *Far-From-Equilibrium Dynamics*, Translations of Mathematical Monographs, Vol. 209, AMS publications, Providence, Rhode Island, (2002).

[26] J. Schnakenberg, *Simple Chemical Reaction Systems with Limit Cycle Behavior*, J. Theoret. Biology, **81**, (1979), p. 389-400.

[27] W. Sun, T. Tang, M. J. Ward, J. Wei, *Numerical Challenges for Resolving Spike Dynamics for Two Reaction-Diffusion Systems*, accepted, Studies in Appl. Math., (2002).

[28] I. Takagi, *Point-Condensation for a Reaction-Diffusion System*, J. Diff. Eq., **61**, (1986), pp. 208-249.

[29] A. Turing, *The Chemical Basis of Morphogenesis*, Phil. Trans. Roy. Soc. B, **327**, (1952), pp. 37-72.

[30] M. J. Ward, J. Wei, *Asymmetric Spike Patterns for the One-Dimensional Gierer-Meinhardt Model: Equilibria and Stability*, Europ. J. Appl. Math., Vol. 13, No. 3, (2002), pp. 283-320.

[31] M. J. Ward, J. Wei, *Hopf Bifurcation of Spike Solutions for the Shadow Gierer-Meinhardt Model*, submitted, Europ. J. Appl. Math., (2002).

[32] J. Wei, *On Single Interior Spike Solutions for the Gierer-Meinhardt System: Uniqueness and Stability Estimates*, Europ. J. Appl. Math., Vol. **10**, No. 4, (1999), pp. 353-378.

[33] J. Wei, M. Winter, *The Gierer-Meinhardt System: Existence and Stability of N-Peaked Solutions*, submitted, Trans. American Math Society, (2001).